Ph. D. Dissertation

Evaluation of Reactivity Improvement Factors using Structured Catalysts to Control Mass Transfer and Proposal for Effective Use

Department of Chemical Engineering

Graduate School of Engineering

Tokyo University of Agriculture and Technology

Hiromu Sasaki

March. 2021

Table of Contents

Chapter 1: Introduction **001**

1.1 Novelty of this study and Contents of this Dissertation 002

1.2 Background 004

1.2.1 Process Intensification (PI) 005

1.2.2 Structured catalyst 010

1.2.3 Micro-Partition Structured Catalyst (MPC) 014

1.2.4 Reactions for Hydrogen Energy and Hydrogen Economy 017

1.3 Purpose 020

1.4 Organization 021

1.5 Conclusions of chapter 1 024

1.6 References 025

Chapter 2: Methodology **034**

2.1 Abstract 035

2.2 Catalyst Preparation 036

2.2.1 Preparation of structured alumite catalyst support 036

2.2.2 Preparation of $Cu/ZnO/Al_2O_3$-MPC 038

2.2.3 Preparation of Pt/Al_2O_3-MPC 040

2.3 Catalyst Characterization 042

2.3.1 Anodized aluminum layer thickness analysis 042

2.3.2 Brunauer–Emmett–Teller specific surface area analysis (BET) 042

2.3.3 Inductively coupled plasma spectroscopy analysis (ICPS) 043

2.3.4 Temperature programmed reduction analysis (TPR) 043

2.3.5 H_2-Pulse titration analysis 045

2.4 Reactor Preparation 046

2.5 Catalytic Activity Test 048

2.5.1 Condition for the SRM Reaction 048

2.5.2 Condition for the WGS Reaction 050

2.5.3 Condition for the CHC Reaction 051

2.6 Simulation Application 053

2.7 Nomenclature 057

2.8 Conclusions of chapter 2 059

2.9 References 060

Chapter 3: Comparison of Reactivity between MPC and Plate-type Structured Catalysts: Experimental studies **064**

3.1 Abstract 065

3.2 Purpose 065

3.3 Methodology 066

3.4 Results and Discussion 067

3.4.1 Catalytic activity test for comparing between MPC and plate for the SRM reaction 067

3.4.2 Catalytic activity test for comparing between MPC and plate for the WGS reaction 071

3.4.3 Catalytic activity test for comparing between MPC and plate for the CHC reaction 075

3.4.4 Discussion of the reactivity improvement 079

3.4.5 Evaluation of the turnover frequency (TOF) 081

3.5 Conclusions of chapter 3 084

3.6 References 085

Chapter 4: Investigation of Factors to Improve Reactivity due to the Structure of MPC and Proposal of Evaluation Index: Numerical Simulation 087

4.1 Abstract 088

4.2 Purpose 088

4.3 Methodology 089

4.4 Results and Discussion 090

4.4.1 Validation of the reactivity improvement using MPC on simulation 090

4.4.2 Reactivity improvement under an external mass transfer rate-limiting step 093

4.4.3 Proposal of evaluation index for reactivity improvement under a catalytic reaction rate-limiting step 096

4.4.4 Identification of structures to affect the reactivity 100

4.5 Conclusions of chapter 4 102

Chapter 5: Investigation of the Effect of the Number of MPC Stacking on the Reactivity 104

5.1 Abstract 105

5.2 Purpose 105

5.3 Methodology 106

5.4 Results and Discussion 107

5.4.1 Effect of the number of MPC stacking on the reactivity for the SRM reaction 107

5.4.2 Effect of the position of MPC in the stacking for the SRM reaction 118

5.4.3 Effect of the number of MPC stacking on the reactivity for the WGS reaction 123

5.4.4 Effect of the number of MPC stacking on the reactivity for the CHC reaction 127

5.5 Conclusions of chapter 5 136

Chapter 6: Proposal for Effective MPC Stacking Method **138**

6.1 Abstract 139

6.2 Purpose 139

6.3 Methodology 140

6.4 Results and Discussion 141

6.4.1 Proposed effective stacking method for MPCs: Numerical simulation 141

6.4.2 Demonstration of the reactivity improvement for the effective stacking method proposed 150

6.4.3 Application of the effective stacking method to the CHC reaction 161

6.5 Conclusions of chapter 6 167

6.6 References 168

Chapter 7: Conclusions and Future Works **169**

7.1 Conclusions 170

7.2 Future works and Outlook 178

7.3 List of published Journal related to this dissertation 181

7.4 Presentation at conferences related to this dissertation 181

7.5 References 182

ACKNOWLEDGMENTS **183**

Chapter 1

Introduction

1.1 Novelty of this study and Contents of this Dissertation

Process Intensification (PI) has attracted attention in the field of chemical engineering. One of the various effective tools for PI is a structured catalyst and a variety of structured catalysts have been applied to a catalytic reaction process. However, there are few reports on the effects on reactivity due to the structure of a structured catalyst, although there have been many reports of energy efficiency improvements when a structured catalyst is used as an alternative catalytic reactor to a conventional particle-packed bed reactor. Most of the few reports are about an improvement of a catalytic reaction process as a device in structured catalyst reactors, and to the best of our knowledge, factors that improve the reactivity of catalytic reaction due to the structure of catalyst have not been examined yet.

Therefore, I focused on the effect on the reactivity of the catalytic reaction due to the structure of the structured catalyst. The unique structured catalyst, which has microscale fins and holes, was prepared and the effect of the structure on the reactivity was examined by comparing that of an unprocessed plate-type structured catalyst. The improvement in reactivity due to the structure of the structured catalyst was confirmed not only under an external mass transfer rate-limiting step but also under a catalytic reaction rate-limiting step. It was a novel report as an effective approach to the catalytic reaction process that is not limited to vector-control of transport phenomena which is one of the expected effects of a structured catalyst so far.

Unique index was proposed to quantitatively evaluate the effect on reactivity due to a structure of a structured catalyst under a catalytic reaction rate-limiting step. The index was used to design a stacking method for the structured catalyst in the reactor to further improve the reactivity of the catalytic reaction process. It was a valuable proposal for engineering as an index to evaluate the effect of using the structured catalysts on reactivity under a catalytic reaction rate-limiting step. The diagram of the construction of this dissertation is displayed in **Fig. 1.1-1**.

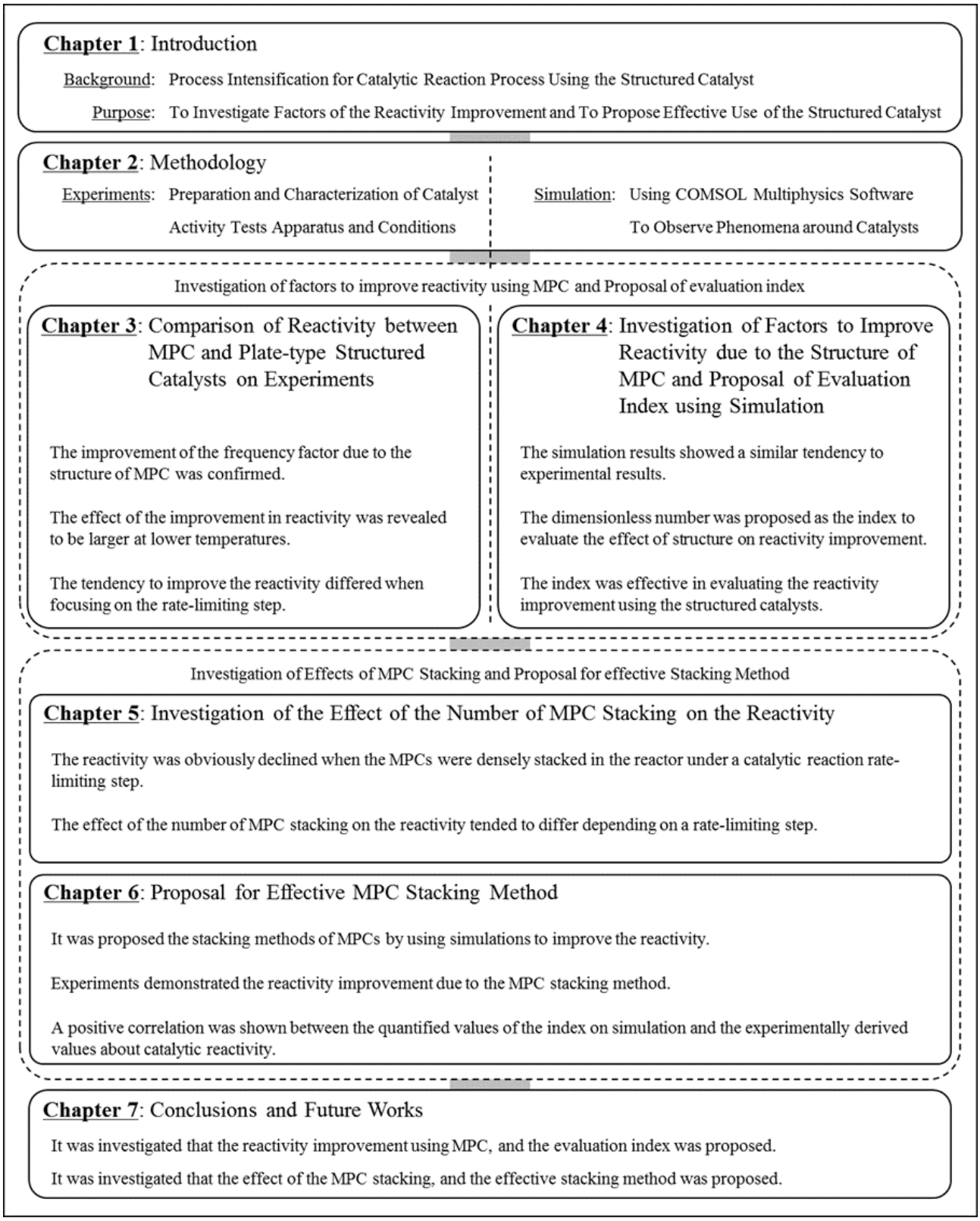

Fig. 1.1-1 Diagram of the contents of this dissertation

1.2 Background

The demand for energy is increasing with the increase of the world population. However, fossil resources are finite, and thus, there is a need to build a sustainable society for us to survive on the Earth. Moreover, since the 19th century, global industrialization has led to serious environmental issues, such as global warming, due to the continuous and massive use of fossil fuels [1-01, 1-02]. There is a close relationship between the energy problem and the environmental problem, and it is an international issue. We must progress from the mass industrial production, consumption, and disposal processes of conventional resources and energy to a new effective use of energy, and the realization of an environmentally harmonious industrial process for a sustainable society. This is a dual challenge (**Fig.1.2-1**). Therefore, chemical processes that have a high energy efficiency and are environmentally friendly should be developed. One such technology development policy is called process intensification (PI), and it is of interest in chemical process engineering [1-03, 1-04].

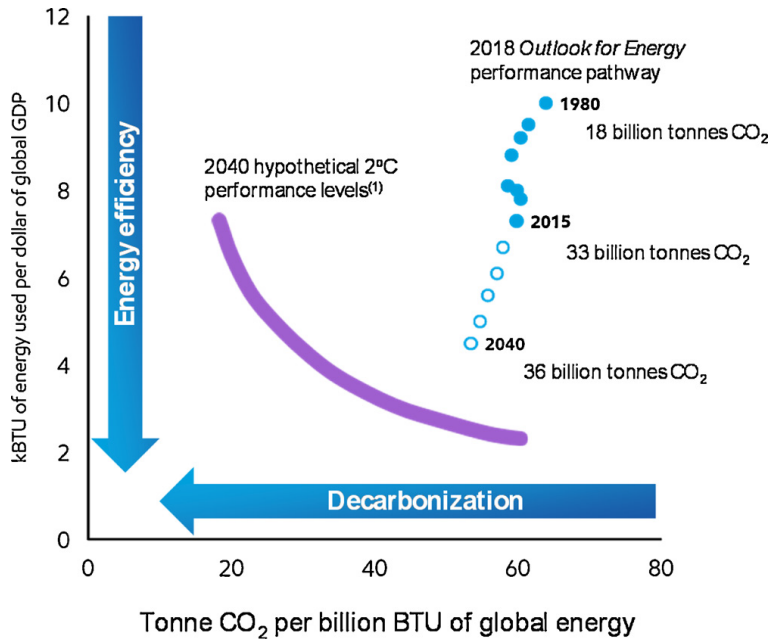

Fig. 1.2-1 World energy-related CO_2 emissions relative to energy intensity and CO_2 emissions intensity [1-05]

1.2.1 Process Intensification (PI)

PI has particularly attracted attention since the 2000s, and is a policy of technological development tailored to current times and purposes. However, there is no universal definition of PI, and its definition has changed over time and based on the international scenario [1-06]. Its flexible interpretation is a very important policy for chemical process development [1-07, 1-08]. It was defined by Stankiewicz *et al.*[1-09] as "Process Intensification is the development of innovative apparatuses and techniques that offer drastic improvements in chemical manufacturing and processing, substantially decreasing equipment volume, energy consumption, or waste formation and ultimately leading to cheaper, safer, sustainable technologies." The components for PI are displayed in **Fig. 1.2-2**.

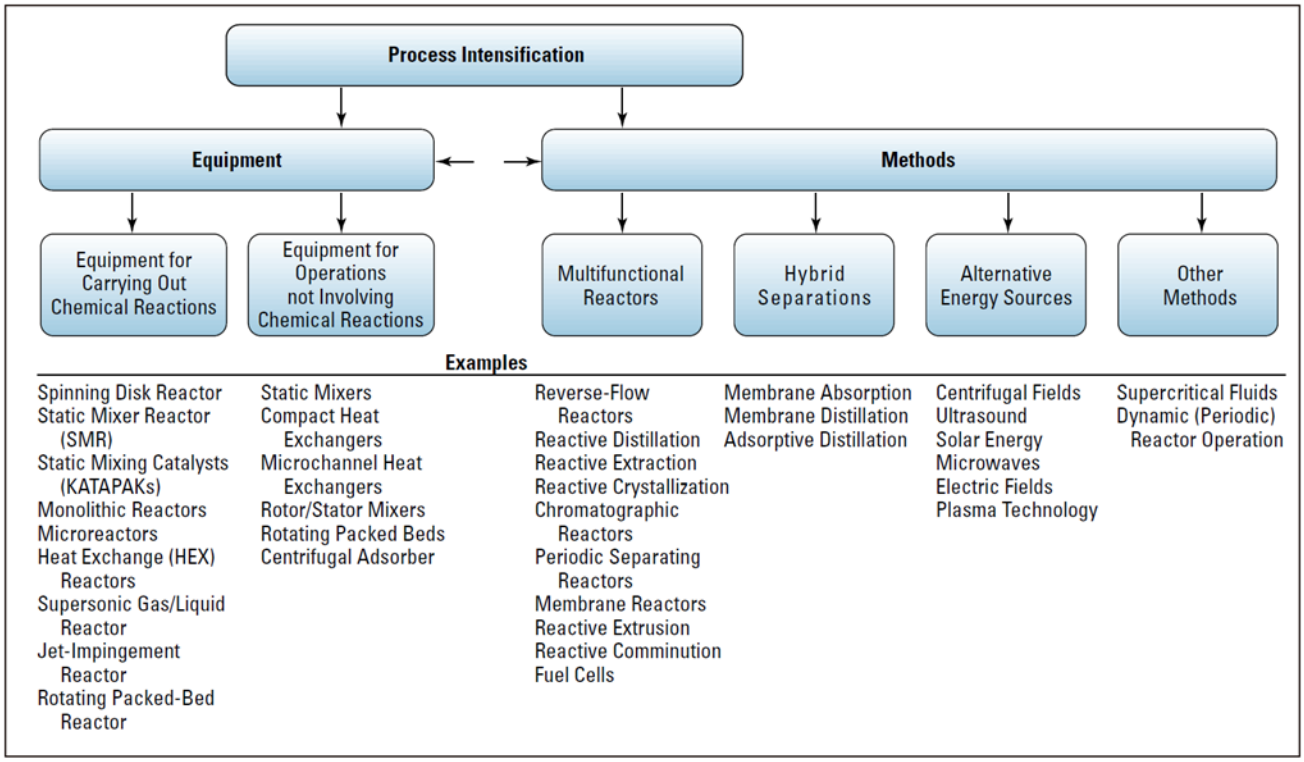

Fig.1.2-2 Process Intensification and its components [1-09]

Moreover, according to Tsouris *et al.* [1-10], "Process Intensification refers to technologies that replace large, expensive, energy–intensive equipment or process with ones that are smaller, less costly, more efficient or that combine multiple operations into fewer devices (or a single apparatus)." Both definitions require miniaturization and increasing the efficiency of chemical process. In recent years, PI has meant an approach aimed at a dramatic improvement in process performance through new connections, high precision, and compactness for each of the important components (e.g., equipment, device and operation) of the process [1-11]. The various definitions for PI was shown in **Table 1.2-1**. There are various technology developments for PI, and some of these approaches are presented in **Table 1.2-2**. It can be seen that PI has a wide range of research targets, including process research, equipment research, and materials research.

Table 1.2-1 Various definitions for PI

Definitions	
drastic improvements in chemical manufacturing and processing, substantially decreasing equipment volume, energy consumption, or waste formation and ultimately leading to cheaper, safer, sustainable technologies	Stankiewicz *et al.* 2000 [1-09]
technologies that replace large, expensive, energy–intensive equipment or process with ones that are smaller, less costly, more efficient or that combine multiple operations into fewer devices (or a single apparatus)	Tsouris *et al.* 2003 [1-10]
dramatic improvement in process performance through new connections, high precision, and compactness for each of the important components of the process	Charpentier *et al.* 2005 [1-11]

Table 1.2-2 Technologies employed for PI (created from the work of [1-04])

Approaches for PI	Technologies	
Dynamic Processes	・Cyclic operation to exploit varying process timescales ・Enabled by rotating equipment, advanced controls ・Examples: true moving beds, simulated moving beds	Process
Combine Unit-operations	・Combine reactions with separations or heat transfer ・Enables by equipment technology R&D ・Examples: hybrid separations, reactive separations	Equipment
Novel Driving Forces	・Unconventional driving forces for reaction/separation ・Unique energy sources: electric fields, microwaves, ultrasound ・Examples: HiGee, fuel cells	
Designed Structured	・Design precise process fluid dynamics & transport phenomena ・Enabled by materials, fabrication R&D ・Examples: monoliths, 3D-printed beds, hollow fibers	Materials

PI has already prompted chemical process development in various fields, equipment, devices, and operations. Representative examples are microfluidic technology, heat integration distillation, and reaction separation [1-12 – 1-14]. Microfluidic technology can improve mass and heat transfer, such as a micro reactor, and drastically improve the energy efficiency [1-15]. For obtaining higher energy-saving efficiency, the internal heat integrated distillation column (HIDiC) (**Fig. 1.2-3**) was developed to decrease the compression ratio, which has a great impact on the usage of electric power [1-14]. Reaction separation is a new combination, similar to reactive distillation, applying a chemical reaction in the separation method (**Fig. 1.2-4**), making multiple operations compact and drastically improve its separation performance [1-16]. The energy for distillation has been greatly reduced by raising the heat transfer efficiency not only via separation but also by changing the shape of the equipment, and by adding a reaction operation [1-17].

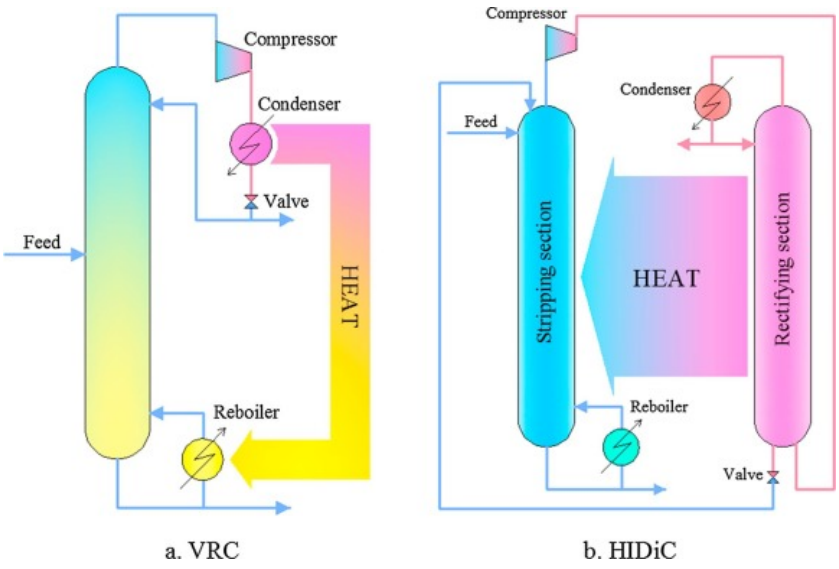

Fig.1.2-3 Conceptual Illustrations of two typical heat integrated configurations [1-14]
(a. VRC: Vapor recompression column, b. HIDiC: Heat integrated distillation column)

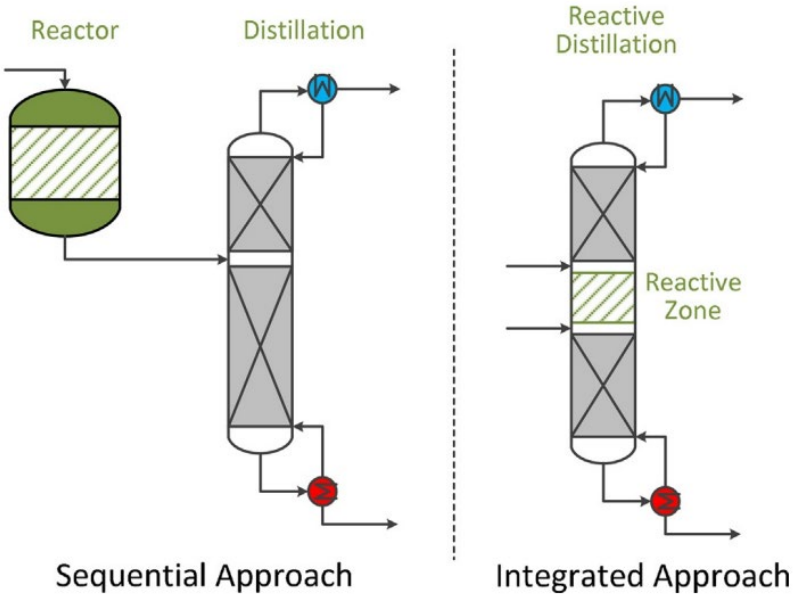

Fig.1.2-4 Sequential approach and integrated approach as reactive distillation [1-18]

In a catalytic reaction, which is an important element of chemical process engineering, the improvement of the reaction performance of not only the catalyst species but also the reaction fields, considering a macro view of the reaction process, leads to PI. Therefore, the creation of reaction fields and the design of the reaction fields are studied for the efficient function of a catalyst. Typical technologies for the creation of reaction fields are ultrafine bubbles [1-19, 1-20] or inorganic–organic porous composite polymers (PCP) and Metal-Organic Frameworks (MOFs) [1-21, 1-22]. MOFs are materials that promote selective adsorption and reaction owing to their regular microstructure and molecular size. These technologies use a field that has not been conventionally controlled as a reaction field. Typical techniques for the design of reaction fields are dynamic operation [1-23, 1-24] or vector control of transport phenomena [1-25, 1-26]. These techniques are expected to improve the reaction performance by actively controlling the reaction conditions and the reaction environment. Structured catalysts are expected to improve the reactivity, owing to their designed macroscopic structure, by controlling the direction of transport phenomena, such as heat transfer and mass transfer, in the reaction field [1-27, 1-28]. The characteristics of these technologies are shown in **Table 1.2-2**. We especially focused on structured catalysts, which is expected to control transport phenomena to realize PI.

Table 1.2-2 Characteristics of PI for chemical reaction fields

Target	Technologies	Characteristics
Creation of reaction fields	Fine bubbles	Gas-phase components are concentrated at the gas-liquid interface in the liquid phase by forming bubbles of 100 μm or less, creating a locally high concentration reaction field.
	Nano-porous material	Porous materials with regular micro-structures such as Porous Coordination Polymer (PCP) and Metal Organic Frameworks (MOF) create selective adsorption and catalytic reaction fields.
Design of reaction fields	Dynamic operation	Actively utilize the dynamics resulting from transport and reactions in chemical processes, or their interactions, as process factors in process design.
	Vector control of transport	The direction of heat and mass transfer is controlled to precisely design the reaction fields, especially in small reactors. A typical device is Structured catalysts and Separation membranes.

1.2.2 Structured catalyst

The structured catalysts can solve the problems of conventional granular packed–bed type catalytic reactors, and it is expected to allow the vector control of the transport phenomena in the reactor by its characteristic structure. The reactivity would dramatically improve using a structured catalyst. A conventional packed–bed type catalytic reactor has serious problems such as severe distributions of temperature in the reactor, leading to a decrease in the catalyst performance, life, and yield of the product. These occur because of the local high–temperature parts in an exothermic reaction or the local low–temperature parts in an endothermic reaction caused by the small heat transfer area between each catalyst [1-29]. Moreover, it has a large pressure drop caused by the limited flow path and increase in the resistance to mass transfer [1-06]. However, in a structure catalyst, the pressure drop is comparatively smaller, the thermal conductivity is improved, and the temperature distribution in the reactor is more uniform. These are expected because the flow path of the fluid is composed of the catalyst continuum itself [1-30]. The characteristics of each catalytic reactor are shown in **Fig. 1.2-5**.

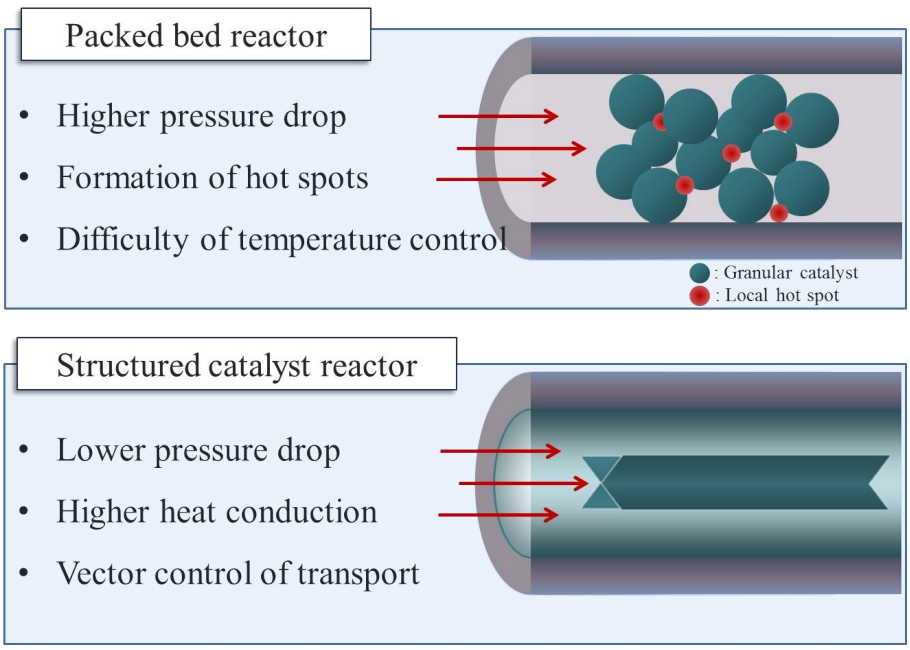

Fig. 1.2-5 Characteristics of each catalytic reactor

Various types of the structured catalysts have been studied [1-26, 1-31, 1-32]. One of the most representative and well-known structured catalysts is a monolithic type catalyst [1-33, 34]. The catalyst support is molded by extrusion in a monolithic type catalyst, and the catalyst component is applied on the surface of the catalyst support by a method called wash coating, to function as a structured catalyst [1-35 – 1-37]. It is frequently used to clean the exhaust gas from automobiles and chemical plants, and to treat high flow rates, because of its small pressure drop [1-38]. Other structured catalysts in the form of fibers [1-39, 1-40], foams [1-41, 1-42], and etching materials [1-43, 1-44] have also been studied. The SEM image of various structured catalysts is displayed in **Fig. 1.2-6.** Each structured catalyst has advantages and disadvantage. For examples, the monolithic type structured catalysts achieve a low-pressure drop, but the larger the diameter of its channels, the less uniform the radial transport becomes. Fiber-type structured catalysts are characterized by high thermal conductivity, but less durable. Foamed type structured catalysts have a very high specific surface area but are more expensive to prepare. Therefore, it is important to understand and use the characteristics of each structure.

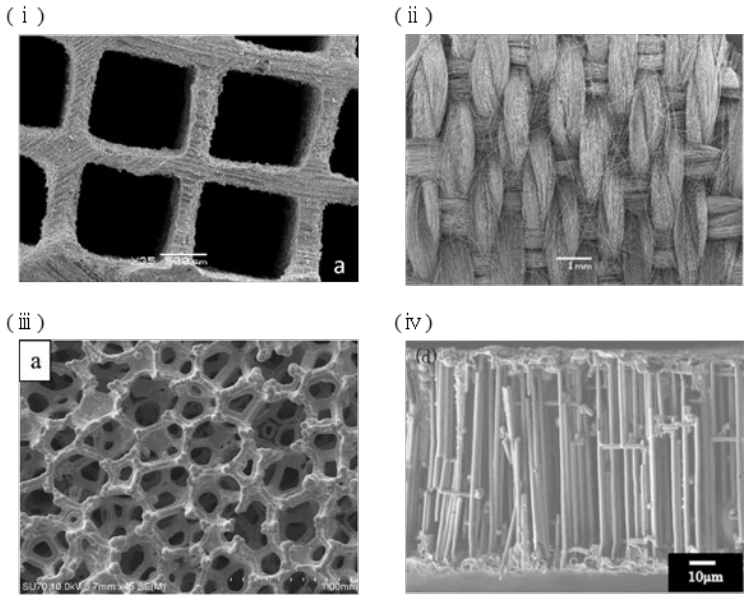

Fig. 1.2-6 SEM image of various structured catalysts
(i) Monolith [1-45], (ii) Gauze [1-39], (iii) Foamed [1-42], (iv) Etched membrane [1-43]

In recent years, achievement of high reactivity via the utilization of structured catalysts have been reported [1-46 – 1-49]. The structured catalysts have gained particular attention because of the recent advances in computer performance and the development of additive manufacturing technology. Research has also been reported on preparing catalyst supports and catalysts directly utilizing three–dimensional (3D) printers [1-47, 1-48, 1-50 – 1-53]. Stainless steel structured catalyst supports was manufactured by the 3D printer, and it was investigated that the effective thermal conductivity and pressure drop due to the structures [1-47]. The impact of the use of the zeolite structured catalyst on its catalytic performance in the methanol-to-olefins reaction are discussed [1-48]. Structured catalysts containing Ce, Cr, Cu, Ga, La, Mg, Y, and Zn as catalyst components, respectively, were prepared [1-51]. Ni-alumina-based structured catalysts were prepared by directly 3D printed from molding a mixture of alumina powder and Ni as a catalytic component for the carbon dioxide reduction reaction, and their catalyst characterization and the reactivity analysis were investigated [1-50]. The samples of structured catalysts prepared using a 3D printer are displayed in **Fig. 1.2-7**.

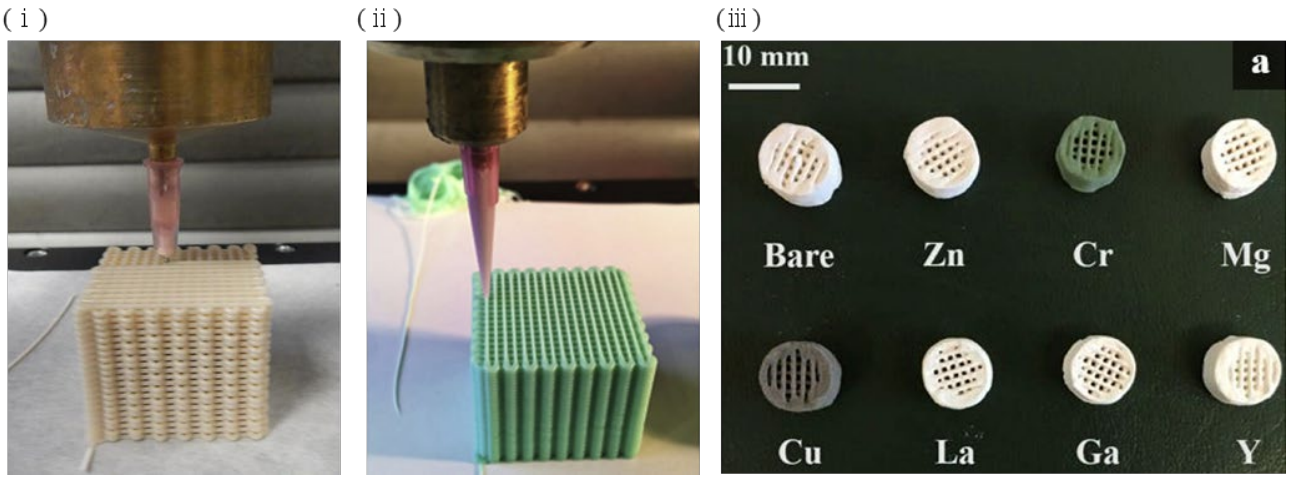

Fig. 1.2-7 Samples of structured catalysts prepared using a 3D printer [1-48, 1-50, 1-51]

In addition, spatially limited and microgravity environments such as the space station and the lunar surface are special applications for structured catalytic reactors. Catalytic reactions on the space station and on the moon are reactions, associated with fuel cells for the use of hydrogen as energy and for air revitalization for human space activities. For both the catalytic reaction processes, there is a need to save resources, save energy, and reduce the size of the process, and PI using structured catalytic reactors are so suited. Moreover, while conventional granular catalysts have the risk of scattering in a microgravity environment, the structured catalyst avoids this risk. The vector control of transport phenomena with the structure of the structured catalyst is effective to improve the reaction performance of the catalytic reaction process because the different forces dominate the heat and mass transfer, especially in the microgravity field.

Table 1.2-3 Advantages of structured catalysts for the aerospace catalytic reaction.

Requirements for Aerospace Catalytic Reactors		Advantages of structured catalysts
Save resources Save Energy	Low Temp. Reactivity	High heat conduction
	High Selectivity	
	Responding on processing variation	Low pressure drop
Limitation	Size	Potential
	Microgravity	Control of transport
Safety	Handling	Continuum

1.2.3 Micro-Partition Structured Catalyst (MPC)

In this study, I adopt a micro–partition (MP) structure that is made of aluminum (A1050), as originally used in a heat sink in precision equipment, not as a catalyst support. The MP was fabricated from 100 μm-thick aluminum plates into a structure with square-shaped 0.375 mm fins and holes. The density of those fins are 196 /cm^2. The overview of MP structure is displayed in **Fig. 1.2-8**, and the microscopic surface observations (Digital Microscope VHX-5000, KEYENCE) for MP are displayed in **Fig. 1.2-9** and **Fig. 1.2-10**.

Our research group has reported on alumite supports made from anodized aluminum materials, and it can be impregnated into a catalytic solution to prepare an alumite catalyst [1-54]. Since the alumite catalyst has features such as a high surface area, high thermal conductivity, and flexibility, a synergy with the structure of the MP can be expected. It is possible to convert an MP into an alumite support using a similar method, and the MP structure was converted into a structured catalyst support with a porous layer composed of γ-alumina by the anodization method [1-54], and the catalyst metal was loaded by an impregnation–supporting method to prepare the MP structured catalyst (MPC).

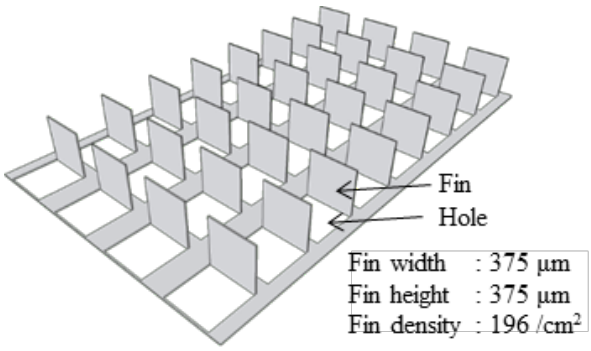

Fig. 1.2-8 Micro‐Partition (MP)

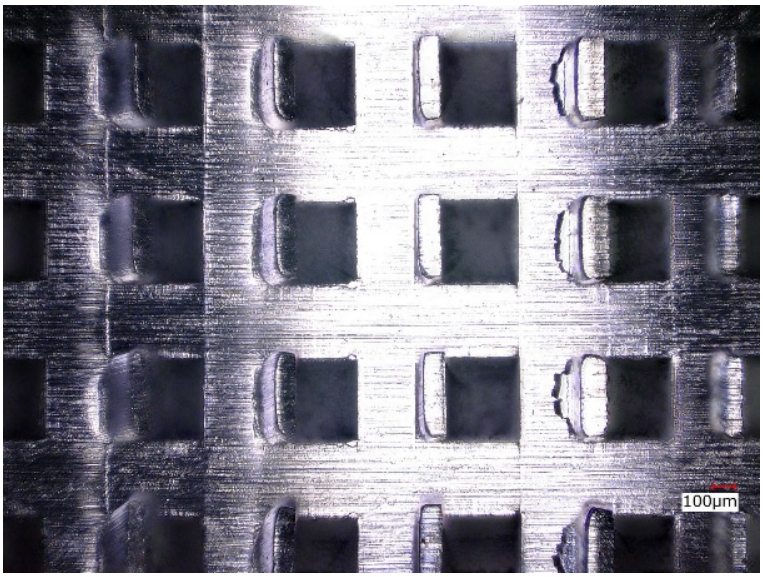

Fig. 1.2-9 Microscopic surface observations of MP (Magnification; x100)

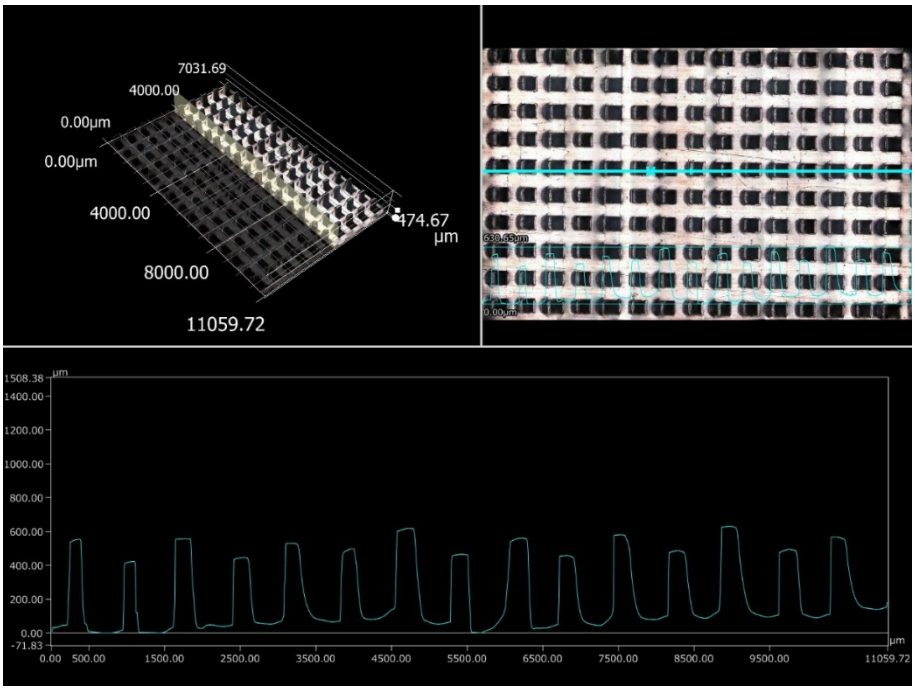

Fig. 1.2-10 The profile of MP structure using Digital Microscope (unit: μm)

When the MP structured catalyst (MPC) is filled into a gas–solid catalytic reactor, the MPC is expected to improve the reactivity by mixing the fluid because the reactant fluid hits the fins and changes the flow direction in the reactor. In a previous study, it was confirmed that this structured catalyst MPC was used to improve the reactivity of the steam reforming of methanol reaction, and the results showed that methanol conversion was affected by the direction of the MPC fins to the reactants fluid [1-55]. The steam reforming of methanol reaction is one of the most important reactions related to the hydrogen energy and the hydrogen economy.

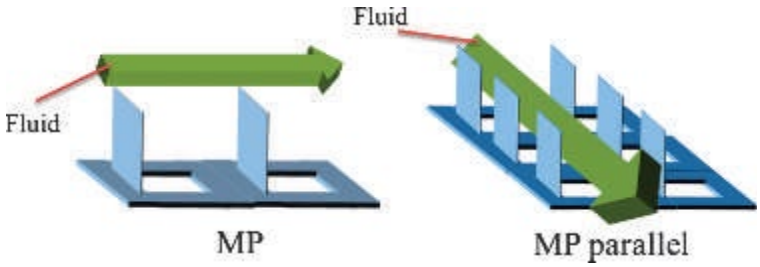

Fig. 1.2-11 Flow image of MP and MP parallel [1-55]

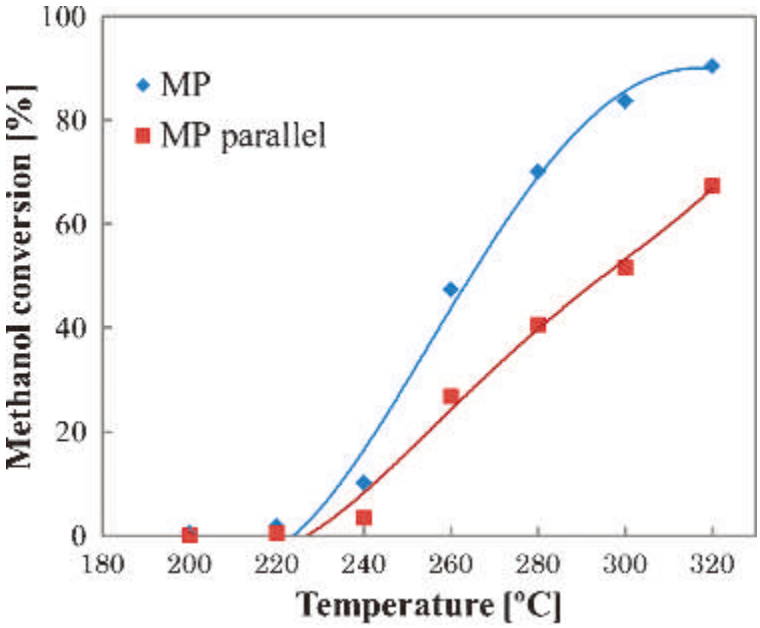

Fig. 1.2-12 Influence of direction of the fin [1-55]

1.2.4 Reactions for Hydrogen Energy and Hydrogen Economy

As described at the beginning of Section 1.2, since the 19th century, global industrialization has led to serious environmental issues, such as global warming, due to the continuous and massive use of fossil fuels [1-01, 1-02]. Therefore, renewable energy and hydrogen energy are attracting attention as clean energy alternatives to fossil fuel-derived energy. Hydrogen, as a clean energy source, is a promising future sustainable energy source owing to its high energy density and low environmental impact [1-56, 1-57]. The commonly used commercial method for hydrogen production is steam reforming of hydrocarbons, which is largely based on methane [1-58, 1-59]. Since this process has an emission of carbon dioxide, one of the greenhouse gases, the environmental impact is not necessarily small. However, the steam reforming of hydrocarbons is necessary for a stable supply of hydrogen. A chemical reaction that has received as much attention as steam reforming of methane is the methanol steam reforming (SRM) reaction (**Eq. 1.2-1**). Methanol is easier to handle than is methane in terms of storage and management because it has high H/C and is liquid at room temperature [1-60, 1-61]. In addition, methanol is a chemical that in the future will constitute a sustainable closed circuit by being produced from carbon dioxide and carbon monoxide [1-62, 1-63].

$$CH_3OH + H_2O \rightarrow H_2 + CO_2 \qquad \Delta H^{\circ}_{298} = 49.4\ \mathrm{kJ/mol} \qquad (\mathbf{Eq.\ 1.2-1})$$

The SRM reaction, in which hydrogen is produced from methanol, has the advantage that the carbon monoxide concentration in the reformed gas is low at lower reaction temperatures due to the thermodynamic equilibrium of the CO shift reaction [1-64 – 1-66]. Steam reforming reactions produce carbon monoxide as a byproduct, typically about 5% in the reformed gas [1-58]. Carbon monoxide poison platinum catalysts or electrodes in a fuel cell, thus impairing the capacity of the reforming process for hydrogen production [1-67]. The concentration of carbon monoxide in the reformed gas can be reduced and the amount of hydrogen produced can be increased by converting of carbon monoxide to carbon dioxide, which is called the water-gas shift (WGS) reaction (**Eq. 1.2-2**).

Although higher temperatures are required to achieve a high reaction rate of the WGS reaction, the increase in the hydrogen production is not expected because the selectivity of carbon monoxide increases for reasons of thermodynamic equilibrium. Therefore, it is important to develop a catalytic unit that allows the WGS reaction to proceed at lower temperatures.

$$CO + H_2O \rightarrow H_2 + CO_2 \qquad \Delta H^{\circ}_{298} = -41.1\ \text{kJ/mol} \qquad (\mathbf{Eq.\ 1.2-2})$$

Fuel cells are one of the most effective ways to use hydrogen as an energy source, in addition to the direct combustion of hydrogen. However, not all hydrogen supplied to a fuel cell stack is necessarily converted into electrical energy. The electrical conversion efficiency is estimated to be less than 95%, and the residual hydrogen produced in excess is discharged [1-68]. The treatment of excess hydrogen is an important process in fuel cell systems as hydrogen gas emission can lead to unknown environmental impacts and hazards [1-69]. Therefore, the catalytic hydrogen combustion (CHC) reaction is used to treat excess hydrogen with oxygen from the air (**Eq. 1.2-3**). Catalytic combustion reactions are specially used for small-scale operations and for processing low-concentration reactants, and catalytic combustion reactions, and CHC is the best way to treat low concentrations of hydrogen at lower temperatures [1-68, 1-70 – 1-72]. The CHC reaction is expected to be safe, controllable, and highly exothermic at low temperatures, and is an important part of the hydrogen economy [1-73]. The heat and water generated by the CHC reaction are used for the endothermic reaction in the steam reforming of hydrocarbons, in other words, the excess hydrogen is converted into heat and reactants to improve the capacity of the hydrocarbon steam reforming process. Controlling the temperature of the catalytic unit is important because the initial temperature of the catalytic bed and the temperature of the reactant feed gas have a significant impact on the hydrogen treatment capacity, according to research reports on the CHC reaction [1-68].

$$2H_2 + O_2 \rightarrow 2H_2O\ (g) \qquad \Delta H^{\circ}_{298} = -242\ \text{kJ/mol} \qquad (\mathbf{Eq.\ 1.2-3})$$

In addition, carbon dioxide reduction to methane (CDR) reaction has been attracting attention for the effective utilization of carbon dioxide, which is a product of hydrocarbon steam reforming and WGS reactions (**Eq. 1.2-4**). This reaction, also known as the Sabatier reaction, is a highly exothermic reaction that produces

methane and water from carbon dioxide and hydrogen. The methane produced from the CDR reaction can be transported through the existing natural gas transportation pipeline network, and the carbon dioxide produced by the combustion of the methane fuel is expected to be captured and reduced again, resulting in a reduction in apparent carbon dioxide emissions. This concept is called P2G, and is being developed systematically in Europe. Platinum group metals such as platinum, rhodium, and ruthenium have been used as catalysts for CDR reaction and have been shown to be highly active, but recently catalysts based on non-precious metals such as cobalt or nickel has been developed [1-74]. In particular, nickel-based catalysts are inexpensive; however, improving their low-temperature activity and durability is a challenge [1-75, 1-76].

$$CO_2 + 4H_2 \rightarrow H_2O + CH_4 \qquad \Delta H^{\circ}_{298} = -165\ \mathrm{kJ/mol} \qquad (\mathbf{Eq.\ 1.2-4})$$

As mentioned above, there are various reaction systems related to hydrogen energy. The number of carbons in the main chemicals in these reactions is one, and hence, this area of chemistry is called C1 chemistry or C1 family and is one of the most important research topics in the world [1-77, 1-78]. Numerous studies regarding catalyst and process design have been reported in each reaction, but a common problem associated with these reactions is the low-temperature activity of the catalyst and the temperature control of the catalyst unit. Novel catalysts are being developed, and the catalyst supports are being investigated separately from the catalyst metal species to solve this problem.

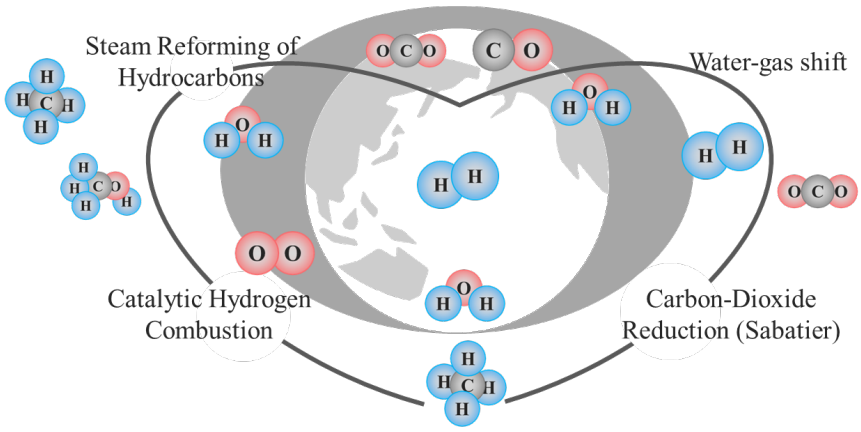

Fig. 1.2-13 Various reaction systems related to hydrogen energy and C1 chemistry

1.3 Purpose

In this study, it was investigated the factors that improve the reactivity due to the structure of MPC and proposed the index for quantitatively evaluating the effect of the reactivity improvement, focusing on a rate-limiting step, using experiments and simulations. Furthermore, the effect of stacking multiple MPCs in the reactor on the reactivity was investigated, and the effective stacking method for MPC was proposed with simulation and demonstrated with experiments.

In chapter 3, the MPC was applied to the SRM, WGS, and CHC reactions, which are important reactions in the hydrogen energy, and experimentally indicated that the MPC improved the reactivity to the unprocessed plate-type structured catalyst, then the factors were investigated with reaction rate analysis. Furthermore, the reaction environment in which the MPC is effective was also investigated by evaluating the tendency of the effect of the reactivity improvement.

In chapter 4, using a numerical simulation, it was investigated the factors that improve the reactivity due to the MPC by evaluating physical phenomena such as flow, heat, and mass transfer around the catalysts. Furthermore, the unique index for evaluating the effect of the structure around the catalysts, focusing on a rate-limiting step, was proposed to identify the structures that contribute to the reactivity improvement.

In chapter 5, the effects of changing the number of MPC stacking on the reactivity for each reaction were investigated. Furthermore, the effects of the stacking on the effect of the structure and the proposed index around the catalysts were also investigated in detail.

In chapter 6, the effective MPC stacking method was proposed by simulation and experimentally investigated for each reaction to improve the reactivity. Furthermore, the correlation between the proposed index to evaluate the reactivity improvement due to the structured catalyst calculated from the simulations and the parameters related to the reaction rate calculated from the experiments were also confirmed.

1.4 Organization

Chapter 1: Introduction

In chapter 1, it was provided the social and technical background of this dissertation, respectively. Process intensification (PI) of the catalytic reaction process with a structured catalytic reactor was proposed for the dual challenge of global environmental and energy issues. MP, a commercially available aluminum precision heat sink, was adopted as the structure for the structured catalyst. One of the purposes of the study in this dissertation is to confirm the effect of the structure on the reactivity, when applying the MP structure catalyst (MPC) to some of the important reactions in the hydrogen energy field, by experiments and to investigate the factors in detail. Furthermore, the index to evaluate the effect of MPC on the reactivity was proposed in the simulation. The method and environment for using MPC to further improve the reactivity were examined and proposed using the index. It was achieved by focusing on a catalytic reaction rate-limiting step process especially.

Chapter 2: Methodology

In chapter 2, it was provided the experimental and simulation methods used to examine the effect of structured catalysts on reactivity, as well as the equations, indexes, and parameters defined for this study. MPC was prepared for each of the model reactions and their catalyst characterization was conducted. The catalyst layer thickness, specific surface area, amount of catalyst loading, reduction properties, and active site characteristics were analyzed. The reactor was prepared in order to examine the effect of MPC in the reactor and to propose their effective stacking. The catalytic activity tests were carried out under comparative conditions with a constant molar flow rate per catalyst loading and were carefully set for each reaction. The simulation software used was COMSOL Multiphysics to observe the physical phenomena around the catalysts, and both 3D and 2D simulations were calculated.

Chapter 3: Comparison of Reactivity between MPC and Plate-type Structured Catalysts: Experimental studies

In chapter 3, it was provided the results of the comparison of the reactivity of each reaction between MPC and the unprocessed plate-type structured catalyst (plate) on experiments. The improvement of the frequency factor due to the structure of MPC was confirmed using the Arrhenius equation as a kinetic analysis, and the effect of the improvement in reactivity was revealed to be larger at lower temperatures by calculating Turnover frequency (TOF), which is a general evaluating index of catalytic performance. Furthermore, it was suggested that the tendency to improve the reactivity differed when focusing on the rate-limiting step.

Chapter 4: Investigation of Factors to Improve Reactivity due to the Structure of MPC and Proposal of Evaluation Index: Numerical Simulation

In chapter 4, it was provided the results of the reactivity between MPC and plate by simulation. The simulation models were prepared referred to the experimental conditions and the values indicated by the experimental results, and these were confirmed to be models that showed similar results to the experimental results. Furthermore, the dimensionless number was proposed as the index to evaluate the effect of structure on reactivity improvement. It was suggested that the index was effective in evaluating the reactivity improvement using the structured catalysts under the condition of a catalytic reaction rate-limiting step.

Chapter 5: Investigation of the Effect of the Number of MPC Stacking on the Reactivity

In chapter 5, it was provided the effect of changing the number of MPC stacking in the reactor was examined on experiments and simulations. The reactivity was obviously declined when the MPCs were densely stacked in the reactor under a catalytic reaction rate-limiting step. The effect of the number of MPC stacking on the reactivity tended to differ depending on a rate-limiting step. It was shown that the proposed unique index was capable of evaluating the reactivity tendency of the catalytic process under a catalytic reaction rate-limiting step condition. It was a valuable proposal for engineering as an index to evaluate the effect of using the structured catalysts on reactivity under a catalytic reaction rate-limiting step.

Chapter 6: Proposal for Effective MPC Stacking Method

In chapter 6, considering the results up to chapter 5, it was proposed the stacking methods of MPCs by using simulations to improve the reactivity, and experiments demonstrated the reactivity improvement due to the MPC stacking method. The effective MPC stacking method was proposed by considering the streamline and concentration distribution, and the evaluation index. The stacking method with contrasting effects was also proposed, and the effects of these stacking methods on reactivity were examined from experiments. Furthermore, the evaluation index around the catalysts when the stacking method was changed was quantified by simulation, and the positive correlation was shown between the quantified values and the experimentally derived values about catalytic reactivity.

Chapter 7: Conclusions and Future Works

In chapter 7, it was provided the conclusions for each chapter, the future works, and the list of published technical papers related to this dissertation.

1.5 Conclusions of chapter 1

Chapter 1 provided a detailed description of the background, purpose, and organization of this dissertation. There is a need for PI approach in the field of chemical engineering in order to achieve a sustainable society. The structured catalyst is one of the various tools to realize PI, and attracting attention in recent years more and more because it has the characteristics to solve the problems of conventional catalytic reactor. In this study, the structured catalysts prepared and applied to the important reactions in the field of hydrogen energy. Furthermore, we focused on the improvement of catalytic reactivity due to the structure of the structured catalyst, while most of the previous studies on the use of structured catalysts have evaluated the improvement of the process performance as a catalytic process. One of the purposes of this dissertation was to clarify the detailed factors that contribute to improved reactivity using a structured catalyst through experiments and simulations. It was also the purpose to propose the index to quantitatively evaluate the improvement of reactivity due to the structure and to propose effective methods for using structured catalysts. The construction of this dissertation was shown in Fig. 1.1-1, and the outline was presented in Section 1.4.

1.6 References

[1-01] R. Singh, D. Kunzru, S. Sivakumar; "Monodispersed ultrasmall NiMo metal oxide nanoclusters as hydrodesulfurization catalyst," Applied Catalysis B: Environmental 185 (2016) 163–173, https://doi.org/10.1016/j.apcatb.2015.12.013.

[1-02] R. Singh, D. Kunzru; "Hydrodesulfurization of dibenzothiophene on NiMo/γ-Al_2O_3 washcoated monoliths," Fuel 163 (2016) 180–188, https://doi.org/10.1016/j.fuel.2015.09.058.

[1-03] M. Baldea; "From process integration to process intensification," Computers and Chemical Engineering 81 (2015) 104–114, http://dx.doi.org/10.1016/j.compchemeng.2015.03.011.

[1-04] C. S. Pereira, B.A. Patel; "The role of process intensification in addressing the dual energy challenge," Chemical Engineering and Processing: Process Intensification 142 (2019), https://doi.org/10.1016/j.cep.2019.107545.

[1-05] ExxonMobil, Outlook for Energy: A View to 2040, (2018) https://corporate.exxonmobil.com/-/media/Global/Files/outlook-for-energy/2018-Outlook-for-Energy.pdf.

[1-06] Y. Tian, S. E. Demirel, M. M. F. Hasan, E. N. Pistikopoulos; "An overview of process systems engineering approaches for process intensification: State of the art," Chemical Engineering and Processing: Process Intensification 133 (2018) 160–210, https://doi.org/10.1016/j.cep.2018.07.014.

[1-07] T. V. Gerven, A. Stankiewicz; "Structure, Energy, Synergy, Time–The Fundamentals of Process Intensification," Industrial & Engineering Chemistry Research 48 (2009) 2465–2474, http://dx.doi.org/10.1021/ie801501y.

[1-08] J.-M. Commenge, L. Falk; "Methodological framework for choice of intensified equipment and development of innovative technologies," Chemical Engineering & Processing: Process Intensification 84 (2014) 109–127, http://dx.doi.org/10.1016/j.cep.2014.03.001.

[1-09] A. Stankiewicz, J. A. Moulijn; "Process Intensification: Transforming Chemical Engineering," Chemical Engineering Progress 96 (2000) 22–33.

[1-10] C. Tsouris, J. V. Porcelli; “Process intensification – Has Its Time Finally Come?,” Chemical Engineering Progress 99 (2003) 50–55.

[1-11] J. C. Charpentier; “Process Intensification by miniaturization,” Chemical Engineering & Technology, 28 (3), (2005) 255–258, http://dx.doi.org/doi:10.1002/ceat.200407026

[1-12] F. J. Keil; “Process intensification,” Reviews in Chemical Engineering 34 (2018) 135–200, https://doi.org/10.1515/revce-2017-0085.

[1-13] F. J. Keil; “Catalytic reactions and reactors,” Chemical Engineering Science 59 (2004) 5473–5478, https://doi.org/10.1016/j.ces.2004.07.065.

[1-14] H. Cong, X. Li, H. Li, J.P. Murphy, X. Gao; “Performance analysis and structural optimization of multi-tube type heat integrated distillation column (HIDiC),” Separation and Purification Technology 188 (2017) 303–315, https://doi.org/10.1016/j.seppur.2017.07.047

[1-15] A.I. Shallan, C. Priest; “Microfluidic process intensification for synthesis and formulation in the pharmaceutical industry,” Chemical Engineering and Processing: Process Intensification 142 (2019) 107559, https://doi.org/10.1016/j.cep.2019.107559

[1-16] G. J. Harmsen; “Reactive distillation: The front-runner of industrial process intensification,” Chemical Engineering and Processing: Process Intensification 46 (2007) 774–780, https://doi.org/10.1016/j.cep.2007.06.005.

[1-17] C. Mduduzi Masuku, and L. T. Biegler; “Recent Advances in Gas-to-liquids Process Intensification with Emphasis on Reactive Distillation,” Current Opinion in Chemical Engineering 25 (2019) 95–100, https://doi.org/10.1016/j.coche.2018.12.009

[1-18] M. Wierschem, A. Górak; “Reactive Distillation,” Reference Module in Chemistry, Molecular Sciences and Chemical Engineering (2018) 1–10, https://doi.org/10.1016/B978-0-12-409547-2.14066-1

[1-19] S. Liu, Y. Kawagoe, Y. Makino, S. Oshita; “Effects of nanobubbles on the physicochemical properties of water: The basis for peculiar properties of water containing nanobubbles,” Chemical Engineering Science 93 (2013) 250–256, https://doi.org/10.1016/j.ces.2013.02.004.

[1-20] M. Matsumoto, T. Fukunaga, K. Onoe; “Polymorph control of calcium carbonate by reactive crystallization

using microbubble technique," Chemical engineering research and design 88 (2010) 1624–1630, https://doi.org/10.1016/j.cherd.2010.02.007.

[1-21] Z. R. Herm, R. Krishna, J. R. Long; "CO_2/CH_4, CH_4/H_2 and $CO_2/CH_4/H_2$ separations at high pressures using Mg_2(dobdc)," Microporous and Mesoporous Materials 151 (2012) 481–487, https://doi.org/10.1016/j.micromeso.2011.09.004.

[1-22] P. Valvekens, E. D. Bloch, J. R. Long, R. Ameloot, D. E. De Vos; "Counteranion effects on the catalytic activity of copper salts immobilized on the 2,2'-bipyridine-functionalized metal–organic framework MOF-253," Catalysis Today 246 (2015) 55–59, http://dx.doi.org/10.1016/j.cattod.2014.08.006.

[1-23] J. J. Brandner, G. Emig, M. A. Liauw, K. Schubert; "Fast temperature cycling in microstructure devices," Chemical Engineering Journal, 101 (2004) 217–224, https://doi.org/10.1016/j.cej.2003.11.020.

[1-24] T. Nakano, M. Sakurai, H. Kameyama; "Operating Temperature Conditions for Periodic Temperature Cycling in a Microreactor," Journal of Chemical Engineering of Japan, 45 (2012) 89–93, https://doi.org/10.1252/jcej.11we151.

[1-25] A. Zamaniyan, Y. Mortazavi, A. A. Khodadadi, Hossein Manafi; "Tube fitted bulk monolithic catalyst as novel structured reactor for gas–solid reactions," Applied Catalysis A: General 385 (2010) 214–223, https://doi.org/10.1016/j.apcata.2010.07.014.

[1-26] E.Tronconi, G. Groppi, C. G. Visconti; "Structured catalysts for non-adiabatic applications," Current Opinion in Chemical Engineering 5 (2014) 55–67, https://doi.org/10.1016/j.coche.2014.04.003.

[1-27] S. Lopatin, P. Mikenin, D. Pisarev, D. Baranov, S. Zazhigalov, and A. Zagoruiko; "Pressure Drop and Mass Transfer in the Structured Cartridges with Fiber-glass Catalyst," Chemical Engineering Journal 282 (2015) 58–65, https://doi.org/10.1016/j.cej.2015.02.026.

[1-28] O. Sanz, I. Velasco, I. Perez-Miqueo, R. Poyato, J. A. Odriozola, and M. Montes, "Intensification of hydrogen production by methanol steam reforming," International Journal of Hydrogen Energy 41 (10) (2016) 5250–5259, https://doi.org/10.1016/j.ijhydene.2016.01.084.

[1-29] V. Palma, M. Martino, E. Meloni, A. Ricca; "Novel structured catalysts configuration for intensification of steam reforming of methane," International Journal of Hydrogen Energy 42 (2017) 1629–1638,

http://dx.doi.org/10.1016/j.ijhydene.2016.06.162.

[1-30] T. Boger, A. K. Heibel; “Heat transfer in conductive monolith structures,” Chemical Engineering Science 60 (2005) 1823–1835, https://doi.org/10.1016/j.ces.2004.11.031.

[1-31] S. Fukahori, H. Koga, T. Kitaoka, M. Nakamura, and H. Wariishi; “Steam Reforming Behavior of Methanol Using Paper-structured Catalysts: Experimental and computational fluid dynamic analysis,” International Journal of Hydrogen Energy 33 (6) (2008) 1661–1670, https://doi.org/10.1016/j.ijhydene.2007.12.063.

[1-32] V. Papetti, P. Dimopoulos Eggenschwiler, A. Della Torre, F. Lucci, A. Ortona and G. Montenegro; “Additive Manufactured Open Cell Polyhedral Structures as Substrates for Automotive Catalysts,” International Journal of Heat and Mass Transfer 126 (2018) 1035–1047, https://doi.org/10.1016/j.ijheatmasstransfer.2018.06.061.

[1-33] I. Aartun, B. Silberova, H. Venvik, P. Pfeifer, O. Gorke, K. Schubert, A. Holmen; “Hydrogen production from propane in Rh-impregnated metallic microchannel reactors and alumina foams,” Catalysis Today 105 (2005) 469–478, https://doi.org/10.1016/j.cattod.2005.06.025.

[1-34] T. Omojola, N. Cherkasov, E. V. Rebrov, D. B. Lukyanov, S. P. Perera; “Zeolite minilith: A unique structured catalyst for the methanol to gasoline process,” Chemical Engineering and Processing: Process Intensification 131 (2018) 137–143, https://doi.org/10.1016/j.cep.2018.07.016.

[1-35] A. Devatine, H. Chaumat, S. Guillaume, B. Tati Tchibouanga, F. Durán Martínez, C. Julcour and A.-M. Billet; “Hydrodynamic Study of a Monolith-type Reactor for Intensification of Gas-liquid Applications,” Chemical Engineering and Processing: Process Intensification 122 (2017) 277–287, https://doi.org/10.1016/j.cep.2017.10.015.

[1-36] C. Fukuhara, K. Hayakawa, Y. Suzuki, W. Kawasaki, and R. Watanabe; “A Novel Nickel-based Structured Catalyst for CO_2 Methanation: A Honey Comb-type Ni/CeO_2 Catalyst to Transform Greenhouse Gas into Useful Resources, Applied Catalysis A: General 532 (2017) 12–18, https://doi.org/10.1016/j.apcata.2016.11.036.

[1-37] S. Ratchahat, M. Sudoh, Y. Suzuki, W. Kawasaki, R. Watanabe, and C. Fukuhara; “Development of a Powerful CO_2 Methanation Process Using a Structured Ni/CeO_2 Catalyst,” Journal of CO_2 Utilization 24 (2018) 210–

219, https://doi.org/10.1016/j.jcou.2018.01.004

[1-38] J. Chen, H. Yang, N. Wang, Z. Ring, T. Dabros; "Mathematical modeling of monolith catalysts and reactors for gas phase reactions," Applied Catalysis A: General 345 (2008) 1–11, https://doi.org/10.1016/j.apcata.2008.04.010.

[1-39] A. N. Zagoruiko, S. A. Lopatin; "Pressure drop of structured cartridges with fiber–glass catalysts," Chemical Engineering Journal 238 (2014) 31–36, http://dx.doi.org/10.1016/j.cej.2013.04.087.

[1-40] J. P. Reymond; "Structured supports for noble catalytic metals: stainless steel fabrics and foils, and carbon fabrics," Catalysis Today 69 (2001) 343–349, https://doi.org/10.1016/S0920-5861(01)00388-1.

[1-41] R. Jiang, Y. Jiao, Y. Xie, Z. Yang, J. Zhang; "SiC foam based structured catalyst for process intensification in oxidative dehydrogenation of 1-butene to butadiene," Chemical Engineering and Processing: Process Intensification 137 (2019) 108–115, https://doi.org/10.1016/j.cep.2019.02.010.

[1-42] W. Zhou, Y. Ke, Q. Wang, S. Wan, J. Lin, J. Zhang, K. S. Hui; "Development of cylindrical laminated methanol steam reforming microreactor with cascading metal foams as catalyst support," Fuel 191 (2017) 46–53, http://dx.doi.org/10.1016/j.fuel.2016.11.058.

[1-43] H. Hiramatsu, M. Sakurai, H. Kameyama; "Application of etched aluminum flow-through membrane as catalyst support," International Journal of Hydrogen Energy 41 (2016) 10161–10169, http://dx.doi.org/10.1016/j.ijhydene.2016.04.232.

[1-44] H. Hiramatsu, M. Sakurai, T. Maki, H. Kameyama; "Stacked etched aluminum flow-through membranes for methanol steam reforming," International Journal of Hydrogen Energy 42 (2017) 9922–9929, http://dx.doi.org/10.1016/j.ijhydene.2017.01.106.

[1-45] C. De los Santos, H. Vidal, Jose Manuel Gatica, M. Pilar Yeste, G. Cifredo, J. Castiglioni; "Optimized preparation of washcoated clay honeycomb monoliths as support of manganese catalysts for acetone total combustion," Microporous and Mesoporous Materials 310 (2021) 110651, https://doi.org/10.1016/j.micromeso.2020.110651.

[1-46] J. G. Khinast, A. Bauer, D. Bolz, and A. Panarello; "Mass-transfer Enhancement by Static Mixers in a Wall-coated Catalytic Reactor," Chemical Engineering Science 58 (2003) 1063–1070,

https://doi.org/10.1016/S0009-2509(02)00648-6.

[1-47] S. Danaci, L. Protasova, R. Try, A. Bengaouer, P. Marty; “Experimental and numerical investigation of heat transport and hydrodynamic properties of 3D-structured catalytic supports,” Applied Thermal Engineering 126 (2017) 167–178, http://dx.doi.org/10.1016/j.applthermaleng.2017.07.155.

[1-48] J. Lefevere, S. Mullens, V. Meynen; “The impact of formulation and 3D-printing on the catalytic properties of ZSM-5 zeolite,” Chemical Engineering Journal 349 (2018) 260–268, https://doi.org/10.1016/j.cej.2018.05.058.

[1-49] J. Lefevere, M. Gysen, S. Mullens, V. Meynen, and J. Van Noyen; The Benefit of Design of Support Architectures for Zeolite Coated Structured Catalysts for methanol-to-olefin Conversion,” Catalysis Today 216 (2013) 18–23, https://doi.org/10.1016/j.cattod.2013.05.020.

[1-50] V. Middelkoop, A. Vamvakeros, D. de Wit, S.D.M. Jacques, S. Danaci, C. Jacquot, Y. de Vos, D. Matras, S.W.T. Price, A.M. Beale; “3D printed Ni/Al_2O_3 based catalysts for CO_2 methanation - a comparative and operando XRD-CT study,” Journal of CO_2 Utilization 33 (2019) 478–487, https://doi.org/10.1016/j.jcou.2019.07.013.

[1-51] X. Li, F. Rezaei, A. Rownaghi; “Methanol-to-olefin conversion on 3D-printed ZSM-5 monolith catalysts: Effects of metal doping, mesoporosity and acid strength,” Microporous and Mesoporous Materials 276 (2019) 1–12, https://doi.org/10.1016/j.micromeso.2018.09.016.

[1-52] A. Elkoro, L. Soler, J. Llorca, I. Casanova; “3D printed microstructured Au/TiO_2 catalyst for hydrogen photoproduction,” Applied Material Today 16 (2019) 265–272, https://doi.org/10.1016/j.apmt.2019.06.007.

[1-53] T.Q. Zheng, W. Zhou, D. Geng, Y.Y. Li, Y.X. Liu, C.Y. Zhang; “Methanol steam reforming microreactor with novel 3D-Printed porous stainless steel support as catalyst support,” International Journal of Hydrogen Energy 45 (2020) 14006–14016, https://doi.org/10.1016/j.ijhydene.2020.03.103.

[1-54] H. Kameyama; “Heat Transfer Material with Porous Alumina Layer,” Suiso Enerugi Shisutemu 20 (1995) 16–23.

[1-55] S. Shimada, M. Sakurai, H. Kameyama; “Development of a Microreactor with a Structured Catalyst,” Journal of Flow Chemistry 3 (2013) 99–102, https://doi.org/10.1556/JFC-D-13-00011.

[1-56] A. Kumar, R. Singh, A.S.K. Sinha; "Catalyst modification strategies to enhance the catalyst activity and stability during steam reforming of acetic acid for hydrogen production," International Journal of Hydrogen Energy 44 (2019) 12983–13010, https://doi.org/10.1016/j.ijhydene.2019.03.136.

[1-57] A. Kumar, A.S.K. Sinha; "Hydrogen production from acetic acid steam reforming over nickel-based catalyst synthesized via MOF process," International Journal of Hydrogen Energy 45 (2020) 24397–24411, https://doi.org/10.1016/j.ijhydene.2020.06.040.

[1-58] J.D. Holladay, J. Hu, D.L. King, Y. Wang; "An overview of hydrogen production technologies," Catalysis Today 139 (2009) 244–260, https://doi.org/10.1016/j.cattod.2008.08.039.

[1-59] J.J. Spivey; "Catalysis in the development of clean energy technologies," Catalysis Today 100 (1–2) (2005) 171–180, https://doi.org/10.1016/j.cattod.2004.12.011.

[1-60] O.O. Fasanya, R. Al-Hajri, O.U. Ahmed, M.T. Myint, A.Y. Atta, B.Y. Jibril; "Copper zinc oxide nanocatalysts grown on cordierite substrate for hydrogen production using methanol steam reforming," International Journal of Hydrogen Energy 44 (2019) 22936–22946, https://doi.org/10.1016/j.ijhydene.2019.06.185.

[1-61] A.A. Lytkina, N.V. Orekhova, M.M. Ermilova, I.S. Petriev, M.G. Baryshev, A.B. Yaroslavtsev; "Ru–Rh based catalysts for hydrogen production via methanol steam reforming in conventional and membrane reactors," International Journal of Hydrogen Energy 44 (2019) 13310–13322, https://doi.org/10.1016/j.ijhydene.2019.03.205.

[1-62] V. Shanmugam, S. Neuberg, R. Zapf, H. Pennemann, G. Kolb; "Hydrogen production over highly active Pt based catalyst coatings by steam reforming of methanol: effect of support and co-support," International Journal of Hydrogen Energy 45 (2020) 1658–1670, https://doi.org/10.1016/j.ijhydene.2019.11.01.

[1-63] M. Behrens, F. Studt, I. Kasatkin, *et al.*; "The Active Site of Methanol Synthesis over $Cu/ZnO/Al_2O_3$ Industrial Catalysts," Science 336 6083 (2012) 893–897, https://doi.org/10.1126/science.1219831.

[1-64] D.Q. Mei, M. Qian, B.H. Liu, B.A. Jin, Z.H. Yao, Z.C. Chen; "A micro-reactor with micro-pin-fin arrays for hydrogen production via methanol steam reforming," Journal of Power Sources 205 (2012) 367–376, https://doi.org/10.1016/j.jpowsour.2011.12.062.

[1-65] Y. Men, G. Kolb, R. Zapf, D. Tiemann, M. Wichert, V. Hessel, H. Löwe; "A complete miniaturized

microstructured methanol fuel processor/fuel cell system for low power applications," International Journal of Hydrogen Energy 33 (2008) 1374–1382, https://doi.org/10.1016/j.ijhydene.2007.12.024.

[1-66] A.A. Lytkina, N.A. Zhilyaeva, M.M. Ermilova, N.V. Orekhova, A.B. Yaroslavtsev; "Influence of the support structure and composition of Ni–Cu-based catalysts on hydrogen production by methanol steam reforming," International Journal of Hydrogen Energy 40 (2015) 9677–9684, https://doi.org/10.1016/j.ijhydene.2015.05.094.

[1-67] W. Fu, Z. Bao, W. Ding, K. Chou, Q. Li; "The synergistic effect of the structural precursors of $Cu/ZnO/Al_2O_3$ catalysts for water–gas shift reaction," Catalysis Communications 12 (2011) 505–509, https://doi.org/10.1016/j.catcom.2010.11.017.

[1-68] C. Zhang, J. Zhang, J. Ma; "Hydrogen catalytic combustion over a $Pt/Ce0.6Zr0.4O_2/MgAl_2O_4$ mesoporous coating monolithic catalyst," International Journal of Hydrogen Energy 37 (2012) 12941–12946, https://doi.org/10.1016/j.ijhydene.2012.05.073.

[1-69] T. K. Tromp, R. L. Shia, M. Allen, J. M. Eiler; "Potential environmental impact of a hydrogen economy on the stratosphere," Science 13 (2003) 1740–1742, https://doi.org/10.1126/science.1085169.

[1-70] D.G. Norton, D.G. Vlachos; "Combustion characteristics and flame stability at the microscale: a CFD study of premixed methane/air mixtures," Chemical Engineering Science 58 (2003) 4871–4882, https://doi.org/10.1016/j.ces.2002.12.005.

[1-71] D. G. Norton, D. G. Vlachos; "A CFD study of propane/air microflame stability," Combustion Flame 138 (1–2) (2004) 97–107, https://doi.org/10.1016/j.combustflame.2004.04.004.

[1-72] V. N. Nguyen, R. Deja, R. Peters, L. Blum, D. Stolten; "Study of the catalytic combustion of lean hydrogen-air mixtures in a monolith reactor," International Journal of Hydrogen Energy 43 (2018) 17520–17530, https://doi.org/10.1016/j.ijhydene.2018.07.126.

[1-73] J. O. M. Bockris; "The hydrogen economy: its history," International Journal of Hydrogen Energy 38 (2013) 2579–2588, https://doi.org/10.1016/j.ijhydene.2012.12.026.

[1-74] P. Frontera, A. Macario, M. Ferraro, P. Antonucci; "Supported catalysts for CO_2 methanation: A review," Catalysts 59 (2017), https://doi.org/10.3390/catal7020059.

[1-75] L. Xu, X. Lian, M. Chen, Y. Cui, F. Wang, W. Li, B. Huang; "CO_2 methanation over Co Ni bimetal-doped ordered mesoporous Al_2O_3 catalysts with enhanced low-temperature activities," International Journal of Hydrogen Energy 43 (2018) 17172–17184, https://doi.org/10.1016/j.ijhydene.2018.07.106.

[1-76] L. Chuanfei, H. Xun, W. Tao, J. Peng, Z. Zhanming, D. Dehua, Z. Shu, L. Qing, H. Guangzhi; "Methanation of CO_2 over Ni/Al_2O_3 modified with alkaline earth metals: Impacts of oxygen vacancies on catalytic activity," International Journal of Hydrogen Energy 44 (2019) 8197–8213, https://doi.org/10.1016/j.ijhydene.2019.02.014.

[1-77] P. Moore; "Carbon dioxide fluctuations," Nature 255 108 (1975), https://doi.org/10.1038/255108a0.

[1-78] W.G. Cui, G.Y. Zhang, T.L. Hu, X.H. Bu; "Metal-organic framework-based heterogeneous catalysts for the conversion of C1 chemistry: CO, CO_2 and CH_4," Coordination Chemistry Reviews 387 (2019) 79–120, https://doi.org/10.1016/j.ccr.2019.02.001.

Chapter 2

Methodology

2.1 Abstract

In chapter 2, it was provided the experimental and simulation methods used to examine the effect of structured catalysts on reactivity, as well as the equations, indexes, and parameters defined for this study. MPC was prepared for each of the model reactions and their catalyst characterization was conducted. The catalyst layer thickness, specific surface area, amount of catalyst loading, reduction properties, and active site characteristics were analyzed. The reactor was prepared in order to examine the effect of MPC in the reactor and to propose their effective stacking. The catalytic activity tests were carried out under comparative conditions with a constant molar flow rate per catalyst loading and were carefully set for each reaction. The simulation software used was COMSOL Multiphysics to observe the physical phenomena around the catalysts, and both 3D and 2D simulations were calculated.

2.2 Catalyst Preparation

Methods of catalyst preparation into an anodized structured catalyst were described for MP, which is consisting of aluminum, applied as a structure for a structured catalyst. The preparation methods for the anodized aluminum catalyst "support" are shown in Section 2.2.1. Furthermore, the preparation methods for the MP catalyst (MPC) to load the appropriate catalyst metal species for each reaction are shown in Section 2.2.2 and 2.2.3.

2.2.1 Preparation of structured alumite catalyst support

The MP catalyst support was prepared by anodizing the MP by the following method [1-54]. The structured alumite catalyst support preparation procedure is shown in **Fig. 2.2-1**. Before anodizing, as a pretreatment, the MP was immersed in 20% sodium hydroxide for 3 min to clean the surface of the MP, followed by immersion in 30% nitric acid for 1 min to acidify the sample surface. After the pre-treatment, the MP sample was immersed in 4 wt% oxalic acid solution and anodized at 50 A/m^2 and 303 K for 4 h. The pore size widening treatment (PWT) was carried out by standing MP sample in the same oxalic acid solution for 4 h, and the specific surface area was increased by calcination at 623 K for 1 h after drying at room temperature for more than 4 h. To further increase the specific surface area, alumina produced by anodization was transformed to boehmite by immersing it in purified water above 353 K for more than 2 h. Finally, γ-alumina with a high specific surface area was prepared by drying it at room temperature for above 4 h, followed by calcination at 773 K, for 3 h. This treatment is called Hot Water Treatment (HWT), and drastically increase the specific surface area of the catalyst support. It was confirmed by microscopic image analysis that the alumite layer thickness of the alumite structured catalyst support prepared in this study was about 30 μm (**Fig.2.2-2**). The results of microscopic surface observations (Digital Microscope VHX-5000, KEYENCE) at each preparation phase are shown in **Fig. 2.2-3**.

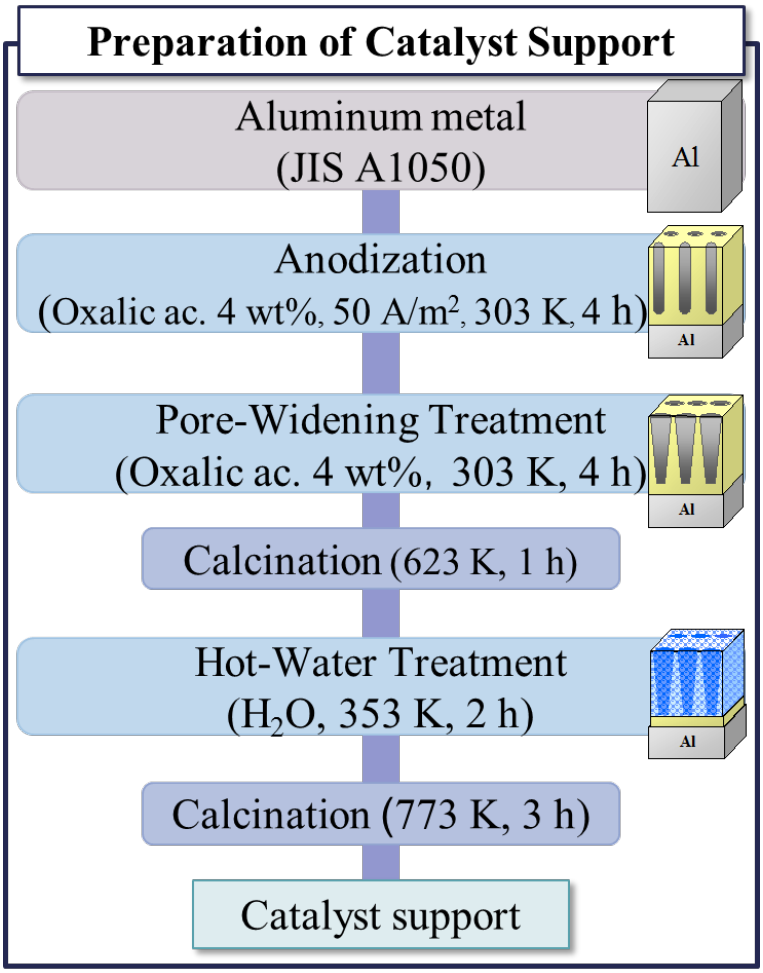

Fig. 2.2-1 Procedure of catalyst support preparation

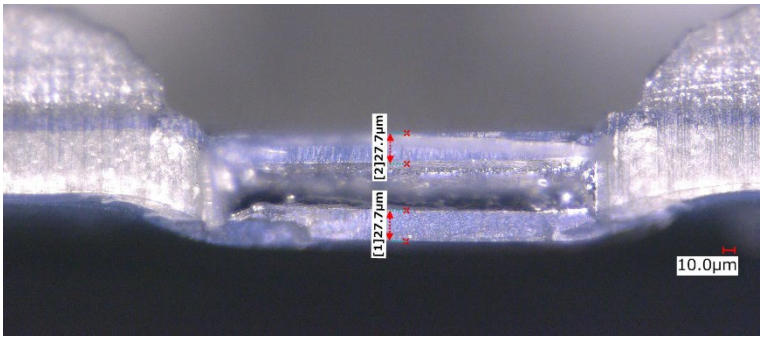

Fig. 2.2-2 Microscopic image analysis for alumite layer thickness

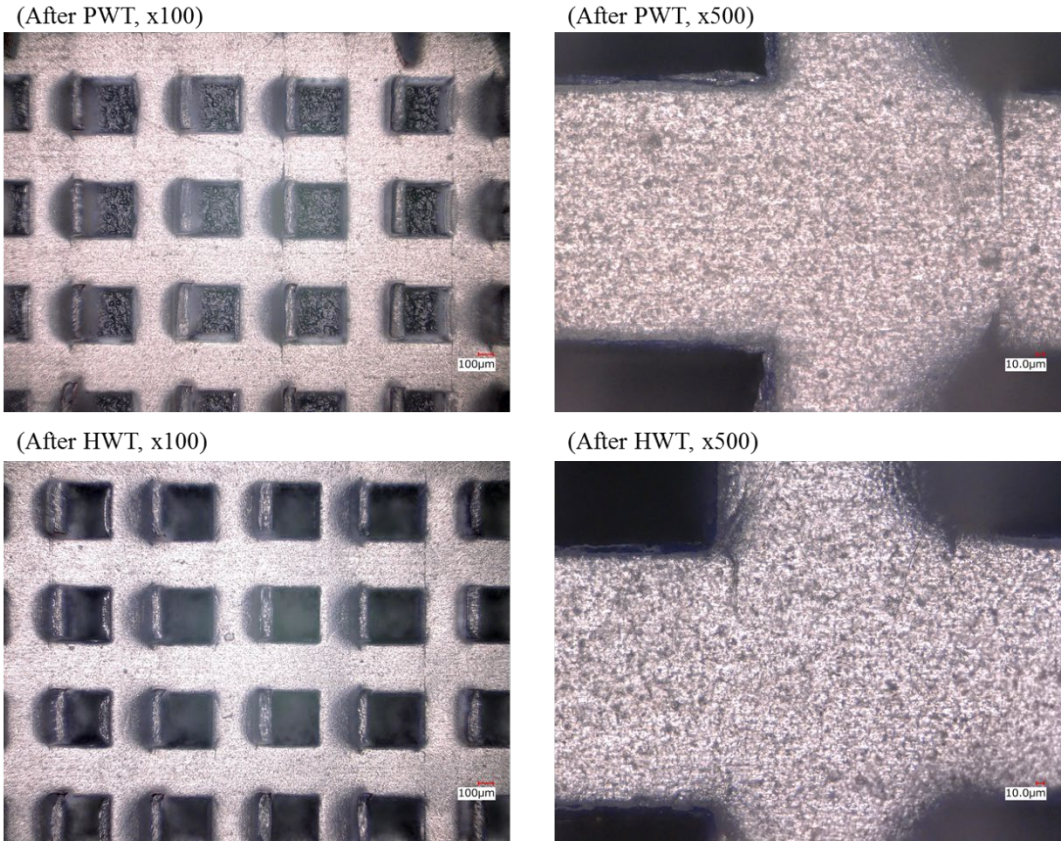

Fig. 2.2-3 Microscopic surface observations at each preparation phase
(Magnification; Left x100, Right x500)

2.2.2 Preparation of Cu/ZnO/Al_2O_3-MPC

For the steam reforming of methanol reaction (SRM), catalytic metals such as Cu, Ni, Pt, and Pd are used. It has been reported on the use of Cu/ZnO/Al_2O_3 catalyst have the advantages of high catalytic activity, durability, and low cost [2-01 – 2-03]. Therefore, Cu/ZnO/Al_2O_3-MPC was prepared for SRM in this study. For the water gas shift reaction (WGS), catalytic metals such as Fe, Cr, and Cu are used in different temperature ranges, and numerous studies have been reported on the catalyst with ZnO added to Cu as a co-catalyst in the low-temperature WGS (LT-WGS) reaction [2-04 – 2-10]. The addition of ZnO is expected to improve the activity at low temperatures and suppress catalytic deterioration. Therefore, Cu/ZnO/Al_2O_3-MPC was also prepared for WGS in this study.

The solution containing 0.49 M-Cu and 0.01 M-Zn at pH 9.5 for impregnation of the catalyst component was prepared with copper nitrate trihydrate and zinc nitrate hexahydrate. A 28% ammonia solution was used to control the pH. The impregnation of the catalyst was carried out twice at 303 K for 3 h. After each impregnation, the samples were dried at room temperature for more than 4 h and then calcined at 623 K, for 1 h. $Cu/ZnO/Al_2O_3$-MPC preparation procedure is shown in **Fig. 2.2-4**.

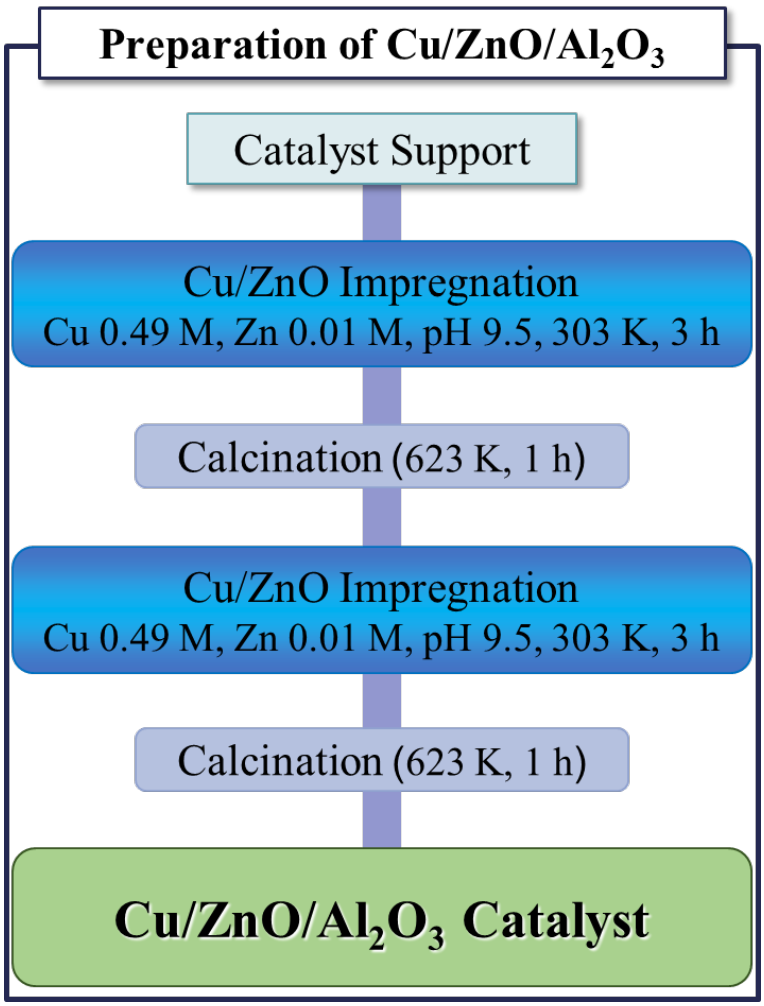

Fig. 2.2-4 Procedure of $Cu/ZnO/Al_2O_3$ catalyst preparation

2.2.3 Preparation of Pt/Al_2O_3-MPC

The use of noble metal catalysts such as Pt or Pd for the catalytic hydrogen combustion reaction (CHC) reaction has been widely reported. In particular, Pt catalysts are known to allow fast CHC reaction in a low-temperature environment close to room temperature [1-72, 2-11 – 2-14]. Therefore, Pt/Al_2O_3-MPC was also prepared for CHC in this study.

The solution containing 5×10^{-4} M-Pt at pH 11.4 for impregnation of the catalyst component was prepared with hydrogen hexachloroplatinate hexahydrate. The same 28% ammonia solution was used to control the pH. The impregnation of the catalyst was carried out only once at 298 K for 1 h. After impregnation, the sample were dried at room temperature for more than 4 h and then calcined at 773 K, for 3 h. Pt/Al_2O_3-MPC preparation procedure is shown in **Fig. 2.2-5**. Moreover, the results of microscopic surface observations (Digital Microscope VHX-5000, KEYENCE) after the Pt impregnation and the calcination are shown in **Fig. 2.2-6**.

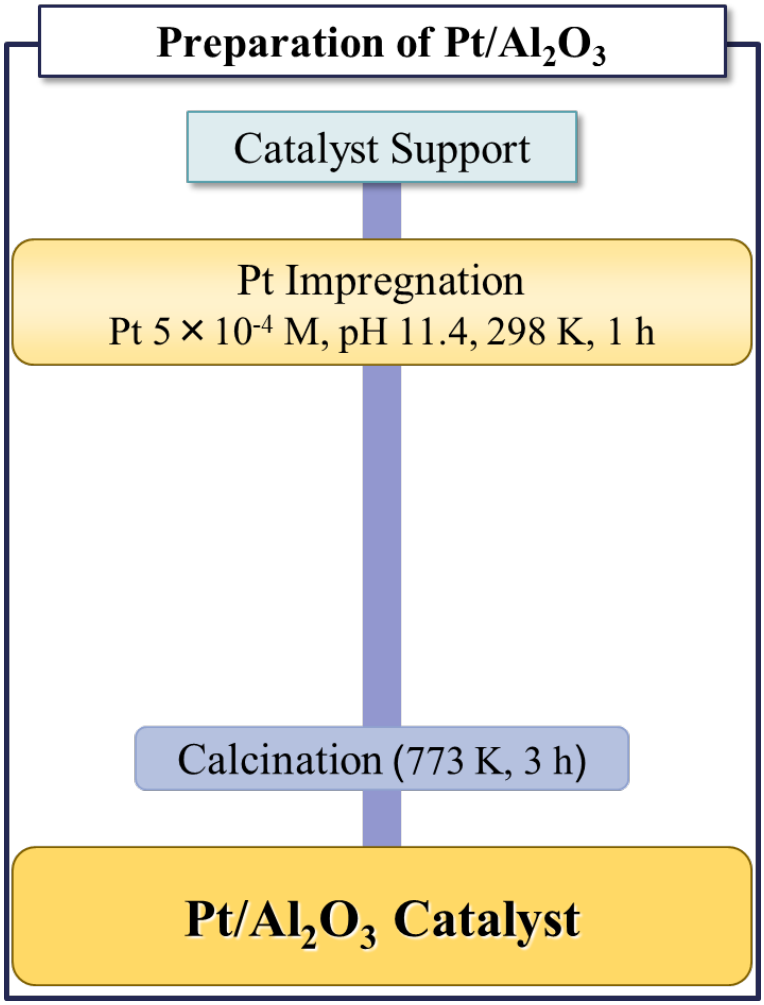

Fig. 2.2-5 Procedure of Pt/Al_2O_3 catalyst preparation

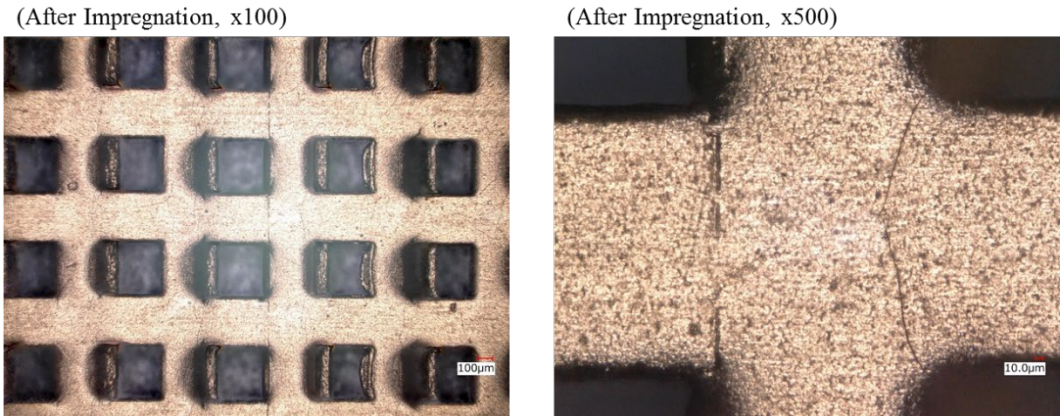

Fig. 2.2-6 Microscopic surface observations after the Pt impregnation
(Magnification; Left x100, Right x500)

2.3 Catalyst Characterization

Layer thickness and specific surface area analysis for the prepared catalyst supports were evaluated. Analyses of the amount of catalyst metals loading, catalytic reduction properties, and catalytic active site characteristics for the prepared anodized structured catalyst were performed. The detailed methods of those analyses were described below.

2.3.1 Anodized aluminum layer thickness analysis

The anodized aluminum layer thickness of the samples after the preparation of the catalyst support was measured using the measuring method of layer thickness by eddy-current thickness tester. It was confirmed by this analysis method that the alumite layer thickness of the alumite structured catalyst support prepared in this study was about 30 μm. This indicated thickness was similar to the results of the microscopic image analysis shown in Fig 2.2-2.

2.3.2 Brunauer–Emmett–Teller specific surface area analysis (BET)

Surface area measurements with BET (ChemBET-3000, Quantachrome Instruments) were performed in order to analyze the specific surface area of the prepared anodized aluminum catalyst support. Each catalyst support sample was cut into pieces (about 100 mg) and the weight was measured using an electronic balance. BET surface area measurements were conducted as follows. First, the adsorbed gas consisting of 30% concentration N_2 (He-based) was completely adsorbed on the samples using liquid nitrogen cooling at low temperatures. Then, the adsorbed components were desorbed from the samples using the water at room temperature and the concentration of the desorbed gas was detected using TCD. The career gas of TCD was Ar and the analysis temperature was 423 K (150 degC). N_2 gas was injected with a syringe as the calibration gas to

equal the detection area as desorption, and the BET surface area was analyzed from the injection volume. The surface area measurements were conducted under three conditions of adsorbed N_2 concentration of 30%, 20%, and 10% and analyzed using the multipoint BET method. The BET specific surface area of the anodized MP catalyst support prepared in this study was 49.9 m^2/g.

2.3.3 Inductively coupled plasma spectroscopy analysis (ICPS)

The amount of catalyst metal loading on each catalyst prepared for each reaction was measured using inductively coupled plasma spectroscopy (ICPS; ICPS-7510, Shimadzu Corporation). Each catalyst sample was cut into pieces with an app. surface area of about 1 cm^2 and dissolved by aqua regia. After the sample was completely dissolved, it was prepared to 50.0 mL with distilled water make a sample solution for analysis. The sample solution was introduced into the ICPS and the amount of catalyst metal loading was measured by emission spectrophotometric analysis method. Results of the amount of catalyst metal loading using ICPS is shown in **Table 2.3-1**.

Table 2.3-1 Results of the amount of catalyst metal loading using ICPS

	$Cu/ZnO/Al_2O_3$ for SRM	$Cu/ZnO/Al_2O_3$ for WGS	Pt/Al_2O_3 for CHC
Catalyst metal loading [g/m^2]	3.10	3.24	0.38

2.3.4 Temperature programmed reduction analysis (TPR)

The catalytic reduction properties of each catalyst prepared for each reaction were analyzed using hydrogen temperature-programmed reduction (H_2-TPR; ChemBET-3000, Quantachrome Instruments). The catalyst sample (about 100 mg) was heated to 773 K under a flow of reducing gas 65%-H_2/35%-Ar at a heating rate of 10 K/min The signal intensity of hydrogen consumption with respect to the reduction temperature was detected by a thermal conductivity detector (TCD).

The TPR results for each catalyst are displayed in **Fig. 2.3-1**. As shown in Fig. 2.3-1, the major peak between 473 K (200 degC) and 573 K (300 degC) was indicated with (i) $Cu/ZnO/Al_2O_3$-MPC. This peak is derived from the reduction of CuO [2-15 – 2-17], and the $Cu/ZnO/Al_2O_3$-MPC was reduced in a hydrogen flow environment at 573 K (300 degC) prior to the catalytic activity tests. And, the major reduction peak at around 643 K (370 degC) was indicated with (ii) Pt/Al_2O_3-MPC. This peak is derived from the reduction of the Pt-O-Al bond [2-18], and the Pt/Al_2O_3-MPC was reduced catalyst surface in a hydrogen flow environment at 723 K (450 degC) prior to the catalytic activity tests.

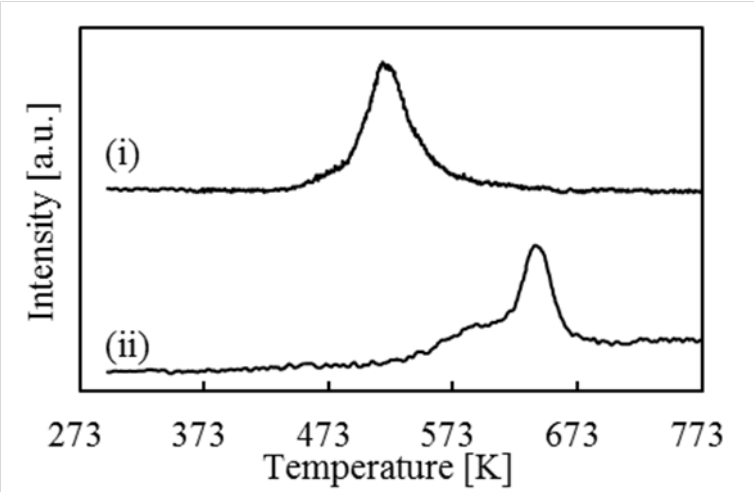

Fig. 2.3-1 TPR results for (i): $Cu/ZnO/Al_2O_3$-MPC and (ii): Pt/Al_2O_3-MPC

2.3.5 H_2-Pulse titration analysis

The catalytic active site characteristics of each catalyst prepared for each reaction were analyzed using H_2-Pulse titration (ChemBET-3000, Quantachrome Instruments). The catalyst sample (about 200 mg) was reduced under a flow of hydrogen at an appropriate temperature, followed by naturally cooling to the required analytical temperature while purging with an inert gas. The chemisorption capacity and surface area of the catalytic metal were analyzed by multiple pulse injections of H_2 gas at a volume of 0.1 mL until adsorption was no longer detected by the TCD. The results of H_2 pulse titration analysis is shown in **Table 2.3-2**.

Table 2.3-2 Results of H_2-Pulse titration analysis

	Metal Surface Area [m^2/g]	Monolayer Uptake Volume [mmol/g]
(i): $Cu/ZnO/Al_2O_3$-MPC	21.9	0.27
(ii): Pt/Al_2O_3-MPC	9.0	0.09

2.4 Reactor Preparation

A reactor with a square channel was prepared so as to reduce the unused space, where the reactant gas does not get in contact the catalyst when the MPCs are stacked in the reactor channel. A bar (diameter 10 mm, length 40 mm, SUS304) was machined, and then a square (5 mm) channel was formed using a wire electrical discharge machine (AQ360L, Sodick). The chemical composition of SUS304 are shown in **Table 2.4-1**. And, the inlet and outlet of the channel were connected to the reducing connectors (1/8 inch). It was confirmed that this reactor has no catalytic activity and the same reactor was used in all the catalytic activity tests. The overview of the reactor prepared is shown in **Fig. 2.4-1**. Moreover, multiple micro-protrusions were designed on the inner wall sides of the reactor flow path to allow for easy orderly stacking of catalysts machined from plates such as MPC. The design diagram is displayed in **Fig. 2.4-2**, and the image of MPC stacking is shown in **Fig. 2.4-3**.

Table 2.4-1 Chemical composition of SUS304 for reactor (JIS G 4303)

SUS304	C	Si	Mn	P	S	Ni	Cr
Composition[%]	0.08	1	2	0.045	0.03	8–10.5	18–20

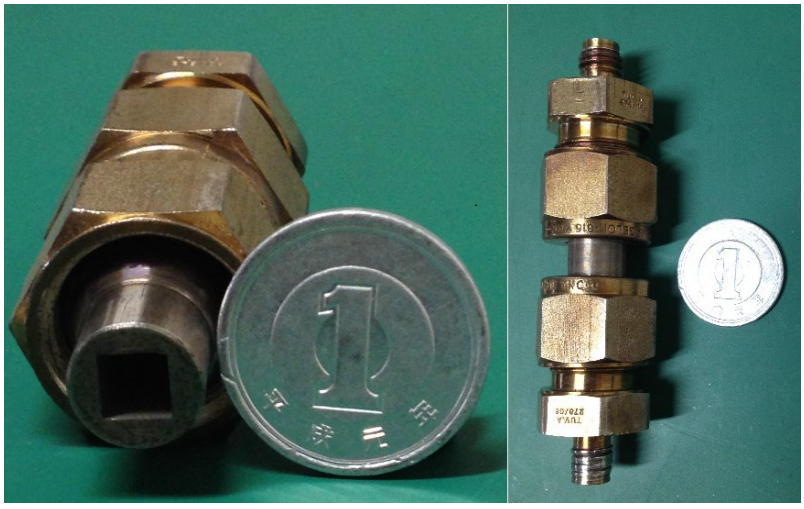

Fig. 2.4-1 Prepared reactor used

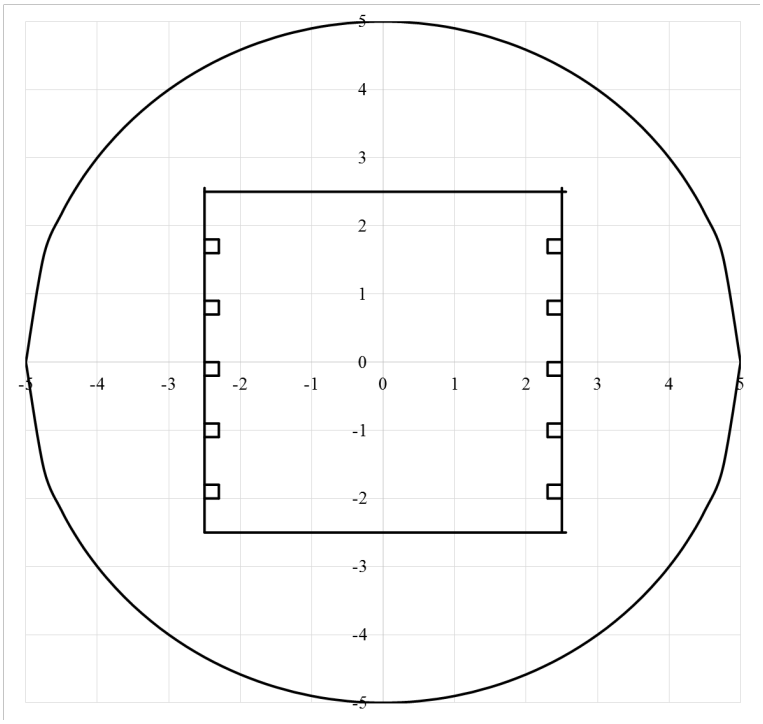

Fig. 2.4-2 Design diagram of multiple micro-protrusions on inner wall (unit: mm)

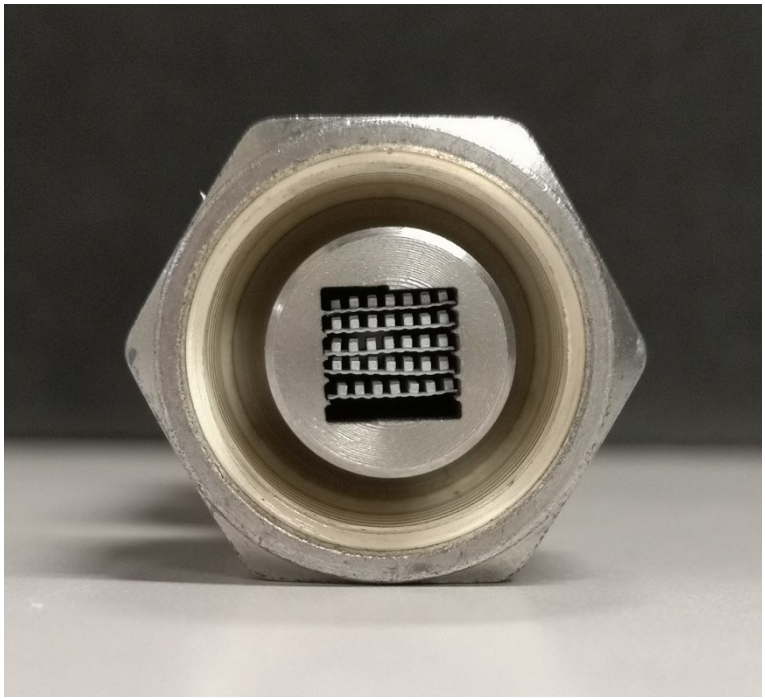

Fig. 2.4-3 Image of MPC stacking

2.5 Catalytic Activity Test

As described in chapter 1, three reactions for hydrogen economy were adopted as model reactions in this study. The catalytic activity test conditions and analytical conditions for each reaction were described, and unless otherwise stand, the catalytic activity tests were conducted under a comparing conditions with a constant ratio of the amount of catalyst metal loading W to the reactant molar flow rate F (W/F) for each reaction (**Eq. 2.5-1**). The reactor was heated by an electric furnace from the outside, and a thermocouple as a sensor was attached to the outer wall of the reactor. The outlet (after reaction) gas was analyzed using a gas chromatograph (GC-14B, SHIMADZU Corp.) with a TCD and a flame ionization detector (FID). The conversion x_i of the reactant material component presented reactivity was calculated using **Eq. 2.5-2**.

$$W/F_i = \frac{\text{(Amount of Catalyst metal loading) [g]}}{\text{(Reactant molar flow rate) [mol/h]}} \qquad (\mathbf{Eq.\ 2.5-1})$$

$$x_i = \frac{F_{\text{i,in}} - F_{\text{i,out}}}{F_{\text{i,in}}} \qquad (\mathbf{Eq.\ 2.5-2})$$

2.5.1 Condition for the SRM Reaction

The catalytic activity tests for the SRM reaction were conducted at W/F_i = 0.644 g/(mol/h). The amount of the Cu/ZnO/Al_2O_3-MPC for SRM reaction used was 3.10 g/m^2, according to the result of measurement with ICPS. The molar steam carbon ratio (S/C) of the inlet reactant gas was set at 1.5 because it was reported that the feed containing the steam molar fraction above the stoichiometry can improve the methanol conversion and prevent the formation of byproducts [2-19 – 2-21]. And then, the feed gas was carried to the reactor by an inert gas (N_2). A methanol/water feed was introduced with nitrogen as the carrier gas, and we calculated the flow rate of the outlet gas on the basis of the flow rate of the inert gas. The flow was regulated, using a mass flow controller,

to a nitrogen: methanol: water molar ratio of 5: 2: 3. The inlet gas was preheated to 423 K (140 degC) before introducing into the reactor, and the test temperature range for the catalytic activity test was controlled at 20 K intervals (7 points) between 473 K (200 degC) and 593 K (320 deg C). The Cu/ZnO/Al_2O_3-MPC was reduced in a hydrogen flow environment (8.0 mL/min) at 573 K (300 degC) for 3 h prior to the catalytic activity tests. The outline of the catalytic activity test apparatus for SRM is shown in **Fig. 2.5-1**, and the catalytic activity test conditions are shown in **Table 2.5-1**. The following equation was used for the reaction rate equation (**Eq. 2.5-3**).

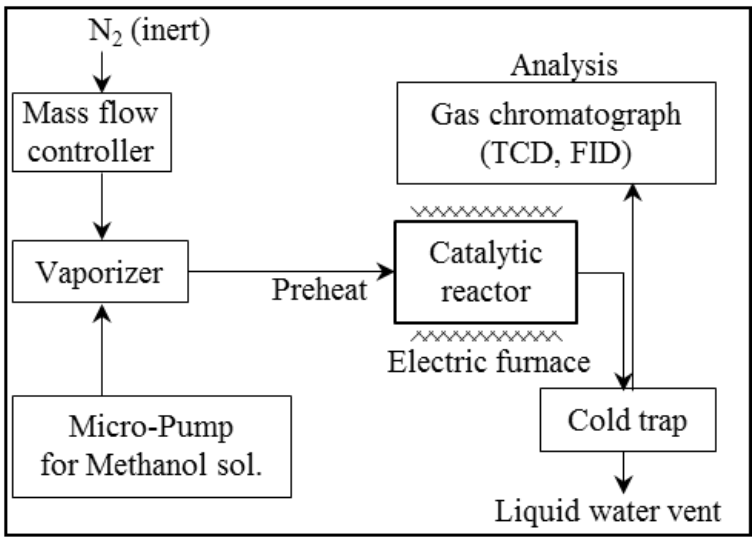

Fig. 2.5-1 Experimental apparatus of catalytic activity test for SRM reaction

Table 2.5-1 Condition of Activity Test for SRM Reaction

Min. Reaction Temperature [K]	Reaction Temperature Interval [K]	Max. Reaction Temperature [K]	Reactant Gas Component Moral Ratio N_2: Methanol: H_2O	W/F [g/(mol/h)]
473	20	593	5: 2: 3	0.644

$$r_{\mathrm{SRM}} = k_{\mathrm{SRM}} \times C_{\mathrm{Methanol}} \qquad \textbf{(Eq. 2.5-3)}$$

2.5.2 Condition for the WGS Reaction

The catalytic activity tests for the WGS reaction were conducted at W/F_i = 0.50 g/(mol/h). The amount of the Cu/ZnO/Al_2O_3-MPC for WGS reaction used was 3.24 g/m^2, according to the result of measurement with ICPS. The composition of the reactant gas was set to S/C = 1.33 because it has been reported that the formation of carbon on the catalyst surface is in general favored at a low H2 to CO ratio, thus decreasing the selectivity of the target product [2-22]. The reactant gas was carried to the reactor with N_2 as an inert gas, and the feed ratio of the reaction gas to inert gas was 35:65. The feed gas was preheated to 413 K (140 degC) before it was in-flowed into the reactor, and catalytic activity tests were conducted between 453 K (180 degC) and 533 K (260 degC) at controlled temperature intervals of 20 K (5 points). This is the typical LT-WGS temperature range [2-23 – 2-25]. The Cu/ZnO/Al_2O_3-MPC was reduced in a hydrogen flow environment (8.0 mL/min) at 573 K (300 degC) for 3 h prior to the catalytic activity tests. The outline of the catalytic activity test apparatus for WGS is shown in **Fig. 2.5-2**, and the catalytic activity test conditions are shown in **Table 2.5-2**. The following equation was used for the reaction rate equation (**Eq. 2.5-4 –Eq. 2.5-6**) [2-26, 2-27].

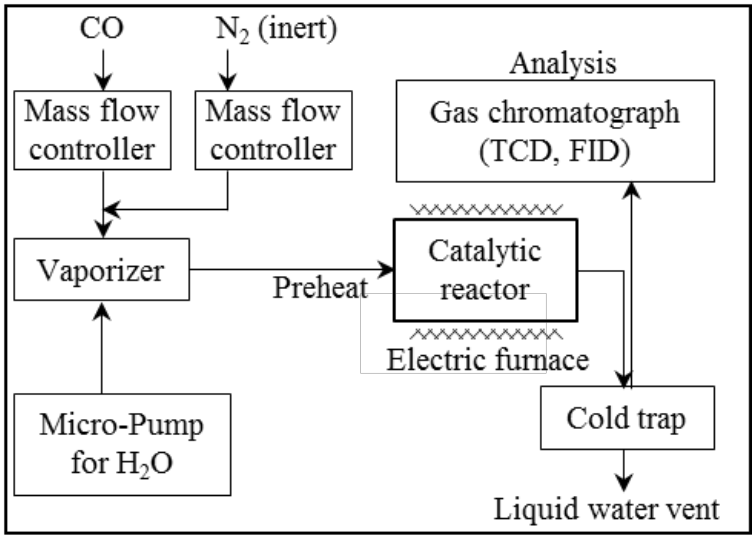

Fig. 2.5-2 Experimental apparatus of catalytic activity test for WGS reaction

Table 2.5-2 Condition of Activity Test for WGS Reaction

Min. Reaction Temperature [K]	Reaction Temperature Interval [K]	Max. Reaction Temperature [K]	S/C	Reactant Gas: N_2	W/F [g/(mol/h)]
453	20	533	1.33	35: 65	0.50

$$r_{\mathrm{WGS}} = k_{\mathrm{WGS}} P_{\mathrm{CO}} P_{H_2O}(1-\beta) \qquad (\mathbf{Eq.\,2.5-4})$$

$$\beta = \frac{p_{\mathrm{CO}_2} p_{H_2}}{p_{CO} p_{H_2O}} \times \frac{1}{K_e} \qquad (\mathbf{Eq.\,2.5-5})$$

$$K_e = \exp\left(\frac{4577.8}{T} - 4.33\right) \qquad (\mathbf{Eq.\,2.5-6})$$

2.5.3 Condition for the CHC Reaction

The catalytic activity tests for the CHC reaction were conducted at $W/F_i = 7.7 \times 10^{-4}$ g/(mol/h). The amount of the Pt/Al_2O_3-MPC for CHC reaction used was 0.38 g/m^2, according to the result of measurement with ICPS. The composition of the reactant gas was set to H_2:O_2: N_2 = 1:5:22, paying attention safely to the mixing ratio of lean H_2 and O_2. Here, N_2 was the inert gas used for dilution. The feed gas was preheated to 333 K (60 degC) before it was in-flowed into the reactor, and catalytic activity tests were conducted between 373 K (100 degC) and 453 K (180 degC) at controlled temperature intervals of 20 K (5 points). This is because the CHC reaction typically proceeded above 353 K (80 degC) [2-12, 2-13]. The Pt/Al_2O_3-MPC was reduced catalyst surface in a hydrogen flow environment (10.0 mL/min) at 723 K (450 degC) for 1 h prior to the catalytic activity tests. The outline of the catalytic activity test apparatus for CHC is shown in **Fig. 2.5-3**, and the catalytic activity test conditions are shown in **Table 2.5-3**. The following equation was used for the reaction rate equation (**Eq. 2.5-7**) [1-72, 2-28].

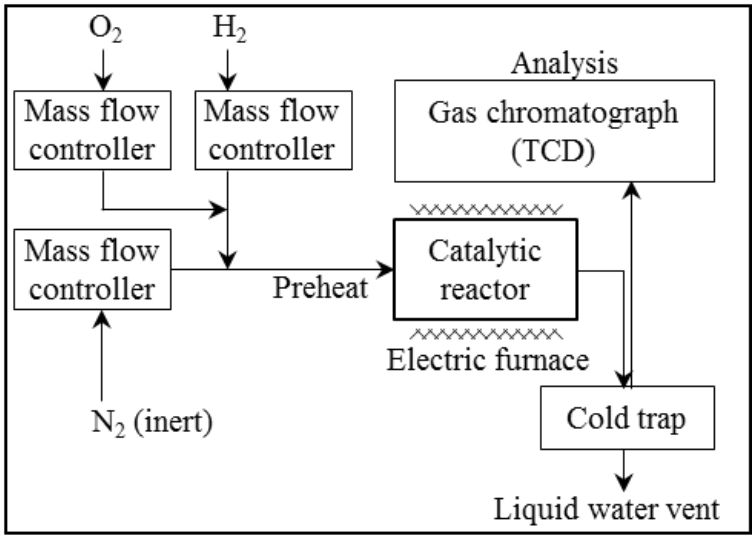

Fig. 2.5-3 Experimental Apparatus of Catalytic Activity Test for CHC Reaction

Table 2.5-3 Condition of Activity Test for CHC Reaction

Min. Reaction Temperature [K]	Reaction Temperature Interval [K]	Max. Reaction Temperature [K]	Reactant Gas Component Moral Ratio H_2: O_2: N_2	W/F [g/(mol/h)]
373	20	453	1: 5: 22	7.7×10^{-4}

$$r_{\mathrm{CHC}} = k_{\mathrm{CHC}} p_{\mathrm{H_2}}^{m} p_{O_2}^{n} \ (m = 1, n = 0) \qquad (\mathbf{Eq.\ 2.5-7})$$

2.6 Simulation Application

The 3D numerical simulation software "COMSOL Multiphysics" was used to observe the physical phenomena such as the fluid flow, the heat transfer, and the mass transfer around the catalysts. The calculated physics were as follows: laminar flow, heat transfer, and dilute species transport; their representative equations and conditions are listed in **Table 2.6-1**. The following assumptions were made for the simulation: ideal gas, non–compressible, steady physicality, and laminar flow. Partial differential equations, such as the Navier–Stokes equation, were used to describe the continuity, momentum, mass, and energy conservations. The equation for mass transfer is a convection–diffusion equation that follows Fick's law. In addition, the initial conditions, such as the flow rate, reactants concentration, and reaction temperature, and boundary conditions were matched to those in the catalytic activity tests; for the parameter of the reaction rate, the value calculated from the experimental results was used. The viscosity, thermal conductivity, and diffusion coefficient of each species in the multi-components system were estimated based on the extension of Chapman–Enskog theory (**Eq. 2.6-1** – **Eq. 2.6-6**). Moreover, the heat of reaction Q was set to be generated as shown in **Eq.2.6-7**, and the reaction rate r_i did not contribute to the mass balance for the calculation model in this study because it is the reaction rate in the gas phase.

Simulation studies were conducted with 2D and 3D simulations. An overview of the basic simulation models in this study is shown in **Fig. 2.6-1** and **Fig. 2.6-2**. It was focused on the changes in physical phenomena in the fin height and flow directions with the simulation model in which the unit MPC structure was cut in half in the width direction was used since the unit MPC structure is symmetrical in the MPC width direction. The mesh number of 2D simulation models was approximately 40,000 and that of 3D simulation models was approximately 100,000. And, a mesh independence verification of them passed about conversions of reactants in the simulation. The conversion of reactants in the simulation was calculated using **Eq. 2.6-8**. All simulation results displayed was adopted side view.

Table 2.6-1 Typical differential equations calculated in simulation

Laminar flow	Navier–Stokes equations $\rho(u \cdot \nabla)u = \nabla \cdot \left[-pI + \mu\left(\nabla u + (\nabla u)^T - \frac{2}{3}\mu(\nabla \cdot u)I\right)\right]$ Continuity equation $\nabla \cdot (\rho u) = 0$
Heat transfer	Heat balance $\rho c_p u \cdot \nabla T + \nabla \cdot q = Q$ Fourier's law $q = -\lambda \nabla T$
Dilute species transport	Mass balance $\nabla \cdot (-D_i \nabla C_i) + u \cdot \nabla C_i = r_i$ Convection–Diffusion equation $N_i = -D_i \nabla C_i + u C_i$

$$\mu_m = \sum_{i=1}^{n} \frac{\theta y_i \mu_i}{\sum_{j=1}^{n} y_j \phi_{ij}} \qquad (\mathbf{Eq.2.6-1})$$

$$\phi_{ij} = \frac{\left[1 + \left(\frac{\mu_i}{\mu_j}\right)^{\frac{1}{2}} \left(\frac{M_j}{M_i}\right)^{\frac{1}{4}}\right]^2}{\left[8\left(1 + \frac{M_i}{M_j}\right)\right]^{\frac{1}{2}}} \qquad (\mathbf{Eq.2.6-2})$$

$$\lambda_m = \sum_{i=1}^{n} \frac{y_i \lambda_i}{\sum_{j=1}^{n} y_j A_{ij}} \qquad (\mathbf{Eq.2.6-3})$$

$$A_{ij} = \kappa \frac{\left[1 + \left(\lambda_i/\lambda_j\right)^{\frac{1}{2}}\left(M_j/M_i\right)^{\frac{1}{4}}\right]^2}{\left[8(1 + M_i/M_j)\right]^{\frac{1}{2}}} \qquad (\mathbf{Eq.\,2.6-4})$$

$$D_i = \frac{1 - y_i}{\sum_{j=1}^{n} \frac{y_j}{D_{ij}}} \qquad (\mathbf{Eq.\,2.6-5})$$

$$D_{ij} = 1.858 \times 10^{-7} T^{\frac{3}{2}} \frac{\left[(M_i + M_j)/(M_i M_j)\right]^{\frac{1}{2}}}{P\sigma_{ij}^2 \Omega} \qquad (\mathbf{Eq.\,2.6-6})$$

$$Q = r_i \times dH_{\text{REACTION}} \qquad (\mathbf{Eq.\,2.6-7})$$

$$x_i = \frac{\iint q_{\text{i,in}} - \iint q_{\text{i,out}}}{\iint q_{\text{i,in}}} \qquad (\mathbf{Eq.\,2.6-8})$$

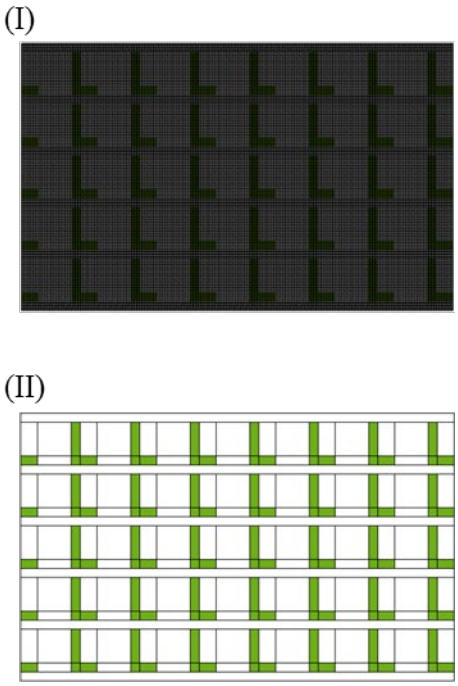

Fig. 2.6-1 Simulation model (I) Mesh, (II) Overall view (2D Simulation Model)

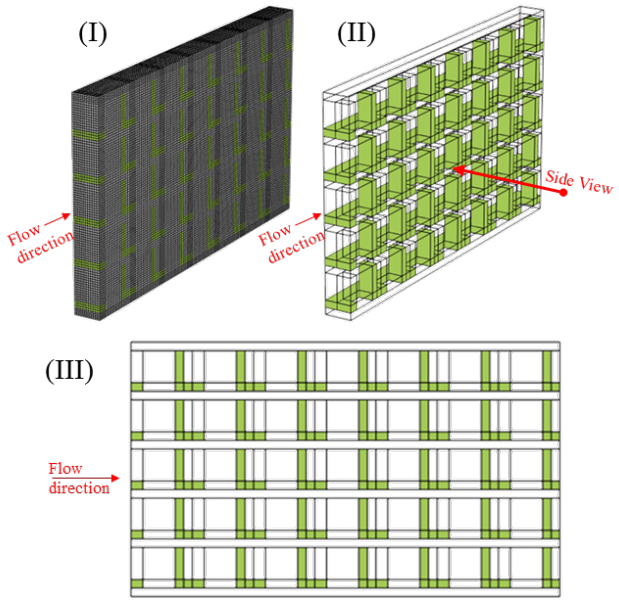

Fig. 2.6-2 Simulation model (I) Mesh, (II) Overall view, (III) Side view (3D Simulation Model)

2.7 Nomenclature

A_{ij}	= interaction parameter for thermal conductivity	[-]
c_p	= specific heat capacity	[J/kg K]
C_i	= molar concentration	[mol/m^3]
D_i	= diffusion coefficient	[m^2/s]
D_{ij}	= mutual diffusion coefficient	[m^2/s]
E_a	= activation energy	[J/mol]
F_i	= molar flow rate	[mol/h]
ΔH°_{298}	= reaction enthalpy	[kJ/mol]
K_e	= equilibrium constant	[-]
M_i	= molecular weight	[kg/mol]
M_s	= surface metal sites of the catalyst	[mol/g]
n	= number of components	[-]
N_i	= molar flux	[mol/(m^2 s)]
p_i	= pressure	[Pa]
q	= heat flux	[W/m^2]
Q	= heat of reaction	[W/m^3]
r_i	= reaction rate in gas phase	[mol/(m^3 s)]
R	= gas constant	[J/(mol K)]
T	= reaction temperature	[K]
u	= flow velocity	[m/s]
W	= catalyst weight	[g]
x_i	= conversion of reactant	[-]
y_i	= mole fraction	[-]

β	= reversibility factor	[-]
κ	= numerical constant	[-]
λ	= thermal conductivity	[W/(m K)]
μ	= viscosity	[Pa s]
ρ	= density	[kg/m^3]
σ_{ij}	= Lennard-Jones force constant	[m]
ϕ_{ij}	= interaction parameter for viscosity	[-]
Ω	= collision integral	[-]

<Subscripts>

b	= bulk
i	= component *i*
j	= component *j*
m	= mixture
s	= surface
in	= inlet
out	= outlet

2.8 Conclusions of chapter 2

In this chapter, the experimental and simulation methods related to this dissertation were provided. For the experiment, the method of preparing an anodized aluminum catalyst was adopted to catalyze a commercial structure made of aluminum. Cu/ZnO/Al_2O_3-MPCs with high catalytic activity and durability and low cost were prepared for the SRM and WGS reactions, and Pt/Al_2O_3-MPCs with low-temperature catalytic activity were prepared for the CHC reaction. The catalyst layer thickness, specific surface area, amount of catalyst loading, reduction properties, and active site characteristics were analyzed as the characterization of those catalysts. Square channel reactors were prepared for the stacking of multiple MPCs and used in all catalytic activity tests. Catalytic activity tests were performed under constant *W/F* comparative conditions in each reaction, with care taken to identify the rate-limiting step.

For the simulation, the software used was COMSOL Multiphysics, which adopted 3D and 2D simulations, respectively. In all the simulation models, parallel calculations were performed for the fluid flow, heat transfer, and mass transfer to evaluate the physical phenomena around the catalyst. All simulation models were conducted and passed mesh independence verification.

2.9 References

[2-01] S. H. Ahn, O.J. Kwon, I. Choi, J.J. Kim; "Synergetic effect of combined use of Cu–ZnO–Al_2O_3 and Pt–Al_2O_3 for the steam reforming of methanol," Catalysis Communications 10 (2009) 2018–2022, https://doi.org/10.1016/j.catcom.2009.07.023.

[2-02] M. M. Günter, T. Ressler, R.E. Jentoft, B. Bems; "Redox behavior of copper oxide/zinc oxide catalysts in the steam reforming of methanol studied by in situ X-ray diffraction and absorption spectroscopy," Journal of Catalysis 203 (1) (2001) 133–149, https://doi.org/10.1006/jcat.2001.3322.

[2-03] P. Kurr, I. Kasatkin, F. Girgsdies, A. Trunschke, R. Schlögl, T. Ressler; "Microstructural characterization of Cu/ZnO/Al2O3catalysts for methanol steam reforming-A comparative study," Applied Catalysis A: General 348 (2008) 153–164, https://doi.org/10.1016/j.apcata.2008.06.020.

[2-04] H.-S. Na, D.-W. Jeong, W.-J. Jang, J.-O. Shim, H.-S. Roh; "The effect of preparation method on Fe/Al/Cu oxide-based catalyst performance for high temperature water gas shift reaction using simulated waste-derived synthesis gas," International Journal of Hydrogen Energy 40 (2015) 12268–12274, https://doi.org/10.1016/j.ijhydene.2015.07.060.

[2-05] D. W. Jeong, W.J. Jang, J.O. Shim, W.B. Han, H.S. Roh, U.H. Jung, W.L. Yoon; "Low-temperature water-gas shift reaction over supported Cu catalysts," Renewable Energy 65 (2014) 102–107, https://doi.org/10.1016/j.renene.2013.07.035.

[2-06] K. Sagata, Y. Kaneda, H. Yamaura, S. Kobayashi, H. Yahiro; "Influence of coexisting Al_2O_3 on the activity of copper catalyst for water–gas-shift reaction," International Journal of Hydrogen Energy 39 (2014) 20639–20645, https://doi.org/10.1016/j.ijhydene.2014.07.021.

[2-07] X. Liu, P. Guo, S. Xie, Y. Pei, M. Qiao, K. Fan; "Effect of Cu loading on Cu/ZnO water-gas shift catalysts for shut-down/start-up operation," International Journal of Hydrogen Energy 37 (2012) 6381–6388, https://doi.org/10.1016/j.ijhydene.2012.01.110.

[2-08] P. Guo, L. Chen, Q. Yang, M. Qiao, H. Li, H. Li, *et al*.; "Cu/ZnO/Al_2O_3 water–gas shift catalysts for practical

fuel cell applications: the performance in shut-down/start-up operation," International Journal of Hydrogen Energy 34 (2009) 2361–2368, https://doi.org/10.1016/j.ijhydene.2008.12.081.

[2-09] J.-O. Shim, H.-S. Na, S.-Y. Ahn, K.-W. Jeon, W.-J. Jang, B.-H. Jeon, *et al.*; "An important parameter for synthesis of Al_2O_3 supported Cu-Zn catalysts in low-temperature water-gas shift reaction under practical reaction condition," International Journal of Hydrogen Energy 44 (2019) 14853–14860, https://doi.org/10.1016/j.ijhydene.2019.04.042.

[2-10] P. Kowalik, K. Antoniak-Jurak, R. Bicki, W. Próchniak, P. Wiercioch, K. Michalska; "The alcohol-modified CuZnAl hydroxycarbonate synthesis as a convenient preparation route of high activity Cu/ZnO/Al_2O_3 catalysts for WGS," International Journal of Hydrogen Energy 44 (2019) 913–922, https://doi.org/10.1016/j.ijhydene.2018.11.051.

[2-11] P. A. Deshpande, G. Madras; "Catalytic hydrogen combustion for treatment of combustible gases from fuel cell processors," Applied Catalysis B: Environmental 100 (2010) 481–490, https://doi.org/10.1016/j.apcatb.2010.08.026.

[2-12] S. Y. Joshi, Y. Ren, M.P. Harold, V. Balakotaiah; "Determination of kinetics and controlling regimes for H_2 oxidation on Pt/Al_2O_3 monolithic catalyst using high space velocity experiments," Applied Catalysis B: Environmental 102 (2011) 484–495, https://doi.org/10.1016/j.apcatb.2010.12.030.

[2-13] G. M. Arzac, O. Montes, A. Fernández; "Pt-impregnated catalysts on powdery SiC and other commercial supports for the combustion of hydrogen under oxidant conditions," Applied Catalysis B: Environmental 201 (2017) 391–399, https://doi.org/10.1016/j.apcatb.2016.08.042.

[2-14] D. Bhatia, M.P. Harold, V. Balakotaiah; "Kinetic and bifurcation analysis of the cooxidation of CO and H_2 in catalytic monolith reactors," Chemical Engineering Science 64 (2009) 1544–1558, https://doi.org/10.1016/j.ces.2008.12.012.

[2-15] S. Gusi, F. Trifiró, A. Vaccari; "Kinetic study of the reduction of copper- zinc-aluminum mixed oxide catalysts," Reactivity of Solids 2 (1986) 59–71, https://doi.org/10.1016/0168-7336(86)80064-X.

[2-16] C. Price, L. Pastor-Pérez, E. le Saché, A. Sepúlveda-Escribano, T.R. Reina; "Highly active Cu-ZnO catalysts for the WGS reaction at medium–high space velocities: effect of the support composition," International

Journal of Hydrogen Energy 42 (16) (2017) 10747–10751, https://doi.org/10.1016/j.ijhydene.2017.02.013.

[2-17] D. Li, Y. Cai, Y. Ding, R. Li, M. Lu, L. Jiang; "Layered double hydroxides as precursors of Cu catalysts for hydrogen production by water-gas shift reaction," International Journal of Hydrogen Energy 40 (2015) 10016–10025, https://doi.org/10.1016/j.ijhydene.2015.05.183.

[2-18] J. Lee, E. J. Jang, D. G. Oh, J. Szanyi, J. H. Kwak; "Morphology and size of Pt on Al_2O_3: The role of specific metal-support interactions between Pt and Al_2O_3," Journal of Catalysis 385 (2020) 204–212, https://doi.org/10.1016/j.jcat.2020.03.019.

[2-19] S. J. Andreasen, S. K. Kær, S. Sahlin; "Control and experimental characterization of a methanol reformer for a 350 W high temperature polymer electrolyte membrane fuel cell system," International Journal of Hydrogen Energy 38 (2013) 1676–1684, https://doi.org/10.1016/j.ijhydene.2012.09.032.

[2-20] A. Iulianelli, P. Ribeirinha, A. Mendes, A. Basile; "Methanol steam reforming for hydrogen generation via conventional and membrane reactors: A review," Renewable and Sustainable Energy Reviews 29 (2014) 355–368, https://doi.org/10.1016/j.rser.2013.08.032.

[2-21] X. Zhang, H. Hu, Y. Zhu, S. Zhu; "Methanol steam reforming to hydrogen in a carbon membrane reactor system," Industrial & Engineering Chemistry Research 45 (2006) 7997–8001, https://doi.org/10.1021/ie060414m.

[2-22] E. Xue, M. O'Keeffe, J.R.H. Ross; "Water-gas shift conversion using a feed with a low steam to carbon monoxide ratio and containing sulphur," Catalysis Today 30 (1996) 107–118, https://doi.org/10.1016/0920-5861(95)00323-1.

[2-23] N. Garcia-Moncada, M. Gonzalez-Castano, S. Ivanova, M.A. Centeno, F. Romero-Sarria, J.A. Odriozola; "New concept for old reaction: novel WGS catalyst design," Applied Catalysis B: Environmental 238 (2018) 1–5, https://doi.org/10.1016/j.apcatb.2018.06.068

[2-24] K. Sagata, N. Imazu, H. Yahiro; "Study on factors controlling catalytic activity for low-temperature water–gas-shift reaction on Cu-based catalysts," Catalysis Today 201 (2013) 145–150, https://doi.org/10.1016/j.cattod.2012.03.064

[2-25] P. Kowalik, W. Próchniak, T. Borowiecki; "The effect of alkali metals doping on properties of $Cu/ZnO/Al_2O_3$

catalyst for water gas shift," Catalysis Today 176 (2011) 144–148, https://doi.org/10.1016/j.cattod.2011.01.028

[2-26] S. Saeidi, F. Fazlollahi, S. Najari, D. Iranshahi, J.J. Klemeše, L.L. Baxter; "Hydrogen production: Perspectives, separation with special emphasis on kinetics of WGS reaction: A state-of-the-art review," Journal of Industrial and Engineering Chemistry 49 (2017) 1–25, https://doi.org/10.1016/j.jiec.2016.12.003.

[2-27] R. L. Keiski, O. Desponds, Y.F. Chang, G.A. Somorjai; "Kinetics of the water-gas shift reaction over several alkane activation and water-gas shift catalysts," Applied Catalysis A: General 101 (1993) 317–338, https://doi.org/10.1016/0926-860X(93)80277-W.

[2-28] F. V. Hanson, M. Boudart; "The reaction between H_2 and O_2 over supported platinum catalysts," Journal of Catalysis 53 (1978) 56–67, https://doi.org/10.1016/0021-9517(78)90007-6.

Chapter 3

Comparison of Reactivity between MPC and Plate-type Structured Catalysts: Experimental studies

3.1 Abstract

In chapter 3, it was provided the results of the comparison of the reactivity of each reaction between MPC and the unprocessed plate-type structured catalyst (plate) on experiments. The improvement of the frequency factor due to the structure of MPC was confirmed using the Arrhenius equation as a kinetic analysis, and the effect of the improvement in reactivity was revealed to be larger at lower temperatures by calculating Turnover frequency (TOF), which is a general evaluating index of catalytic performance. Furthermore, it was suggested that the tendency to improve the reactivity differed when focusing on the rate-limiting step.

3.2 Purpose

Most of the conventionally report on improving the process performance of catalytic processes using structured catalysts was on improving the performance of catalytic reactors as devices. On the other hand, the factor for the improved reactivity due just to the structure of the structural catalyst is not clear. In the previous report (Shimada et al., 2013), it shows that MPC improved reactivity compared with plate and that the orientation relationship between flow direction and MPC fins affected reactivity. And they conducted simulations to show streamline and only concluded that the reactivity was improved because of the MPC disarrangements the fluid.

In this chapter, MPC was applied to the SRM, WGS, and CHC reactions, and the catalytic activity tests for comparing the reactivity to the unprocessed plate catalyst were carried out. The conversions from the experimental results and the results of the reaction rate analysis according to the Arrhenius equation were used to compare the activation energy and the frequency factor in both structures to investigate the factors affecting reactivity and the effect of the structure on those factors. It was also investigated that the effects of MPC for each reaction condition with a focus on the rate-limiting step, especially. Furthermore, the turnover frequency

(TOF), is a general index of catalytic performance, was calculated for each condition, and the ratio of the TOF to that of the unprocessed plate was evaluated in order to evaluate the effect and tendency of the reactivity enhancement. It was suggested that the factor that improved the reactivity by using the structured catalyst from these results.

3.3 Methodology

The model catalyst reactions adopted the SRM and WGS reactions and CHC reactions. MPCs were prepared as $Cu/ZnO/Al_2O_3$-MPC for the SRM and WGS reactions, and Pt/Al_2O_3-MPC for CHC reaction as described in Section 2.2. Plate as a structured catalyst to compare the reactivity of MPC was prepared by flattening the fins of MPC. The plate exhibited similar reactivity to that of the catalyst prepared using the same procedure from an unprocessed aluminum plate of the same thickness. Therefore, the amount of catalyst metal loading per unit surface area was the same for the MPC and the plate in each reaction. The catalytic reactors used were shown in Section 2.4, Fig. 2.4-1. The catalytic activity test conditions for each reaction were shown in Section 2.5. All catalytic activity tests were carried out under constant W/F comparative conditions for each reaction, and conversion and reaction rates were compared for both MPC and plate structures. The effect of the reactivity improvement was investigated by calculating TOF as an index of catalytic performance. Details of each experimental method were described in chapter 2.

3.4 Results and Discussion

3.4.1 Catalytic activity test for comparing between MPC and plate for the SRM reaction

The catalytic activity tests were carried out to compare the difference of the reactivity between using MPC and using plate under constant *W/F* as a comparison condition. The plate was prepared by flattening the fins of Cu/ZnO/Al_2O_3-MPC as shown in **Fig. 3.4-1**. The plate exhibited similar reactivity to that of the catalyst prepared using the same procedure from an unprocessed aluminum plate of the same thickness. Therefore, the amount of catalyst metal loading per unit surface area was the same for the MPC and the plate.

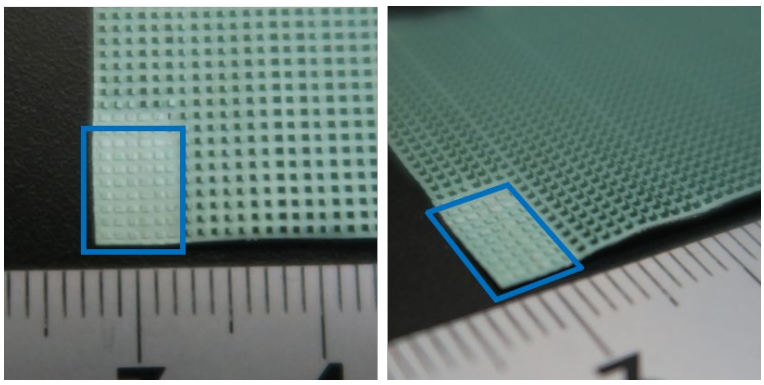

Fig. 3.4-1 Plate with flattened fins of Cu/ZnO/Al_2O_3-MPC (in blue frame)

The rate-limiting step for the SRM reaction was determined from "experiments with varying feed velocity of reactant gas". **Fig. 3.4-2** shows the reaction rate with a different feed velocity of reactant gas for the SRM reaction. Based on the results, a rate-limiting step was carefully determined. Fig. 3.4-2 suggested that the feed velocity of reactant gas did not affect the reaction rate beyond a certain value ($0.006 < u$ [m/s]), indicating that the external boundary film resistance did not affect the reactivity.

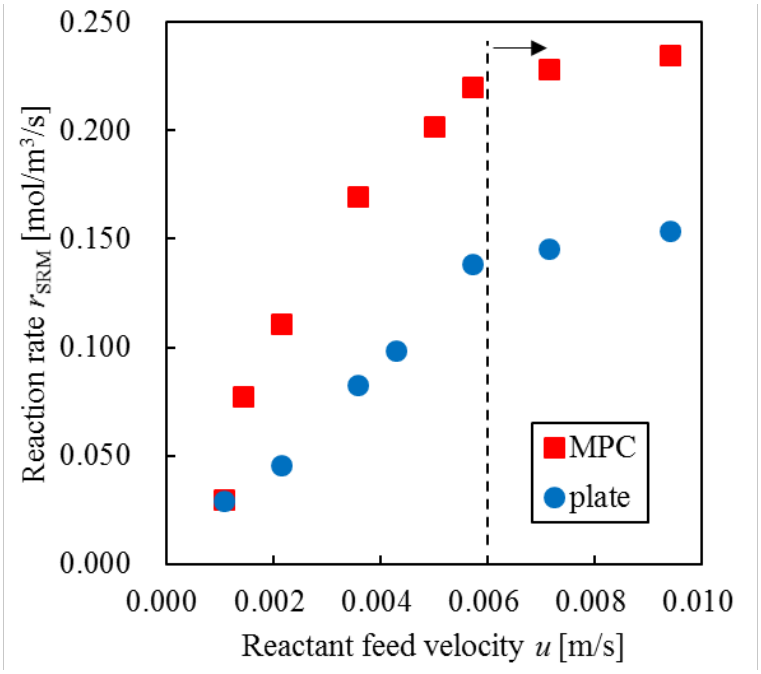

Fig. 3.4-2 The reaction rate with a different feed velocity of reactant gas for the SRM reaction

The conversions in the activity tests on SRM by the MPC and plate are shown in **Table 3.4-1** and **Fig. 3.4-3**; further results of the reaction rate analysis according to the Arrhenius equation (**Eq. 3.4-1)** are shown in **Table 3.4-2** and **Fig. 3.4-4**. MPC improved the methanol conversion compared to plate, and the conversion by the MPC increased by 80% at 553 K, compared with that by the plate. Fig. 3.4-4 shows that the activation energies of MPC and plate were almost the same (98.6 kJ/mol and 95.4 kJ/mol) because the slopes of the Arrhenius plots were similar for both catalyst structures and did not change within the range of this activity test conditions. Furthermore, those values were similar to the data reported for $Cu/ZnO/Al_2O_3$ based catalysts on the same reaction [3-01 – 3-03], and it was indicated that a catalytic reaction rate-limiting step, not an external mass transfer rate-limiting step. The rate-limiting step did not change depending on a reaction temperature. It was suggested that a catalytic reaction rate dominated the overall reactivity in the temperature range of this test on both structures. These results also indicated that the reactivity improved due to a frequency factor was increased using MPC because the results of Arrhenius plots indicated. In other words, an improvement in the contact frequency between the reactants and the catalyst owing to the structure of MPC.

$$k = k_0 \times \exp\left(-\frac{E_a}{RT}\right) \qquad \textbf{(Eq. 3.4 - 1)}$$

Table 3.4-1 Conversions in the activity tests on SRM using MPC and plate

T [K]	Methanol conversion [%]	
	MPC	plate
473	8.0	2.9
493	19.1	6.5
513	37.8	13.4
533	65.7	25.1
553	87.9	48.0
573	98.0	72.2
593	100.0	92.2

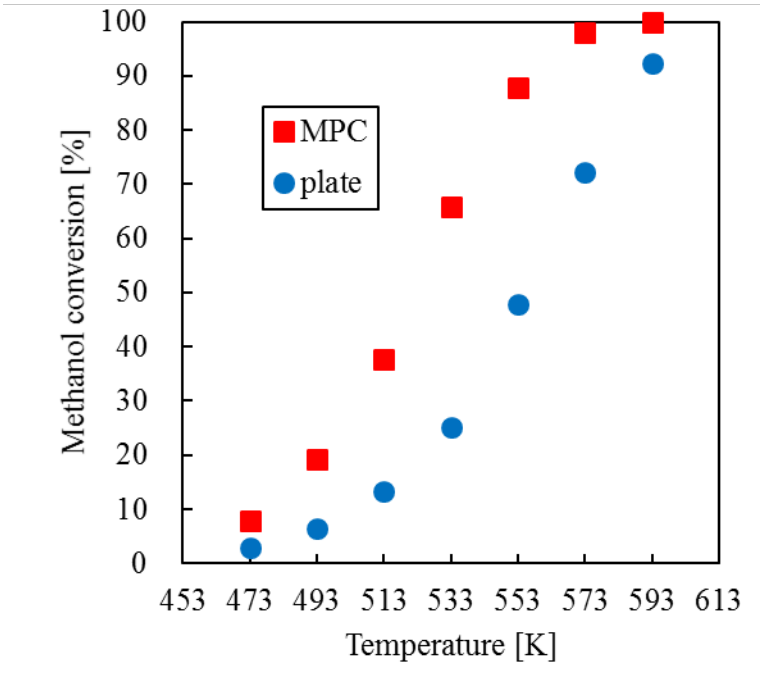

Fig. 3.4-3 Methanol conversions of MPC and plate for the SRM reaction

Table 3.4-2 Reaction rate analysis according to the Arrhenius equation for SRM reaction

T [K]	ln k_{SRM} [-]	
	MPC	plate
473	-10.6	-11.6
493	-9.7	-10.8
513	-8.9	-10.1
533	-8.0	-9.4
553	-7.4	-8.5
573	-6.7	-7.9
593	–	-7.2

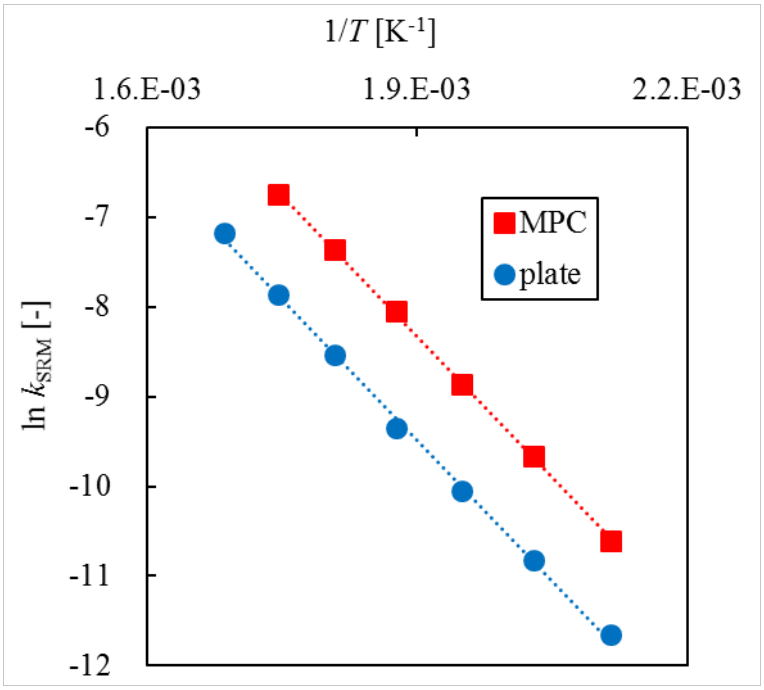

Fig. 3.4-4 Arrhenius plots of MPC and plate for the SRM reaction

3.4.2 Catalytic activity test for comparing between MPC and plate for the WGS reaction

For the WGS reaction, catalytic activity tests were carried out to compare the reactivity between MPC and plate. The plate was prepared by flattening the fins of Cu/ZnO/Al_2O_3-MPC. The rate-limiting step for the WGS reaction was also determined from "experiments with varying feed velocity of reactant gas". **Fig. 3.4-5** shows the reaction rate with a different feed velocity of reactant gas for the WGS reaction. Based on the results, a rate-limiting step was carefully determined. Fig. 3.4-5 suggested that the feed velocity of reactant gas did not affect the reaction rate beyond a certain value ($0.009 < u$ [m/s]), indicating that the external boundary film resistance did not affect the reactivity.

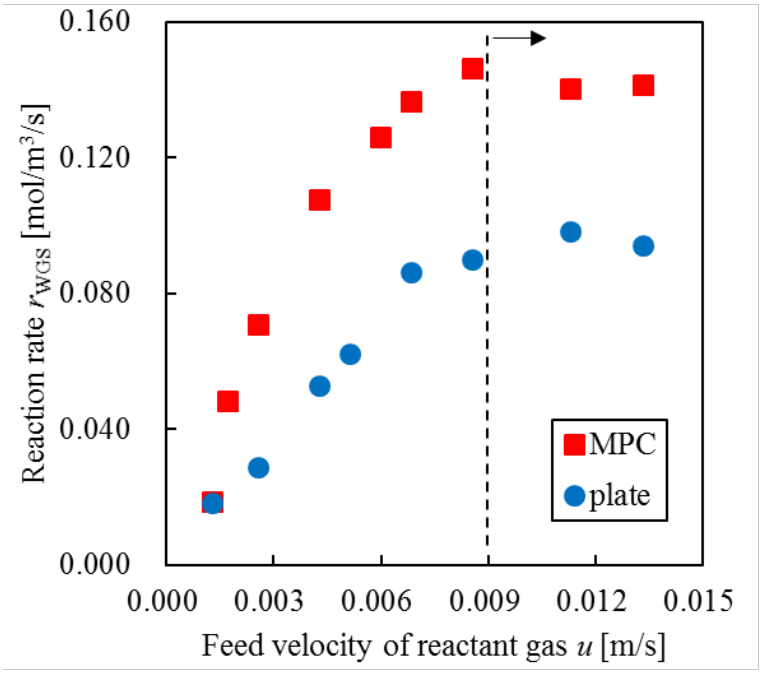

Fig. 3.4-2 The reaction rate with a different feed velocity of reactant gas for the WGS reaction

The results of the CO conversions are presented in **Table 3.4-3** and **Fig. 3.4-6**, and the Arrhenius plot as the reaction rate analysis are presented in **Table 3.4-4** and **Fig. 3.4-7**. The MPC showed a higher CO conversion than did the plate. The Arrhenius plot showed that the activation energies for both structures were similar (MPC: 43.9 kJ/mol; plate: 45.4 kJ/mol) and the frequency factor was increased when using MPC. The activation energy values obtained experimentally were comparable to those reported in literature using the same component catalysts [2-26, 2-27, 3-04]. This indicates that the rate-limiting step was a catalytic reaction under the experimental conditions of the WGS reaction in this study. The improvement in the frequency factor due to the MPC implied an increase in the frequency of contact between the reactants and the catalysts. Therefore, it was suggested that the reactivity was improved on the WGS reaction under a catalytic reaction rate-limiting step due just to the structure of MPC. These results of conversion and the reaction rate analysis and the condition was a catalytic reaction rate-limiting step, were similar to SRM.

Table 3.4-3 Conversions in the activity tests on WGS using MPC and plate

T [K]	CO conversion [%]	
	MPC	plate
453	26.0	13.2
473	46.1	23.9
493	63.6	37.9
513	75.9	51.0
533	82.3	57.9

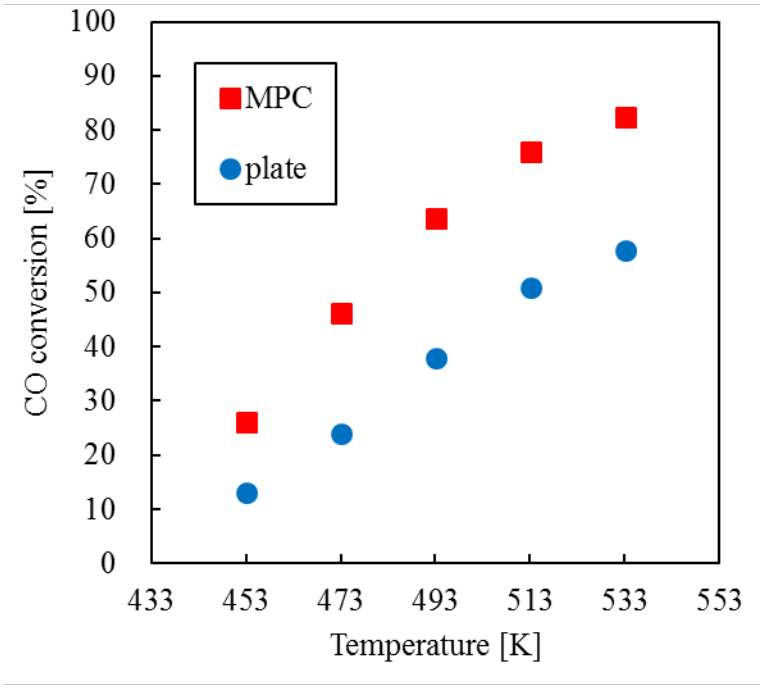

Fig. 3.4-6 Carbon monoxide conversions of MPC and plate for the WGS reaction

Table 3.4-4 Reaction rate analysis according to the Arrhenius equation for the WGS reaction

T [K]	ln k_{WGS} [-]	
	MPC	plate
453	-8.9	-9.7
473	-8.2	-9.0
493	-7.7	-8.5
513	-7.4	-8.1
533	-7.2	-7.9

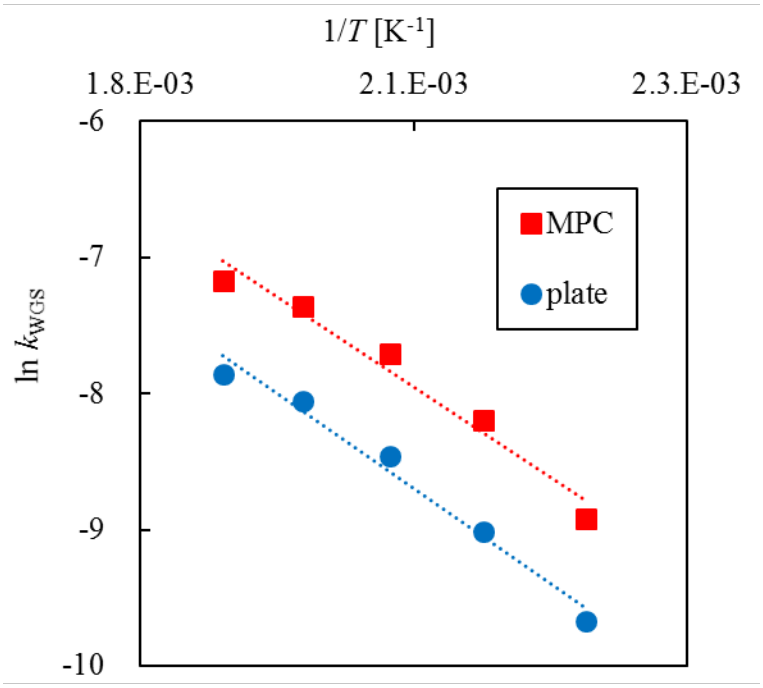

Fig. 3.4-7 Arrhenius plots of MPC and plate for the WGS reaction

3.4.3 Catalytic activity test for comparing between MPC and plate for CHC reaction

For the CHC reaction, catalytic activity tests were carried out for comparing the catalytic activities of MPC and plate. The plate was prepared by flattening the fins of Pt/Al_2O_3-MPC. The rate-limiting step for the CHC reaction was also determined from "experiments with varying feed velocity of reactant gas". **Fig. 3.4-8** shows the reaction rate with a different feed velocity of reactant gas for the WGS reaction. Based on the results, a rate-limiting step was carefully determined. Fig. 3.4-8 suggested that the feed velocity of reactant gas affected the reaction rate ($0.040 < u < 0.20$ m/s), indicating that the external boundary film resistance affected the reactivity. In all the experiments for CHC reaction in this study, the conditions of reactant gas feed velocity were set such that the external mass transfer resistance affected the reactivity.

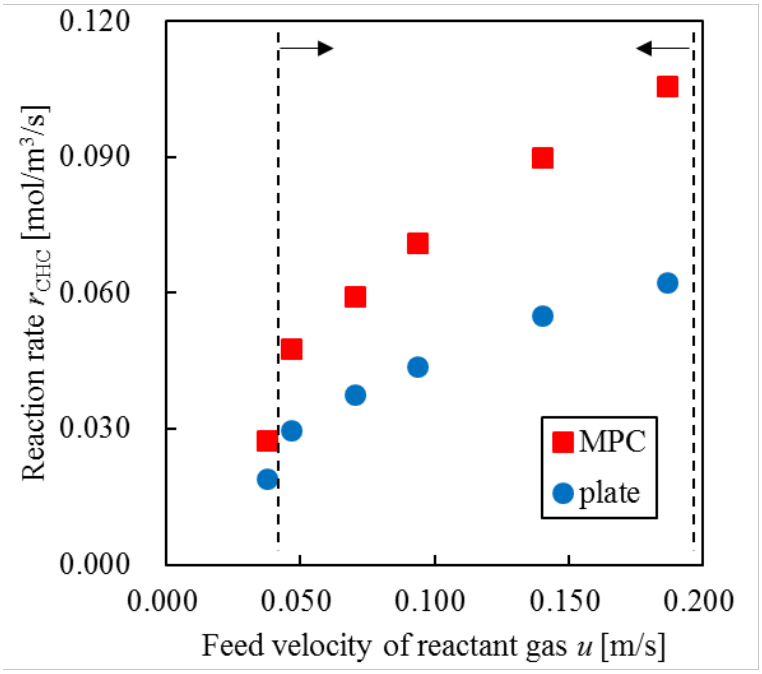

Fig. 3.4-8 The reaction rate with a different feed velocity of reactant gas for the CHC reaction

The results of hydrogen conversion are presented in **Table 3.4-5** and **Fig. 3.4-9**, and the Arrhenius plots as the reaction rate analysis are presented in **Table 3.4-6** and **Fig. 3.4-10**. The MPC showed a higher hydrogen conversion than did the plate. The catalytic activities in this case were similar to those observed for the SRM and WGS reactions; MPC was superior to the plate in terms of both the conversion and reaction rate analysis. Thus, the activation energies for both structures were similar (MPC: 11.1 kJ/mol; plate: 10.1 kJ/mol), and the frequency factor increased when using MPC. It was identified that the rate-limiting step of the CHC reaction in this study was influenced by an external mass transfer because the values of the apparent activation energy calculated from the experiments were similar to those reported in the literature [3-05, 3-06].

It was considered that the MPC structure was improved the reactivity of the CHC reaction under an external mass transfer rate-limiting step because the resistance of the external film mass transfer was reduced and the external mass transfer was promoted due just to the structure of MPC.

Table 3.4-5 Conversions in the activity tests on CHC using MPC and plate

T [K]	Hydrogen conversion [%]	
	MPC	plate
373	58.4	45.5
393	66.4	51.5
413	74.8	58.9
433	77.1	61.9
453	81.1	64.8

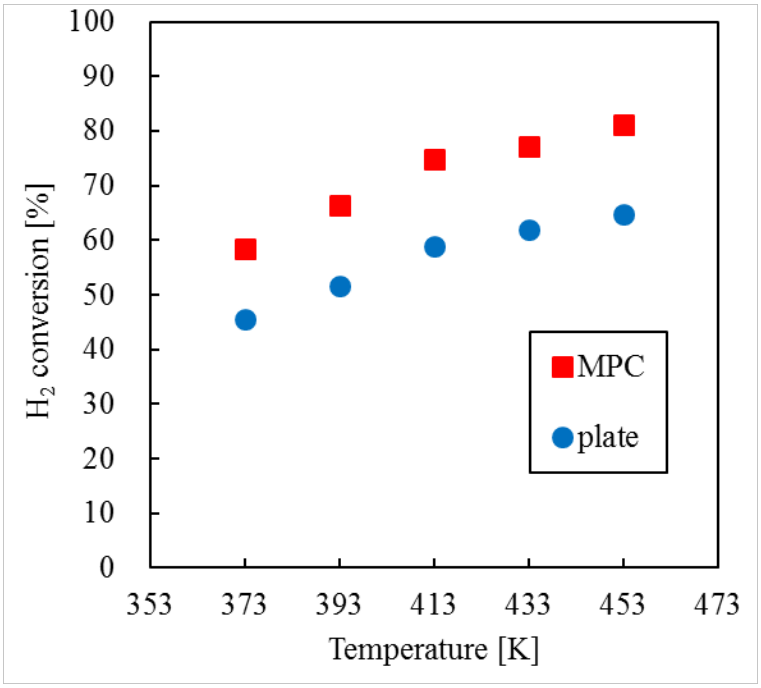

Fig. 3.4-9 Hydrogen conversions of MPC and plate for the CHC reaction

Table 3.4-6 Reaction rate analysis according to the Arrhenius equation for the CHC reaction

T [K]	ln k_{CHC} [-]	
	MPC	plate
373	-3.9	-4.3
393	-3.7	-4.1
413	-3.4	-3.9
433	-3.4	-3.8
453	-3.2	-3.7

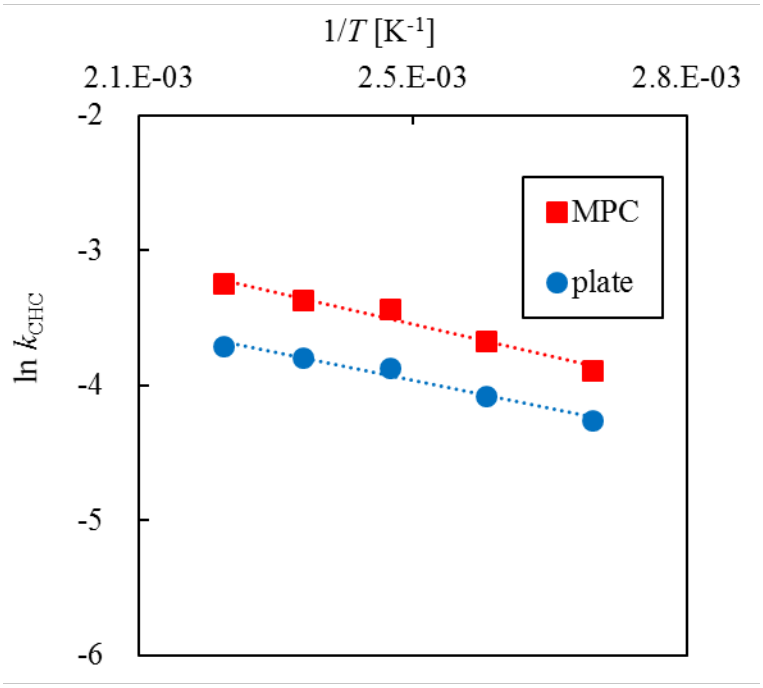

Fig. 3.4-10 Arrhenius plots of MPC and plate for the CHC reaction

3.4.4 Discussion of the reactivity improvement

First, the factors for the reactivity improvement due to the structure of MPC for SRM and WGS reactions under a catalytic reaction rate-limiting step shown in Subsection 3.4.1 and 3.4.2 were discussed. It showed that the frequency factor increased in MPC when both structures were compared.

According to the molecular collision theory, a frequency factor is generally expressed as a product of the collision frequency *Z*, the steric factor *P*, between the reactant molecules and the catalyst active site, and the fraction of collisions with enough energy *f* (**Eq. 3.4-2** and **Eq. 3.4-3**). The frequency factor in the Arrhenius equation (Eq. 3.4-1) is the product of the collision frequency *Z* and the steric factor *P* (**Eq. 3.4-4**). The collision frequency *Z* is the rate at which molecules collide and the steric factor *P* is the probability of the reactant molecules colliding with the right orientation and positioning to achieve a product. In other words, the frequency factor k_0 is the frequency of total collisions that collide with the right orientation.

$$k = Z \cdot P \cdot f \qquad (\mathbf{Eq.\,3.4-2})$$

$$f = \exp\left(-\frac{E}{\mathrm{R}T}\right) \qquad (\mathbf{Eq.\,3.4-3})$$

$$k_0 = Z \cdot P \qquad (\mathbf{Eq.\,3.4-4})$$

An increase in a frequency factor means an increase in a number of active collision molecules and a steric factor. Due to a change in flow pattern caused by the catalyst structure, a number of collisions between the reactant molecules and the catalyst metals or the steric factor increases, thus improving reactivity under a rate-limiting step of a chemical reaction. So, the frequency factor increased just due to the catalyst structure as shown in Fig. 3.4-4 and Fig. 3.4-7. In other words, the structure of the MPC improved the reactivity in a catalytic reaction rate-limiting step by improving a number of active collision molecules and a steric factor between the reactants and the catalyst, which led to an increase in a frequency factor.

Here, I confirmed whether the internal diffusion of the catalyst layer affected the overall reaction rate. The

modified Weisz modulus Φ_{n}, which doesn't include the true reaction rate constant, is defined by the following equation [3-07].

$$\Phi_{\mathrm{n}} \equiv m^2\eta = \left(\frac{\mathrm{V_{cat}}}{\mathrm{S_{cat}}}\sqrt{\frac{\mathrm{n}+1}{2}\times\frac{\rho_{\mathrm{cat}}k_{mn}C_{\mathrm{AS}}^{\mathrm{n}-1}}{D_{e\mathrm{A}}}}\right)^2 \times \frac{(-r_{\mathrm{A}m})}{k_{mn}C_{\mathrm{AS}}^{\mathrm{n}}}$$

$$\Phi_{\mathrm{n}} = \frac{\mathrm{n}+1}{2}\times\frac{\mathrm{V_{cat}^2}\rho_{\mathrm{cat}}(-r_{\mathrm{A}m})}{\mathrm{S_{cat}^2}D_{e\mathrm{A}}C_{\mathrm{AS}}} < 0.1 \qquad (\mathbf{Eq.\,3.4-5})$$

m : Generalized Thiele modulus, η : Catalyst effectiveness factors, n : Reaction order,
$\mathrm{V_{cat}}$: Catalyst volume, $\mathrm{S_{cat}}$: Catalyst surface area, ρ_{cat} : Catalyst density,
$r_{\mathrm{A}m}$: Reaction rate per catalyst loading, $D_{e\mathrm{A}}$: Effective diffusion coefficient, C_{AS} : Reactant concentration

We estimated the effective diffusion coefficient $D_{e\mathrm{A}}$. The diffusion in the pores was Knudsen diffusion dominated since the ratio of pore radius r_e to mean free path λ_{A} was smaller than 0.1. The effective diffusion coefficient in the Knudsen diffusion region $D_{K\mathrm{A}}$ were then calculated, and the effective diffusion coefficient $D_{e\mathrm{A}}$ and the modified Weisz modulus Φ_{n} were calculated. Since the value of the modified Weisz modulus Φ_{n} was sufficiently small in all conditions under a rate-limiting step of a catalytic reaction, the catalyst effectiveness factors were almost 1, confirming that the reaction conditions were such that the influence of internal diffusion was ignored. Therefore, it was insisted that the frequency of effective collisions between the reactant molecules and the catalyst active sites (frequency factor) was improved due to the structure of MPC.

Next, the factors that led to improved reactivity due to the structure of the MPC for the CHC reaction under an external mass transfer rate-limiting step shown in Subsection 3.4.3 were discussed. It was suggested that the structure of MPC promoted an external mass transfer under that reaction conditions. Generally, the larger the Sherwood number (Sh), which is positively correlated with mass transfer Péclet number ($\mathrm{Pe_M}$), the lower the external film mass transfer resistance [2-12]. In other words, the increase in $\mathrm{Pe_M}$ around the catalysts due to the structure of MPC can be evaluated to provide the improvement in reactivity, this investigation was conducted in chapter 4. It was expected that convection around the catalyst was promoted due to the structure of MPC since $\mathrm{Pe_M}$ is the ratio of the convection time and diffusion time, and therefore, the structure of MPC was expected to promote external mass transfer.

3.4.5 Evaluation of the turnover frequency (TOF)

The use of MPC was shown to improve the reactivity compared to plate for all reactions, but the effect of reactivity improvement was different for the SRM and WGS reactions under a catalytic reaction rate-limiting step and the CHC reaction under an external mass transfer rate-limiting step. Therefore, the turnover frequency (TOF), which is generally defined as the moles of reactant converted per unit time per mole of active catalytic sites, was calculated and compared with that of the plate under each condition to quantitatively evaluate the effect of reactivity improvement due to the structure of MPC. I focused on the TOF as having a meaning similar to that of "reactant-catalyst frequency factor". The TOF was calculated using **Eq. 3.4-6** [3-08 – 3-11], where M_S was measured by H_2 pulse titration analysis. The effect of reactivity improvement was evaluated for each reaction temperature as the lowest temperature i.e., lowest temperature (LT), middle temperature (MT), and highest temperature (HT) of each reaction. The results are presented in **Table 3.4-7** and **Fig. 3.4-11**.

As shown in Fig. 3.4-11, for the CHC reaction, the effect of reactivity improvement when using MPC, represented as the TOF ratio was almost constant, independent of the reaction temperature. For the WGS and SRM reactions under a catalytic reaction rate-limiting step, it was clarified the effect of improving reactivity tended to get larger at lower temperatures. It was because the frequency of contact between the reactants and the catalyst increased at lower temperatures due to the MPC structure. In this dissertation, it was realized that the evaluation of the increase in the frequency factor as the effect of reactivity improvement by evaluating the TOF ratio.

$$\mathrm{TOF}\ [/\mathrm{h}] = \frac{F_{\mathrm{i}}\ [\mathrm{mol/h}]\ \times x_i\ [-]}{W\ [\mathrm{g}] \times M_s\ [\mathrm{mol/g}]} \qquad (\mathbf{Eq.\ 3.4-6})$$

Table 3.4-7 TOF ratio calculated for each reaction

Temperature	CHC	WGS	SRM
LT	1.28	1.97	2.96
MT	1.27	1.68	2.62
HT	1.25	1.42	1.36

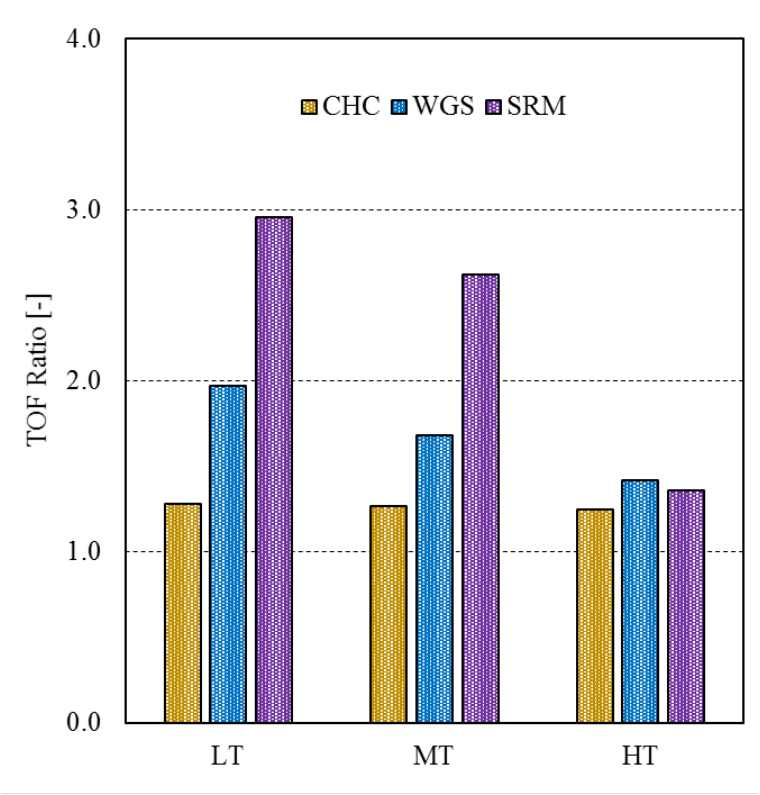

Fig. 3.4-11 TOF Ratio calculated for each reaction

The effect for the SRM and WGS reactions was larger than that for the CHC reaction. Although each reaction had different reaction conditions such as catalyst species, feed gas, or reaction temperature, I focused on the rate-limiting step in this study. Moreover, the effect of reactivity improvement for the SRM reaction was larger than that of the WGS reaction. A simple comparison of the effect between both reactions under a catalytic reaction rate-limiting step was not appropriate because of the different reaction conditions described above. Since the adsorption of a reactant molecule on an active sites of the catalyst metal has a suitable orientation, it was considered that the adsorption probability and adsorption capacity due to the complexity of the reactant molecules contribute to the effect of reactivity improvement for both reactions. Therefore, a detailed comparison of the effect for both reactions will be achieved by thermodynamic studies, such as measuring the adsorption capacity of the reactant molecules on the active sites, or by quantum mechanics studies, such as first-principles calculation of the relation between the reactant molecules and the active sites.

3.5 Conclusions of chapter 3

MPC was applied to the SRM, WGS, and CHC reactions, and the catalytic activity tests for comparing the reactivity to the unprocessed plate catalyst were carried out. MPC showed higher conversions than plate for all reactions, and reaction rate analysis according to the Arrhenius equation showed that there was no change in a rate-limiting step dependent on the reaction temperature and the activation energy was similar in both structures of MPC and plate for each reaction. Furthermore, the results of the reaction rate analysis revealed that the frequency factor was increased by the structure of MPC, suggesting that the contact frequency between reactants and catalysts was improved by the structure. The reactivity of the SRM and WGS reactions was improved under a catalytic reaction rate-limiting step, and this factor was investigated in detail because it was never reported. It is generally known that a frequency factor is expressed as a product of a number of collision molecules and a steric factor, and the improved a number of collision molecules or a steric factor due to the effect of the structure due to the structure of MPC was considered to provide the improvement of reactivity. On the other hand, for CHC reaction, the structure of MPC promoted the mass transfer around the catalyst and improved the reactivity for CHC reaction because the CHC reaction was an external mass transfer rate-limiting step.

The TOF, which is a general index of catalytic performance, was calculated and compared with that of the plate under each condition to quantitatively evaluate the effect of reactivity improvement due to the structure of MPC. For the CHC reaction, which is an external mass transfer rate-limiting step, the effect was almost constant independent of the reaction temperature. On the other hand, the effects of the SRM and WGS reactions, which were a catalytic reaction rate-limiting step, were getting larger at lower temperatures. It was suggested that the contact frequency between the reactants and the catalysts was promoted at lower temperatures due to the effect of the structure. In this study, it was realized that the evaluation of the increase in the frequency factor as the effect of reactivity improvement by evaluating the TOF ratio.

3.6 References

[3-01] A. Chougule, and R. R. Sonde; "Modelling and Experimental Investigation of Compact Packed Bed Design of Methanol Steam Reformer," International Journal of Hydrogen Energy 44 (2019) 29937–29945, https://doi.org/10.1016/j.ijhydene.2019.09.166.

[3-02] M. Turcoa, G. Bagnasco, C. Cammarano, P. Senese, U. Costantino, and M. Sisani; "Cu/ZnO/Al_2O_3 Catalysts for Oxidative Steam Reforming of Methanol: The Role of Cu and the Dispersing Oxide Matrix," Applied Catalysis B: Environmental 77 (2007) 46–57, https://doi.org/10.1016/j.apcatb.2007.07.006.

[3-03] J. K. Lee, L. B. Ko, and D. H. Kim; "Methanol Steam Reforming over Cu/ZnO/Al_2O_3 Catalyst: Kinetics and Effectiveness Factor," Applied Catalysis A: General 278 (2004) 25–35, https://doi.org/10.1016/j.apcata.2004.09.022.

[3-04] M. J. L. Ginés, N. Amadeo, M. Laborde, C.R. Apesteguía; "Activity and structure-sensitivity of the water-gas shift reaction over Cu–Zn–Al mixed oxide catalysts," Applied Catalysis A: General 131 (1995) 283–296, https://doi.org/10.1016/0926-860X(95)00146-8.

[3-05] K. M. Ogle, J.M. White; "The low temperature water formation reaction on Pt(111): a static SIMS and TDS study," Surface Science 139 (1984) 43–62, https://doi.org/10.1016/0039-6028(84)90007-4

[3-06] O. Deutschmann, R. Schmidt, F. Behrendt; "Interaction of transport and chemical kinetics in catalytic combustion of H_2/O_2 mixtures on Pt. From Transport Phenomena in Combustion," S.H. Chan (Ed.), Proceedings of the 8th international symposium on transport phenomena in combustion,, San Francisco, July 16–20, 1995, Volume 1, vol. 1 (1996) 166–175.

[3-07] P. B. Weisz, C. D. Prater; "Interpretation of Measurements in Experimental Catalysis," Advances in Catalysis 6 (1954) 143–196, https://doi.org/10.1016/S0360-0564(08)60390-9.

[3-08] S. Sengupta, K. Ray, G. Deo; "Effects of modifying Ni/Al_2O_3 catalyst with cobalt on the reforming of CH_4 with CO_2 and cracking of CH_4 reactions," International Journal of Hydrogen Energy 39 (22) (2014) 11462–11472, https://doi.org/10.1016/j.ijhydene.2014.05.058.

[3-09] R. Kumari, S. Sengupta; "Catalytic CO_2 reforming of CH_4 over $MgAl_2O_4$ supported Ni-Co catalysts for the

syngas production," International Journal of Hydrogen Energy 45 (2020) 22775–22787, https://doi.org/10.1016/j.ijhydene.2020.06.150.

[3-10] K. Ray, S. Sengupta, G. Deo; "Reforming and cracking of CH_4 over Al_2O_3 supported Ni, Ni-Fe and Ni-Co catalysts," Fuel Processing Technology 156 (2017) 195–203, https://doi.org/10.1016/j.fuproc.2016.11.003.

[3-11] A. K. Yadav, P.D. Vaidya; "A study on the efficacy of noble metal catalysts for butanol steam reforming," International Journal of Hydrogen Energy 44 (2019) 25575–25588, https://doi.org/10.1016/j.ijhydene.2019.07.191

Chapter 4

Investigation of Factors to Improve Reactivity due to the Structure of MPC and Proposal of Evaluation Index: Numerical Simulation

4.1 Abstract

In chapter 4, it was provided the results of the reactivity between MPC and plate by simulation. The simulation models were prepared referred to the experimental conditions and the values indicated by the experimental results, and these were confirmed to be models that showed similar results to the experimental results. Furthermore, the dimensionless number was proposed as the index to evaluate the effect of structure on reactivity improvement. It was suggested that the index was effective in evaluating the reactivity improvement using the structured catalysts under the condition of a catalytic reaction rate-limiting step.

4.2 Purpose

In this chapter, the physical phenomena around the catalysts were observed by numerical simulations using COMSOL Multiphysics software in order to investigate the factors contributing to the improvement in reactivity due to the catalyst structure. The model reactions on simulation to be calculated are the SRM reaction with the largest effect on the reactivity improvement due to the structure of MPC and the CHC reaction with the smallest effect. The simulation used a 2D simulation model for the calculations to confirm Streamline and a 3D simulation model for the investigation of all others. First, the validity of the simulation model was investigated by comparing the experimental and calculated conversion results for each reaction. Next, the dimensionless number was proposed as the index to evaluate the reactivity improvement due to the structure of MPC, and the effect of the reactivity improvement was explained by this index. Furthermore, the simulation models of the non-hole MPC, which have no holes in the MP structure but only fins, were prepared and the changes in the proposed index were evaluated in order to identify the structures to improve the reactivity of the MPC structure catalyst.

4.3 Methodology

COMSOL Multiphysics software was used to create a numerical simulation model in order to observe the physical phenomena around the catalyst, to obtain computational results similar to the experimental results. The overview of the prepared simulation models is shown in Figs. 2.6-1 and 2.6-2. The equations used for the calculations were described in Table 2.6-1. The initial values and boundary conditions of those models were set to be consistent with the experiments, and the parameters related to the reaction rate were derived from the experimental results. The calculation of the fluid properties, which depend on the composition of the fluid changing as the reaction proceeds, was calculated from Eqs. 2.6-1 - 2.6-6. The results from those simulation models were verified as mesh-independent study, and it was confirmed that the calculation results did not change regardless of the number of meshes. The features of the simulation were used to evaluate local physical phenomena and the fluid physical properties in the reactor, which cannot be derived from experimental results, to investigate the factors that improve the reactivity shown in the experiments. The structure of the structured catalyst was varied and the effect of the structure on the reactivity was examined. Details of these numerical simulation methods were provided in Section 2.6.

4.4 Results and Discussion

4.4.1 Validation of the reactivity improvement using MPC on simulation

A three-dimensional simulation was carried out to verify how the frequency factor was improved by the MP structure, and how the factor that affected the improvement became large at lower temperatures. The simulation was carried out using the COMSOL Multiphysics software (COMSOL Inc.) to model the reaction conditions around the catalyst. Three kinds of physics were used for the calculations: laminar flow, heat transfer, and dilute species transport; their representative equations and conditions are listed in Table 2.6-1. Detailed information and conditions for the simulation were described in Section 2.6. The model of the applied MPC catalytic reactor was shown in Fig. 2.6-1 and 2.6-2. Partial differential equations, such as the Navier–Stokes equation, were used to describe the continuity, momentum, mass, and energy conservations. The following assumptions were made for the simulation: ideal gas, non-compressible, steady physicality, laminar flow. In addition, the initial conditions, such as the flow rate, reactants concentration, and reaction temperature, and boundary conditions were matched to those in the catalytic activity tests; for the parameter of the reaction rate, the value calculated from the experimental results was used. The model was subsequently used to characterize and evaluate the reaction-coupled transport phenomena occurring within the reactor. The comparison results of the conversions for confirming the consistency between the constructed simulation models and experimental results for the SRM and CHC reactions are shown in **Fig. 4.4-1** and **4.4-2**. As shown in the figure, it was confirmed that the calculation results of the simulation models were valid with respect to the experimental results.

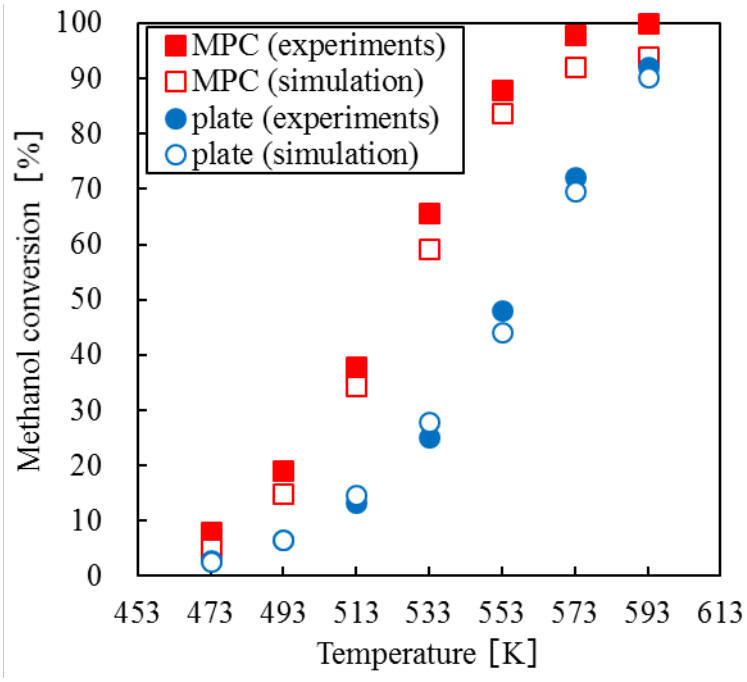

Fig. 4.4-1 Comparison of the conversions between the simulation and experiments for SRM reactions

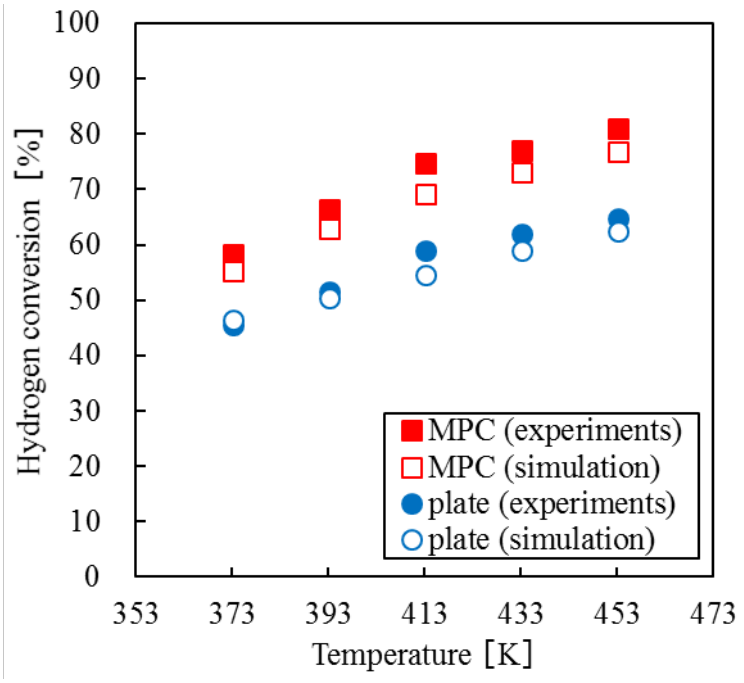

Fig. 4.4-2 Comparison of the conversions between the simulation and experiments for CHC reactions

Fig. 4.4-3 and **Fig. 4.4-4** show the streamlines around both the catalyst structures via simulation. The arrows in these figures indicate the flow direction and green area indicate the part of the catalyst. It was observed that the flow was disarranged by the fins and holes in Fig. 4.4-4, and recognized that the flow from the left side hit the MP fins and that direction was changed toward the holes. The change in the flow direction was also shown a similar trend in the latter part of the MP fins. In other words, it was shown that MPC have the ability to control mass transfer vectors and that MPC is suitable for Process Intensification of catalytic reaction processes.

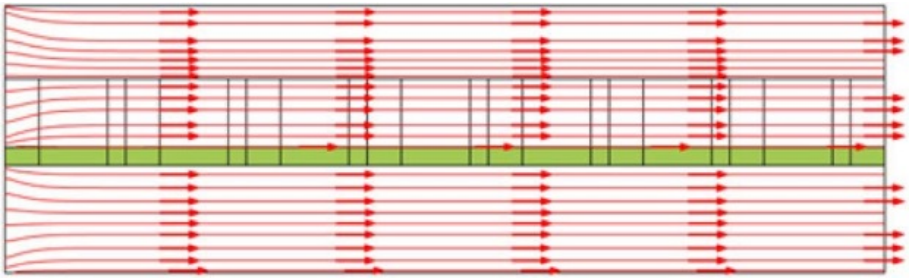

Fig. 4.4-3 Streamline (plate, Side view)

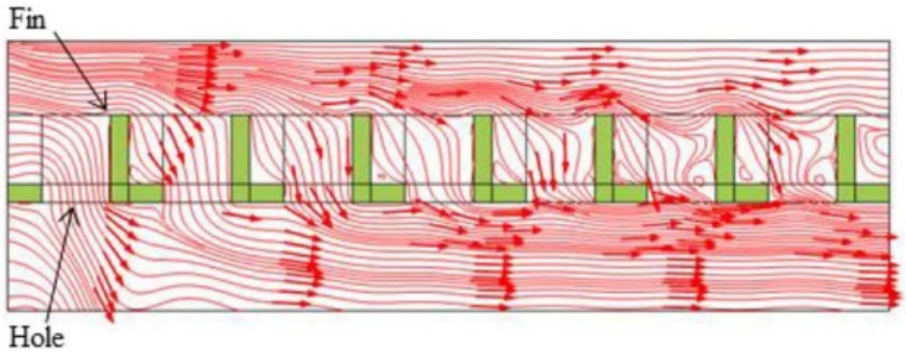

Fig. 4.4-4 Streamline (MPC, Side view)

4.4.2 Reactivity improvement under an external mass transfer rate-limiting step

As mention in Subsection 3.4.4, the improvement of the reactivity for the CHC reaction due to the structure of MPC was investigated by calculating the Péclet number for mass transfer (Pe_M) around the catalysts appropriate for evaluating the reactivity under an external mass transfer rate-limiting step. This is because the mass transfer flux N_i to the catalyst surface can be regarded as the reaction rate under an external mass transfer rate-limiting step. The mass transfer flux to the catalyst surface is represented by **Eq. 4.4-1**. The external mass transfer coefficient k_e in Eq. 4.4-1 is equivalent to the reaction rate constant k, and k_e depends on Sherwood number (Sh). Furthermore, Sh is generally known to be positively correlated with Pe_M. The numerical simulation results of Pe_M around the catalyst in the reactor are displayed in **Fig. 4.4-5** and **Fig. 4.4-6**. Pe_M is generally expressed in the ratio of convection and diffusion related to fluid transport phenomena and was calculated from **Eq. 4.4-3** with the simulation in this study. This index was evaluated over the direction of the MPC fin height in the reactor, considering the structure of MPC. The calculated distribution of Pe_M around the MPC at the temperature where the TOF ratio as the effect of reactivity improvement was calculated is shown in **Fig 4.4-7**. Under the activity test conditions of this study (calculation conditions), no significant change in Pe_M around the catalyst was observed with reaction temperature. This tendency obtained from simulating was similar to that of the TOF ratio, the results obtained from the experiment.

$$N_i = k_e(C_b - C_s) \quad (\mathbf{Eq.4.4-1})$$

$$k_e = \frac{\text{Sh}\,[-] \times \text{Diffusion coefficient}\,[\text{m}^2/\text{s}]}{\text{Length}\,[\text{m}]} \quad (\mathbf{Eq.4.4-2})$$

$$\text{Pe}_\text{M} = \frac{\text{Flow velocity}\,[\text{m}/\text{s}]}{\text{Diffusion coefficient}\,[\text{m}^2/\text{s}]\ /\ \text{Length}\,[\text{m}]} \quad (\mathbf{Eq.4.4-3})$$

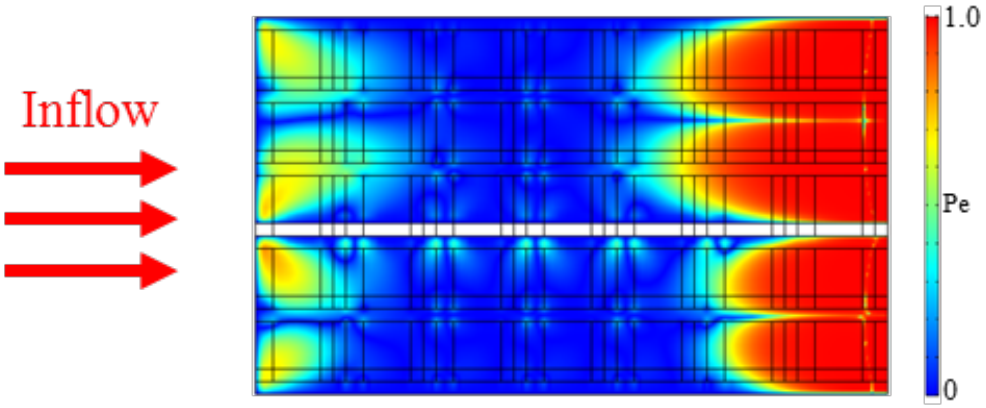

Fig. 4.4-5 Simulation results for Pe_M of plate (CHC reaction, 413 K)

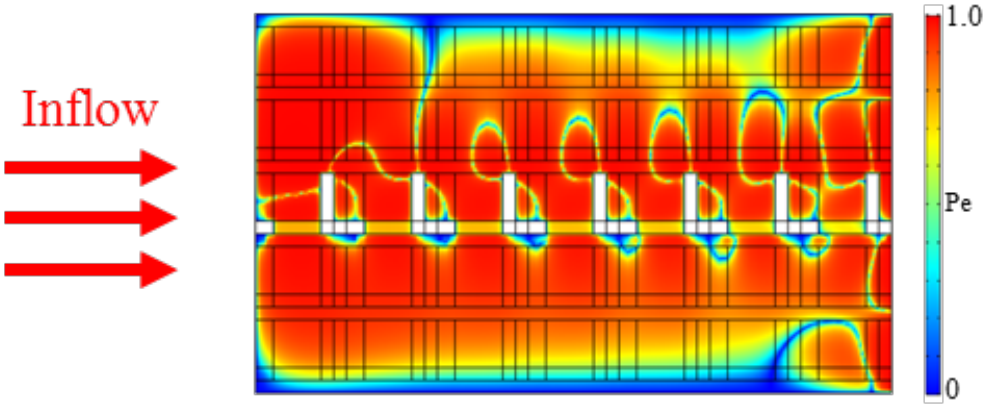

Fig. 4.4-6 Simulation results for Pe_M of MPC (CHC reaction, 413 K)

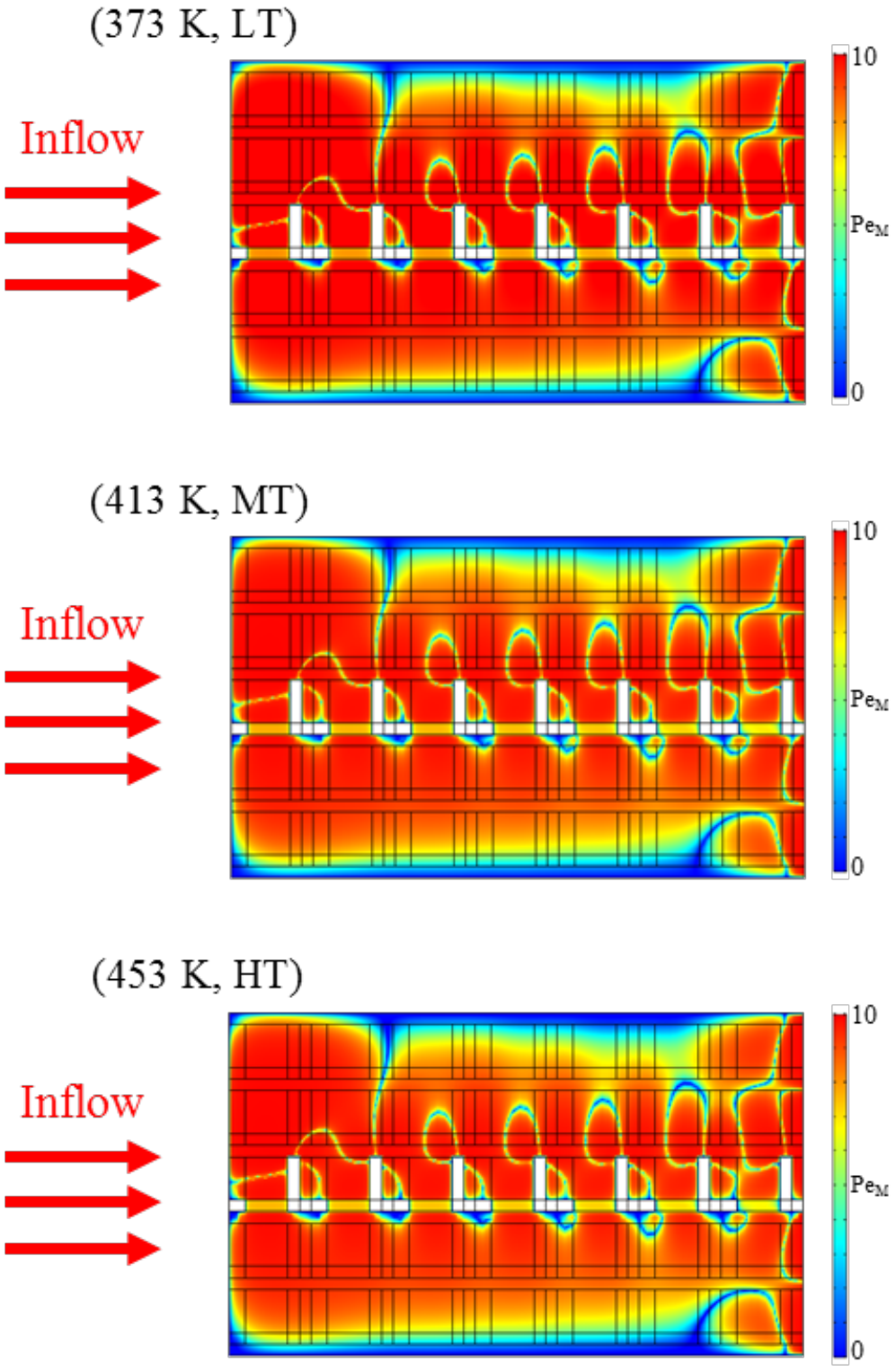

Fig. 4.4-7 Pe_M when changing the reaction temperature of the MPC for CHC reaction (373 K as LT, 413 K as MT, and 453 K as HT)

4.4.3 Proposal of evaluation index for reactivity improvement under a catalytic reaction rate-limiting step

One of the purposes of carrying out the numerical simulation was to investigate the factor by which the reactivity improved depending on the structure of MPC. The structure of MPC was expected to disarrange the fluid and then the reactivity was improved by it; they did not occur about the plate. For the CHC reaction under an external mass transfer rate-limiting step, it is not difficult to guess that the structure promoted the external mass transfer. On the other hand, I have to consider the reason for reactivity improvement under a catalytic reaction rate-limiting step. The reaction rate under a catalytic reaction rate-limiting step is not affected by an external mass transfer flux and therefore cannot be evaluated by Sh. Therefore, I proposed a quantitative evaluation index, the "Degree of convective mixing (Dcm [-])" to evaluate the flow changes due to the structure of the structured catalyst (**Eq. 4.4-4**). Dcm was defined as the ratio of the flux of mass transfer due to "convection" to the flux of mass transfer due to "convection and diffusion." This ratio showed that the index, Dcm became larger when the mass transfer was promoted by convection rather than by diffusion. This index was evaluated over the direction of the fin height in the reactor, considering the structure of MPC. Dcm indicated the proportion of mass transfer flux due to convection caused by the catalytic structure and evaluates the effects of the structure under a catalytic reaction rate-limiting step.

$$\mathrm{Dcm} = \frac{\text{Convective mass flux } [\mathrm{mol/m^2 s}]}{\text{Convective mass flux } [\mathrm{mol/m^2 s}] + \text{Diffusive mass flux } [\mathrm{mol/m^2 s}]} \quad (\mathbf{Eq.\,4.4-4})$$

The simulation results of Dcm of the MPC and plate at 533 K are displayed in **Fig. 4.4-8** and **Fig. 4.4-9**. As shown in these figures, it was obvious that the flux of mass transport due to convection was not produced around the plate, and the mass transfer in that direction was shown to be controlled by diffusion. On the other hand, it was observed that around the MPC, Dcm had a large value, especially at the parts where the fluid collided with the front of the first fin, and at the parts between the latter fins.

This means that the distribution of the effect of the structure around the MPC was depicted and the degree of change in flow direction due to the structure was evaluated. The frequency factor k_0 (the product of the collision frequency Z and the steric factor P) discussed in Subsection 3.4.4 increased, suggesting that reactivity was improved under the catalytic reaction rate-limiting step. Most of the purposes of the conventional use of structured catalysts for PI was to suppress the transition from a catalytic reaction rate-limiting step to an external mass transfer rate-limiting step when the reaction rate increases with increasing reaction temperature. It was a concept that was valid under the reaction conditions of an external mass transfer rate-limiting step, but not applicable to a catalytic reaction rate-limiting step such as this study. However, the results of this study provided that the effect of mixing the reactant fluids, as I call it the effect of the structure, can improve the overall reactivity by using the structured catalysts with MPC-like structures even under a catalytic reaction rate-limiting step. Furthermore, that effect was evaluated with the value of Dcm around the catalysts. In other words, it was suggested the proposal of the effective using method and the structure of structured catalysts from the numerical simulation for evaluating Dcm can be further improved the reactivity under a catalytic reaction rate-limiting step. It was a novel report for the field of process intensification of a catalytic reaction process using a structured catalyst.

The calculation results for the Dcm when changing the reaction temperature of the MPC for SRM reaction are displayed in **Fig. 4.4-10**. There were many places where the Dcm was larger around the MP at lower temperatures. The index "Dcm", which indicates the ratio of convective mass transfer to total mass transfer (sum of convection and diffusion), depends on temperature. This was because the flux of mass transfer caused by diffusion became small at low temperature, whereas that caused by convection due to the structure of the MP became relatively large. As described above, the similar tendency was shown by the results of experiments (Fig.3.4-11); the improvement ratio of the conversion was higher at lower temperatures, which suggested that the Dcm around the catalyst had an effect on the improvement in the reactivity, and the evaluation of the value of Dcm around the catalyst is an indicator to evaluate the improvement of reactivity under a catalytic reaction rate-limiting step.

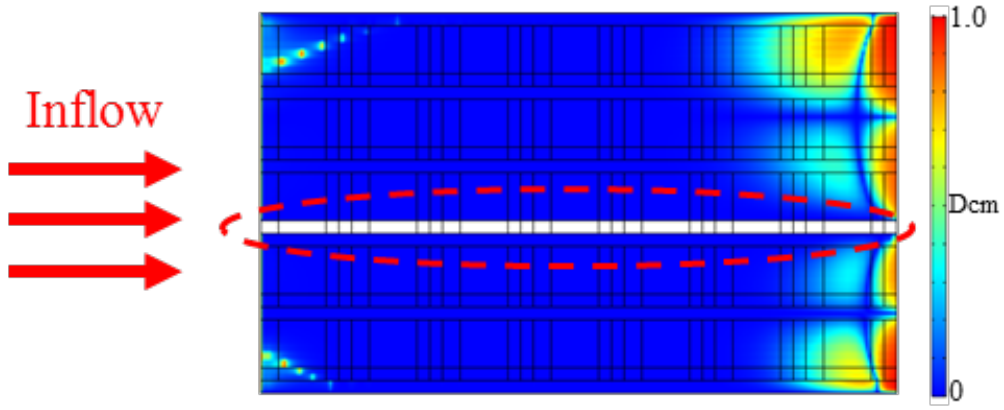

Fig. 4.4-8 Simulation results for Dcm of plate (SRM reaction, 533 K)

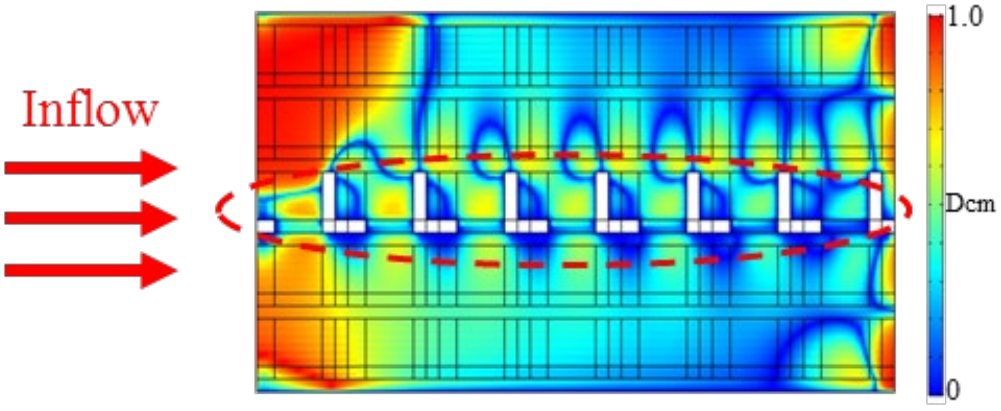

Fig. 4.4-9 Simulation results for Dcm of MPC (SRM reaction, 533 K)

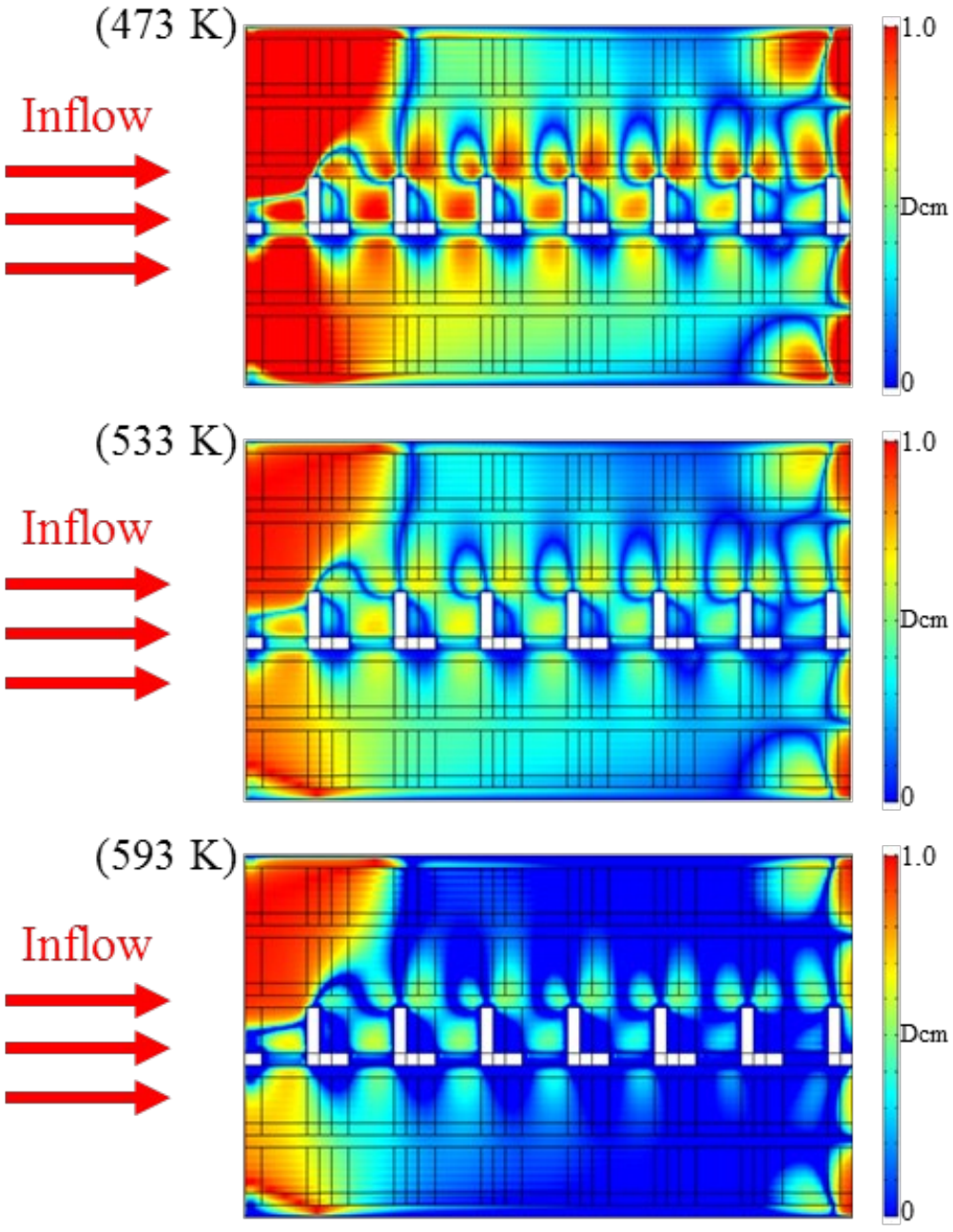

Fig. 4.4-10 Dcm when changing the reaction temperature of the MPC for SRM reaction (473 K as LT, 533 K as MT, and 593 K as HT)

4.4.4 Identification of structures to affect the reactivity

It was identified the structure in MPC required for improved reactivity by comparing the reactivity of MPC with that of non-hole MPC, which have no holes in the MP structure but only fins. The non-hole MPC was already reported in our research group to be less reactive than the MPC on experiments. It was discussed these results using Dcm in simulation. The streamline around the non-hole MPC is displayed in **Fig. 4.4-11**, and the result of Dcm at 533 K is displayed in **Fig. 4.4-12**. The change in fluid flow behavior was observed such that fluid hitting on the fins remained in the space between the fins owing to the no holes in Fig. 4.4-11. Although Dcm increased at the front of the first fin, there was no increase in the Dcm between the fins after that. Dcm around the non-hole MPC was larger than the plate, but smaller than the MPC. This suggests a correlation between Dcm values and reactivity.

These results implied that not only the fins but also the holes were indispensable for increasing Dcm, suggesting that they were necessary structures for improving the contact frequency of the reactants and the catalyst. In other words, the vector control of transport phenomena is possible using the structured catalysts with both fins and holes structures. The PI for the catalytic reaction process is realized because the effective use of structured catalysts with those structures increases the frequency factor and improves the reactivity even under a catalytic reaction rate-limiting step.

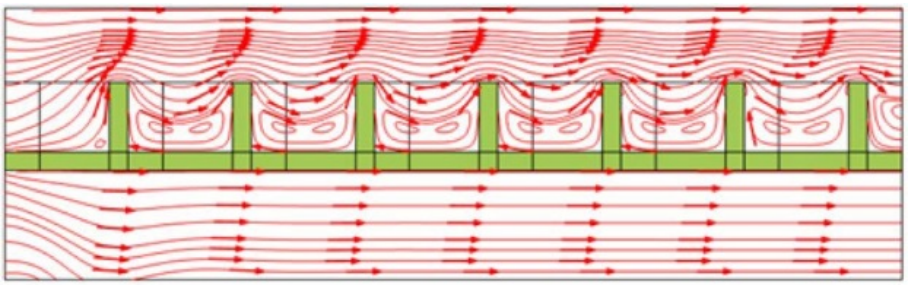

Fig. 4.4-11 Streamline (non-hole MPC)

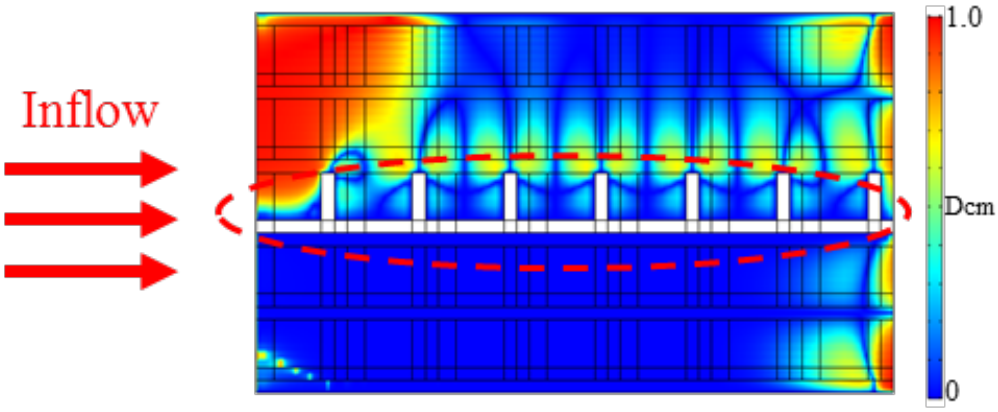

Fig. 4.4-12 Simulation results for Dcm of the non-hole MP (533 K)

4.5 Conclusions of chapter 4

In this chapter, it was investigated the factors on reactivity improvement when the use of MPC comparing with unprocessed plate-type catalysts with COMSOL Multiphysics software as numerical simulations. The SRM reaction, which had the largest reactivity improvement effect due to the structure of MPC, and the CHC reaction, which had a smaller effect, were adopted in the simulation models. The initial and boundary conditions were set to match the experimental conditions, and the parameters related to the reaction rate were calculated from the experimental results. The results of the calculations for both reactions by their prepared simulation models showed similar conversion to those of the experimental results, thus confirming the validity of the simulation model. The change in streamline due to the structure of MPC using the simulation models was evaluated, and it was demonstrated that the MPC is a suitable tool for PI, as it showed that the MPC is capable of vector control of transport phenomena.

For the CHC reaction, which was an external mass transfer rate-limiting step, the Pe_M around MPC was calculated with simulation to evaluate the overall reactivity. The results showed that the use of MPC significantly increased the value of Pe_M around MPC. It was suggested that the factors of the reactivity improvement when the use of MPC for the CHC reaction.

Dcm, which evaluates the effect of the structure, was proposed as the index to evaluate the reactivity improvement due to the structure of MPC under a catalytic reaction rate-limiting step. The Dcm was defined as the ratio of the mass transfer flux due to convection caused by the catalytic structure to the mass transfer flux due to diffusion, with a higher value indicating that the changes in the reactants fluid flow were larger. Dcm was evaluated in the direction of MPC fin height, considering the structure of MPC. Therefore, Dcm was found to be almost zero around the plate. On the other hand, Dcm around the MPCs was found to be larger in front of or behind the MPC fins. It was suggested that the factor of the reactivity improvement when the use of MPC for the SRM reaction. For the WGS reaction, it was the same reason for the reactivity improvement when MPC was used because a rate-limiting step was the same as the SRM reaction. In addition, numerical simulations were

performed for the SRM reaction at different reaction temperatures in order to investigate the tendency of larger TOF ratios at lower temperatures as the effect of the reactivity improvement under a catalytic reaction rate-limiting step presented in Subsection 3.4.5 The evaluation of Dcm at each reaction temperature showed that the Dcm values around MPC were higher at lower temperatures, indicating good accordance between the calculated and experimental results. In other words, it was suggested that Dcm is a suitable index for evaluating the reactivity of structured catalysts such as MPC under a catalytic reaction rate-limiting step. It was a novel report for the field of process intensification of a catalytic reaction process using a structured catalyst.

Finally, the simulation model was prepared for the non-hole MPC and its streamlines and Dcm were evaluated. The streamlines and the value of Dcm around MPC indicated that the effect of the structure was small because there were no holes, and the reason for the decreased reactivity of the non-hole MPCs by experiments was verified. In other words, it was suggested that not only the fins but also the holes are important for improving the reactivity due to the structure of MPC.

Rate-limiting step	External mass transfer	Catalytic reaction
Factors of the reactivity improvement using structured catalyst	Increase in the external mass transfer coefficient k_e	Increase in the frequency factor k_0
Evaluation index	Sh (Pe_M) The larger Pe_M is, the larger the external mass transfer is.	Dcm The larger Dcm is, the larger the effect of the structure is.

Fig. 4.4-13 Summary of chapter 4

Chapter 5

Investigation of the Effect of the Number of MPC Stacking on the Reactivity

5.1 Abstract

In chapter 5, it was provided the effect of changing the number of MPC stacking in the reactor was examined on experiments and simulations. The reactivity was obviously declined when the MPCs were densely stacked in the reactor under a catalytic reaction rate-limiting step. The effect of the number of MPC stacking on the reactivity tended to differ depending on a rate-limiting step. It was shown that the proposed unique index was capable of evaluating the reactivity tendency of the catalytic process under a catalytic reaction rate-limiting step condition. It was a valuable proposal for engineering as an index to evaluate the effect of using the structured catalysts on reactivity under a catalytic reaction rate-limiting step.

5.2 Purpose

The comparison of the MPC and a plate–type catalyst taken as the reaction surface of a monolithic type catalyst was performed on the SRM, WGS, and CHC reactions in chapter 3. A drastic improvement in the reactivity was reported. It was revealed from the results of the reaction rate analysis that the frequency factor, which affects the frequency of contact between the reactants and the catalysts due to the structure of MPC under a catalytic reaction rate-limiting step, significantly improved the reactivity. For the CHC reaction under an external mass transfer rate-limiting step, the external mass transfer was promoted due to the structure of MPC, and the reactivity was improved. It was suggested that the index, Dcm, was effective in evaluating the reactivity improvement using the structured catalysts under the condition of a catalytic reaction rate-limiting step.

In this chapter, considering an MPC for a chemical industrial application, I studied the effect of a multiple MPC stacked inside a reactor on the reactivity. Experiments and numerical simulations were performed. The number and position of the MPC were used as the parameters to evaluate the reactivity. In addition, the influence on the distribution of Dcm and Pe_M caused by the changes in the reaction environment around the MPC was also evaluated.

5.3 Methodology

The model reactions adopted the SRM and WGS reactions and CHC reactions for investigation of the effect of the number of MPC stacking. MPCs were prepared as $Cu/ZnO/Al_2O_3$-MPC for the SRM and WGS reactions, and Pt/Al_2O_3-MPC for CHC reaction as described in Section 2.2. The number of stacked MPCs was 1, 3, and 5. The catalytic reactors used were shown in Section 2.4, Fig. 2.4-1. The catalytic activity test conditions for each reaction were shown in Section 2.5. The effect of the reactivity improvement and tendency of that were investigated by calculating TOF ratio. Details of each experimental method were described in chapter 2.

Furthermore, the numerical simulation was conducted using COMSOL Multiphysics software to observe the physical phenomena around the MPC stacking. The overview of the prepared simulation models was shown in Fig. 2.6-1 and 2.6-2. The equations used for the calculations were described in Table 2.6-1. The results from those simulation models were verified as a mesh-independent study, and it was confirmed that the calculation results did not change regardless of the number of meshes. Moreover, the quantifications of the Dcm and Pe_M distribution around the MPCs in the reactor was conducted in simulations in order to evaluate the effect of changing the stacking method on reactivity. Details of these numerical simulation methods were provided in Section 2.6.

5.4 Results and Discussion

5.4.1 Effect of the number of MPC stacking on the reactivity for the SRM reaction

W/F is constant and the rate-limiting step is a chemical reaction, so it was predicted that a similar conversion can be obtained regardless of the amount of the catalyst in the activity test under a catalytic reaction rate-limiting step condition. However, when multiple MPCs were stacked in the reactor, it was expected that the effect of the structure would be promoted and the reactivity would be improved depending on the number of stacked MPC. To investigate the effect of the stacked MPCs, activity tests were carried out for the SRM reaction by orderly stacking MPCs in the reactor, and the effect of the number of stacked MPCs on the reactivity for the SRM reaction was examined. The stacking methods were such that the distances between all the adjacent catalysts were maximally similar. The number of stacked MPCs was 1, 3, and 5 under each condition, and these were referred to as “One”, “Three” and “Five,” respectively. The maximum number of MPC that could be stacked in the reactor was 5, and the stacked MPCs were densely packed, in that case. The images of MPC packing in the reactor under each condition for each number of stacked MPC samples are displayed in **Fig. 5.4-1**.

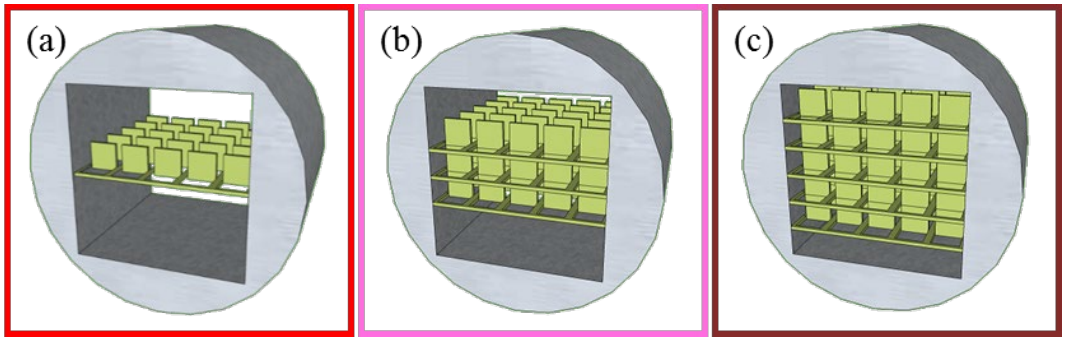

Fig. 5.4-1 Stacking method of the MPCs in the reactor (a) One, (b) Three, (c) Five

The activity tests were carried out under each condition, and the results of the methanol conversion are presented in **Table 5.4-1** and **Fig. 5.4-2,** and the Arrhenius plots as the reaction rate analysis are presented in **Table 5.4-2** and **Fig. 5.4-3**. It was provided that condition ”Three” had a higher conversion than condition “One”, whereas condition “Five” had a much lower conversion than condition “One”. It was confirmed that there was no change in the rate-limiting step in the temperature range under these stacking conditions; it was confirmed that a rate-limiting step was a catalytic reaction. This indicated that the effect of the structure was promoted and subsequently the reactivity was improved by the number of stacking, from the experimental results of condition “Three”. However, the results under condition “Five” showed that the reactivity was significantly reduced, suggesting that the densely packed MPCs in the reactor had a negative effect on the reactivity. Therefore, the reaction environment around the MPCs was observed using numerical simulation, because it was assumed that the MPCs packed in the reactor did not work uniformly.

The TOF ratio as the index of the effect of the reactivity improvement, as discussed in subsection 3.4.5, was then applied to the experimental results in this chapter when changing the number of MPC stacking for the SRM reaction. The results of the evaluation of them are displayed in **Table 5.4-3** and **Fig. 5.4-4**. Its value for condition “Three” was larger than that for condition “One”, which indicated the effect of MPC stacking when multiple MPCs were used under a catalytic reaction rate-limiting step because the catalytic activity tests were carried out under constant *W/F* comparative conditions. However, for condition “Five”, the TOF ratio as an effect of the reactivity improvement was obviously reduced. The TOF ratio was lower at the evaluation temperature HT because the high-temperature (HT) was a reaction environment that showed higher reactivity even in plate. Furthermore, the TOF ratio was found to be higher at lower temperatures for condition One and Three. On the other hand, the TOF ratio for condition Five was almost similar and small at all reaction temperatures conditions. It was implied that Dcm increased in reaction environments where the reactant diffusion rate was low at lower temperatures, resulting in an increase in the frequency of the contact between the reactants and catalyst by convection due to the structure of MPC for also these conditions.

Table 5.4-1 Conversions of (a) One, (b) Three, and (c) Five for the SRM reaction

T [K]	Methanol Conversion [%]		
	One (MPC)	Three	Five
473	8.0	7.6	3.2
493	19.1	19.2	8.1
513	37.8	39.2	18.5
533	65.7	70.3	37.0
553	87.9	91.4	64.1
573	98.0	99.2	91.3

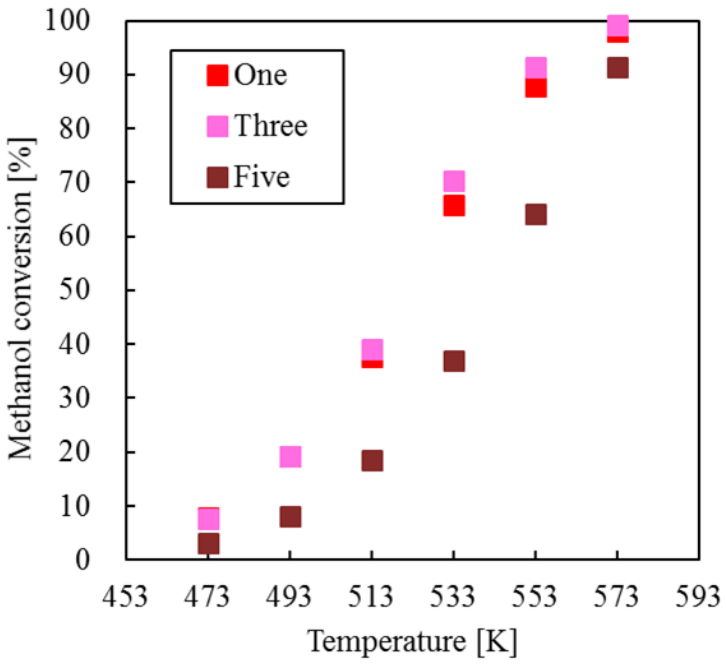

Fig. 5.4-2 Methanol Conversions of (a) One, (b) Three, and (c) Five for the SRM reaction

Table 5.4-2 Reaction rate constant of (a) One, (b) Three, and (c) Five for the SRM reaction

T [K]	ln k_{SRM} [-]		
	One (MPC)	Three	Five
473	-10.7	-10.7	-11.7
493	-9.7	-9.6	-10.7
513	-8.8	-8.7	-9.7
533	-7.9	-7.7	-8.8
553	-7.1	-6.9	-7.9
573	-6.4	-	-7.0

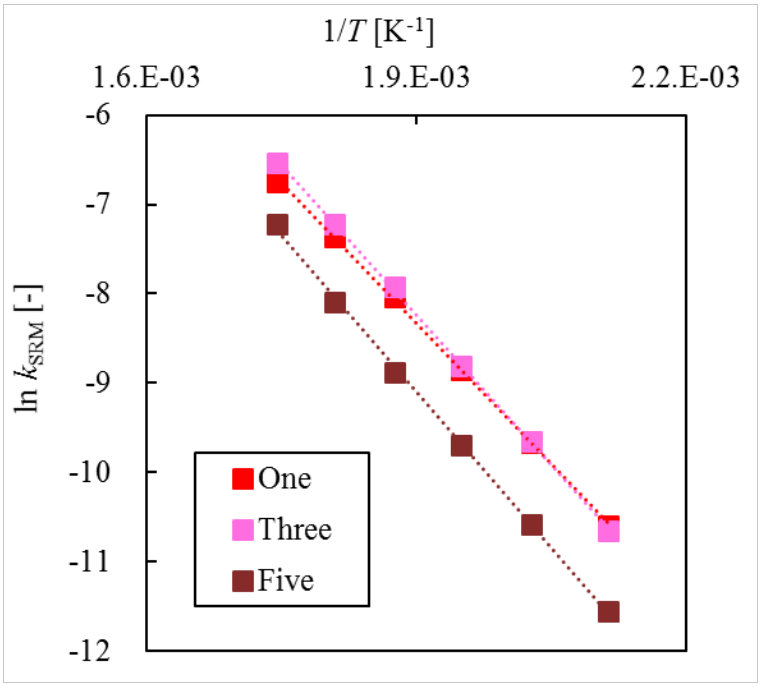

Fig. 5.4-3 Arrhenius plots of (a) One, (b) Three, and (c) Five for the SRM reaction

Table 5.4-3 TOF ratio for each stacking condition for the SRM reaction

Temperature	One (MPC)	Three	Five
LT	2.96	2.97	1.25
MT	2.62	2.80	1.48
HT	1.36	1.37	1.26

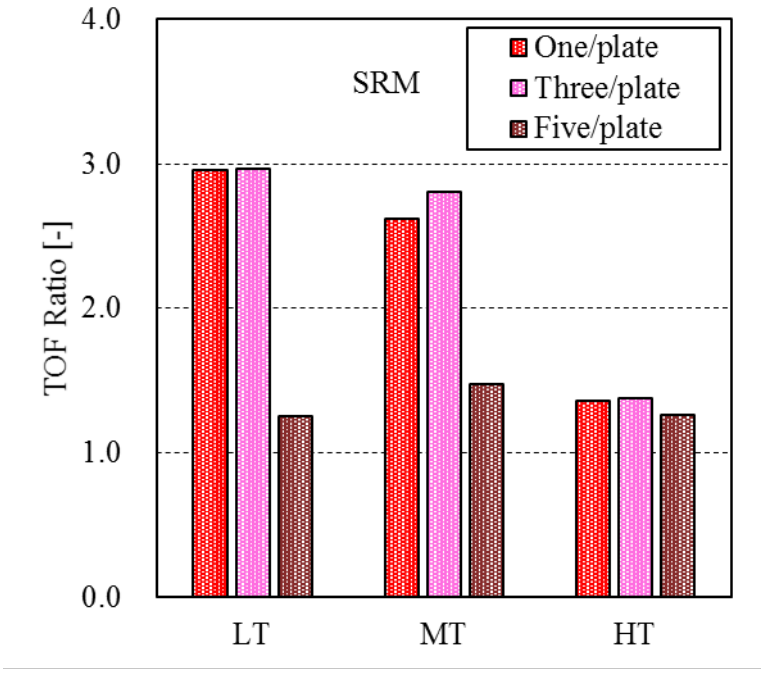

Fig. 5.4-4 TOF ratio when changing the number of MPC stacking for the SRM reaction

As the first result of the simulation, streamlines under conditions “Three” and “Five” are displayed in **Fig. 5.4-5 (b-1, c-1)**, to observe the changes in the fluid flow behavior around the MPCs due to the number of stacked MPCs. For condition “One”, the streamline was already shown in Fig. 4.4-4 because condition “One” was the same as the condition MPC in Chapter 3. In these figures, the reactant fluid in the reactor flowed from left to right, and the green area depicted the MPC parts. Under condition “One” and “Three,” the inflowing fluid hit the fins and flowed over the fins or in the direction of the holes in front of the fins. Furthermore, the flow direction was changed so that most of the fluid passed through the holes of the MPCs. In addition, for condition “Three”, the fluid that passed through the hole of MPC stacked upper flowed toward the fins of the MPC stacked lower, and it was expected to have a synergistic effect of adding the effect of the structure of stacking multiple MPCs to the effect of a single MPC. Specifically, it was remarkably displayed that the inflowing fluid flowed from the upper MPC of the stack to the lower MPC, as the reaction proceeded. These results demonstrated the vector control of fluid and that MPCs are suitable for PI.

However, under condition “Five,” it was presented that the change in the fluid flow from the upper to the lower MPC of the stack was smaller than that under condition “Three.” This was owing to the characteristic flow direction change due to the difference between the flow in the space where the MPC was not packed and the flow in the MPC stacked part under condition “Three.” It was assumed that the effect of the structure was smaller under condition “Five” because that difference was smaller when the MPCs was densely packed, the flow direction change was smaller.

The distribution of the Dcm under condition “Three” and “Five” at 533 K, to evaluate the effect of the structure, is displayed in **Fig. 5.4-6 (b-2, c-2)**. For condition “One”, the distribution of the Dcm was already shown in Fig. 4.4-9. The fluid flows from left to right in the figures, and the white area depicts the MPCs. It was demonstrated that the Dcm was larger around the MPCs under conditions “One” and “Three,” whereas obviously smaller as a whole stacking under condition “Five.” It was suggested that the effect of the structure was smaller, as shown by the streamline.

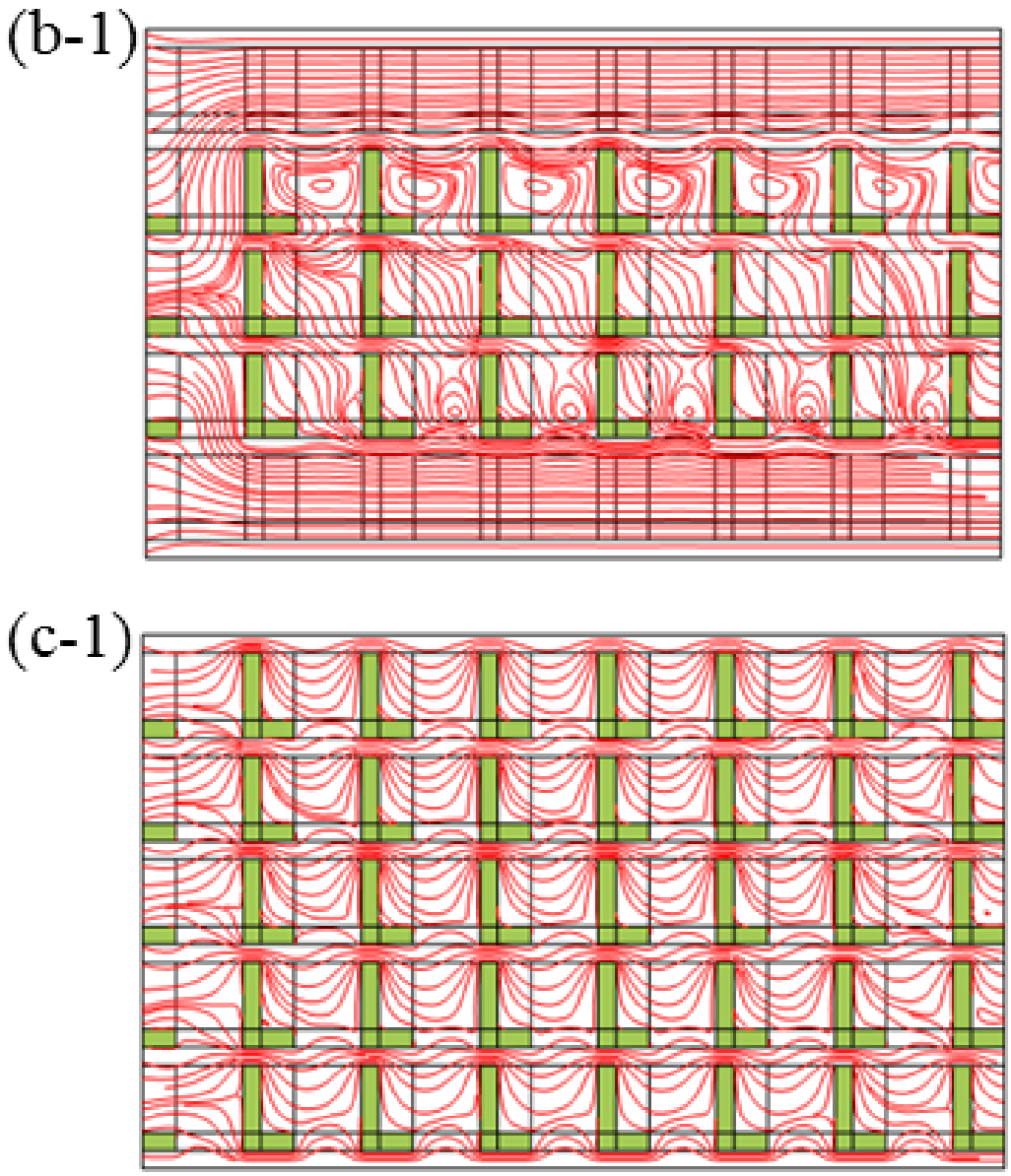

Fig. 5.4-5 Streamlines under condition “Three” and “Five”

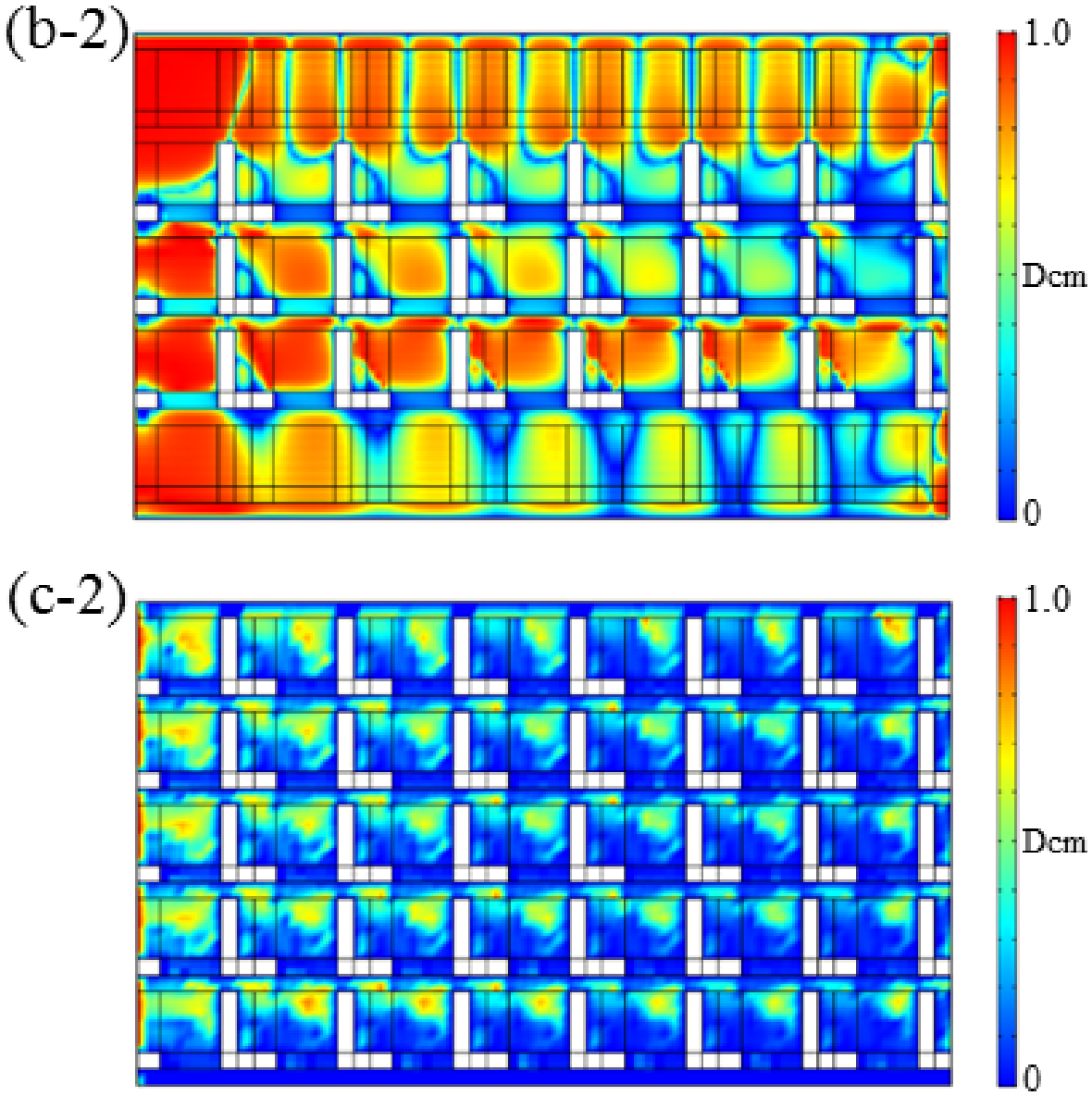

Fig. 5.4-6 Distribution of Dcm under condition “Three” and “Five” (533 K)

Moreover, the quantification of the Dcm distribution around the MPCs was conducted. The calculation domain to evaluate the Dcm quantitatively with simulation was around each packing MPC under the conditions respectively, not whole inside the reactor because the higher Dcm value around a catalyst means the improvement of the reactivity. For example, under the condition "One", it was evaluated the Dcm in the domain of the space volume based on the width, length, and height of one MPC. The designated domain for quantification of the Dcm around the MPCs under condition "Five" as an example is displayed in **Fig. 5.4-7.**

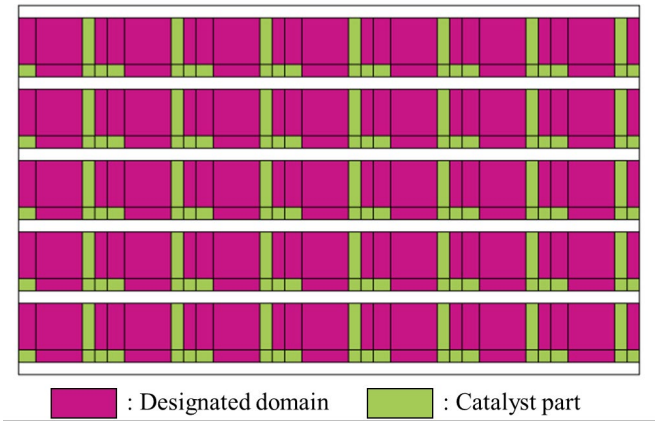

Fig. 5.4-7 Designated domain for quantification of the Dcm distribution

The quantitative evaluated value as $(Dcm)_{int}$ (**Eq. 5.4-1**) was obtained by dividing the integrated value of Dcm in each element, where the computational domain was minutely divided, by the space volume of the calculation domain to evaluate, and these values are listed in **Table 5.4-4**. It was found that the higher conversion in the experimental results, the larger $(Dcm)_{int}$ calculated by the simulation. The Dcm represents the ratio of the "mass transfer by convection" to the "total mass transfer" about reactants in the direction of the stacking. It is able to evaluate by Dcm the effect of the structure for the reaction environment around an MPC. That is, it became clear that it was possible to propose the stacking method when using multiple MPC to improve the reactivity by referring to the value of $(Dcm)_{int}$ with the numerical simulation.

$$(\mathrm{Dcm})_{\mathrm{int}} = \frac{(\text{Integrated value of Dcm in the designated domain})}{(\text{Volume of the designated domain for quantification})} \qquad (\mathbf{Eq.\ 5.4-1})$$

Table 5.4-4 $(Dcm)_{int}$ in conditions (a) One, (b) Three, (c) Five

Stacking Condition	(a) One	(b) Three	(c) Five
$(Dcm)_{int}$	0.49	0.60	0.21

The methanol conversion under the condition "Five" was significantly reduced. It was predicted for this result that the MPC stacking did not work uniformly. The distribution of the relative reactant concentration to the inflow reactant concentration (C/C_0) under each condition are depicted in **Fig. 5.4-8 (a-1, b-1, c-1)**. In these figures, the fluid flows from left to right and the white area depicts the MPCs. Under especially condition "Five," a remarkable reactant concentration distribution was confirmed from the upper layer to the lower layer of the stacking, which was the range indicated by the dashed arrow. This result exhibited that the reactant concentration around the MPCs in the lower layer was significantly smaller and that the reaction rate around that MPCs was lower than those in the upper layer under condition "Five." It was believed that the conversion reduced because the reaction rate was not uniform toward the direction in which the flow changed by the MPC stacking. The distribution of the reactant concentration occurred because the flow change was small in the direction of the stacking flowing into the lower layer.

In conventional particle-packed bed or monolithic-type catalytic reactors, the reactant flow in the radial direction of the reactor is uniformity distributed, so the distribution of reactivity by catalyst position is ignored. On the other hand, in a reactor that utilizes structured catalysts with directional flow changes, such as MPC, a concentration distribution in the radial direction of the reactor occurs due to the structure of the catalyst and the method it is stacked. Designing and controlling this distribution through structure and stacking methods will improve the reactivity of the structured catalytic reactors.

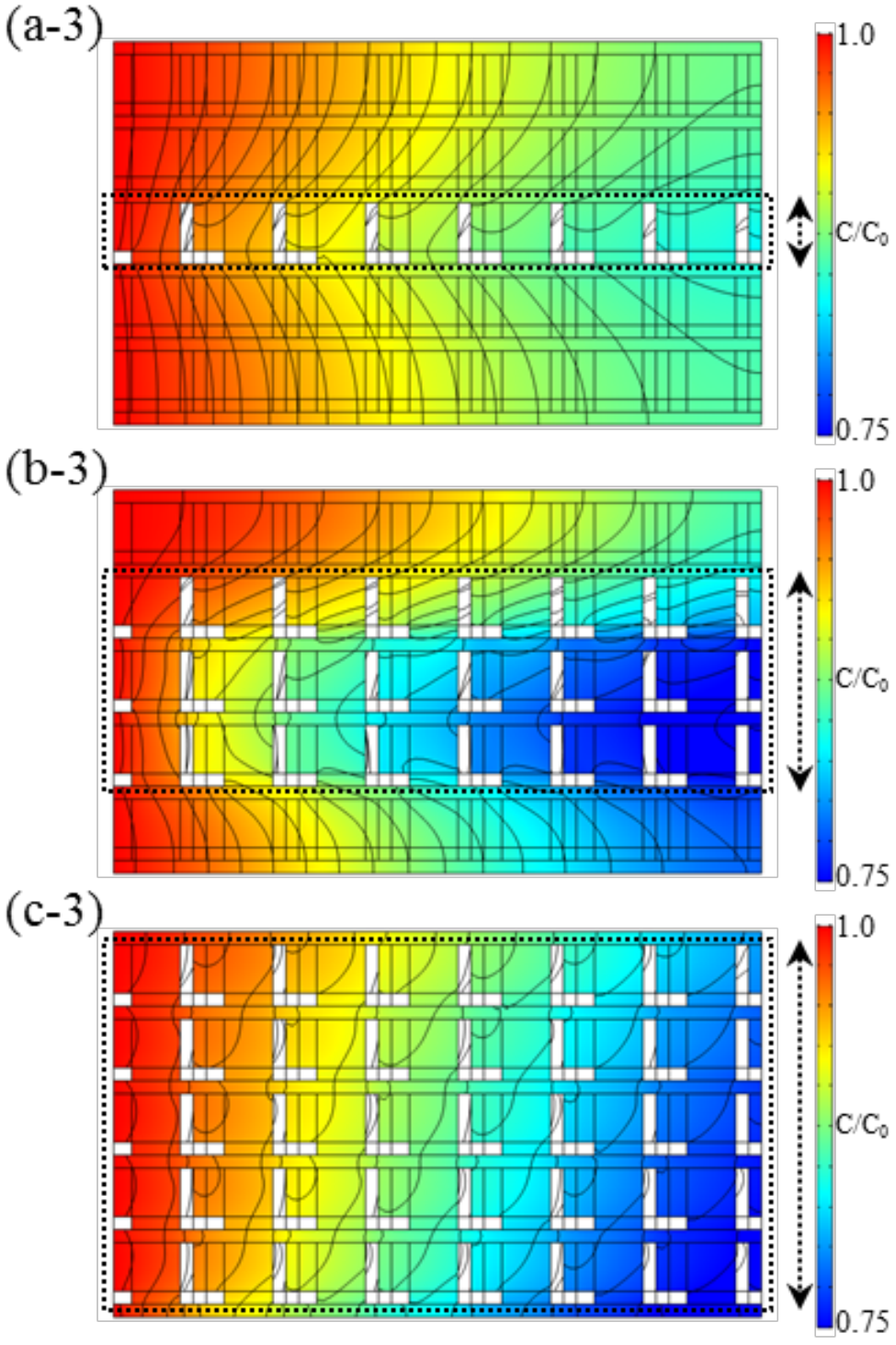

Fig. 5.4-8 Distribution of reactant concentration

5.4.2 Effect of the position of MPC in the stacking for the SRM reaction

Condition “Five” had a lower reactivity for the SRM reaction than condition “One;” therefore, the effect of the position of the MPCs on the reactivity was examined, to clarify the relationship between the MPC stacking and the reactivity in more detail. Only one layer in the five-stacking case was the MPC and the other four layers were replaced by the uncatalyzed MP, and activity tests were performed under the condition changed in the MPC position. It was previously ascertained that the uncatalyzed MP has no catalytic activity. The images of the packing in the reactor under each condition for the position of MPC are displayed in **Fig. 5.4-9 (d, e, f)**, and the condition are referred as “TOP,” “MIDDLE,” and “BOTTOM” as displayed in the figure. In addition, the activity test was performed in which the reactor of condition “TOP” was rotated 180° around the longitudinal direction of the reactor (“TOP180”) to deal with the influence of the temperature distribution due to biased heating. The methanol conversions are displayed in **Table 5.4-5** and **Fig. 5.4-10**, and the Arrhenius plots under each condition including the result of condition “One” for comparison are displayed in **Table 5.4-6** and **Fig. 5.4-11**.

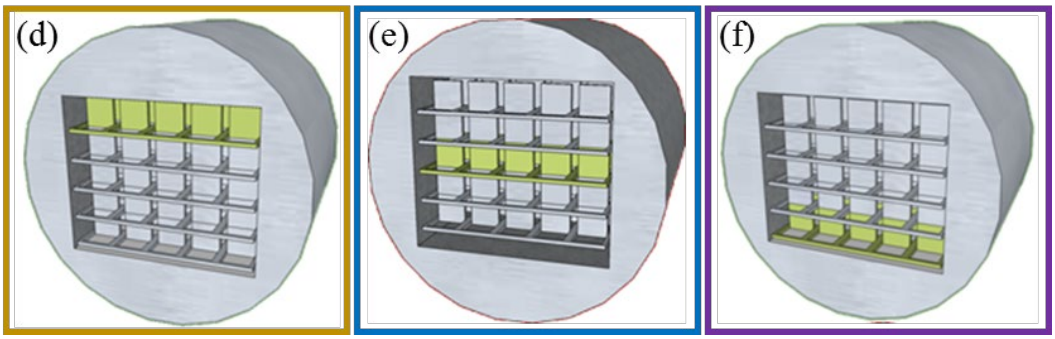

Fig. 5.4-9 Stacking method of the MPCs in the reactor (d) TOP, (e) MIDDLE, and (f) BOTTOM

Table 5.4-5 Conversions of (d) TOP, (e) MIDDLE, and (f) BOTTOM for the SRM reaction

T [K]	Methanol conversion [%]			
	TOP	TOP 180	MIDDLE	BOTTOM
473	5.9	8.0	–	4.8
493	22.4	20.1	14.6	12.0
513	41.3	39.1	31.0	23.7
533	69.3	70.5	57.5	45.0
553	90.2	90.9	80.8	71.2
573	99.0	97.9	95.6	90.7
593	100.0	100.0	100.0	97.5

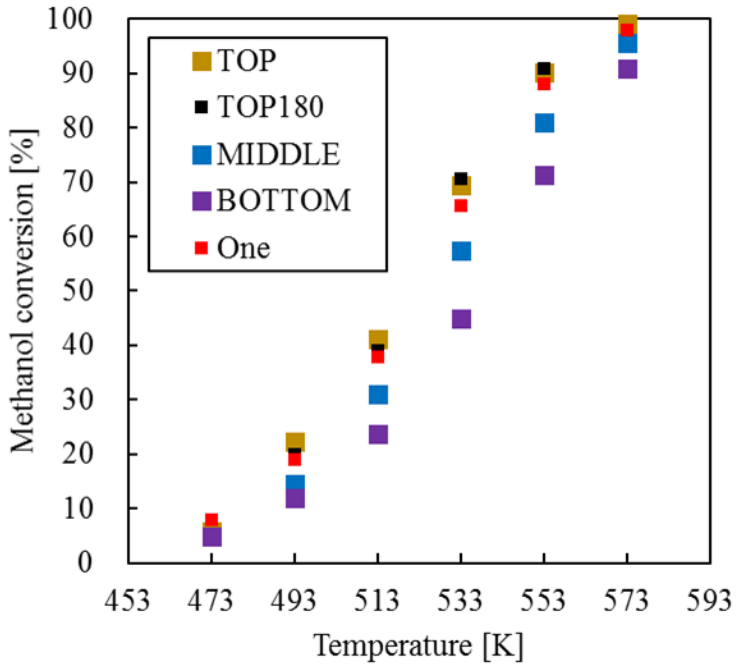

Fig. 5.4-10 Methanol conversions of (d) TOP, (e) MIDDLE, and (f) BOTTOM for the SRM reaction

Table 5.4-6 Reaction rate constants of (d) TOP, (e) MIDDLE, and (f) BOTTOM for the SRM reaction

T [K]	ln k_{SRM} [-]			
	TOP	TOP 180	MIDDLE	BOTTOM
473	-10.7	-10.7	–	-11.2
493	-9.5	-9.7	-10.0	-10.2
513	-8.7	-8.8	-9.1	-9.4
533	-7.8	-7.8	-8.2	-8.5
553	-7.0	-7.0	-7.4	-7.7
573	-6.3	-6.5	-6.7	-7.0
593	–	–	–	-6.5

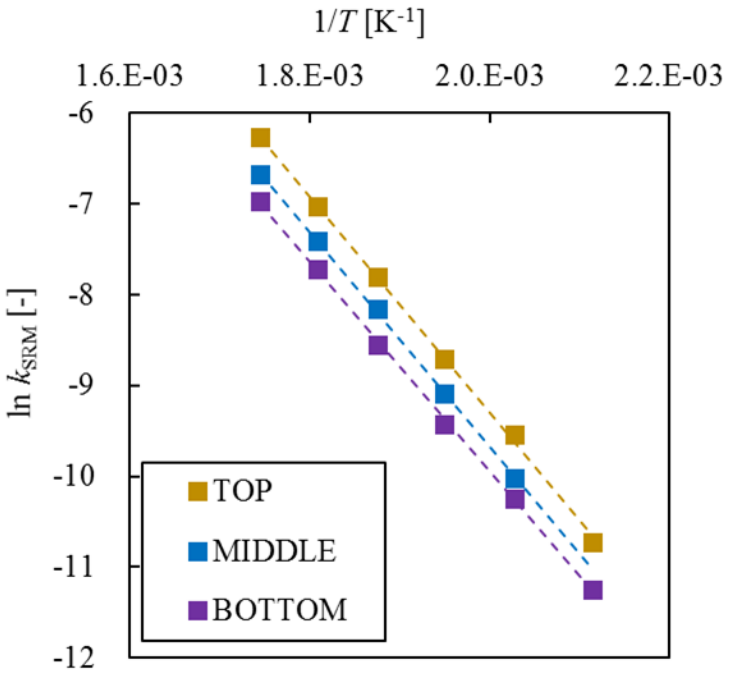

Fig. 5.4-11 Arrhenius plots of (d) TOP, (e) MIDDLE, and (f) BOTTOM for the SRM reaction

Condition “TOP” obtained a high conversion, whereas condition “BOTTOM” achieved the lowest conversion. Moreover, there was no change in the rate-limiting step, which was the catalytic reaction, under all the conditions, from the results of the Arrhenius plots. Furthermore, it was supported that the reactivity depended on the change in the fluid flow caused by the stacking method, from the result of condition “TOP180”. Condition “TOP” realized a similar reactivity to condition “One.” It was suggested that the reaction environment under condition “TOP” was similar to that under condition “One.” Moreover, the conversion was lower under condition “BOTTOM”, because there was little space for the product fluid to flow out from the stack and it was predicted the effect of the structure decreased.

The calculation results of the $(Dcm)_{int}$ for each condition are listed in **Table 5.4-7**. Under each condition, it was evaluated the Dcm only in the domain of the space volume based on the width, length, and height of the catalyzed MP (MPC) part, not the entire stacking. It was demonstrated a similar tendency, the higher the conversion obtained by the experiments, the larger the $(Dcm)_{int}$ calculated by the simulation. The MPCs were placed at the top of the stack under condition “TOP”, therefore, they were not affected by the effect of the structure of the other stacked MPs. The reaction environment under condition “TOP” was similar to that under condition “One” because $(Dcm)_{int}$ and the reactivity were similar. Condition “MIDDLE” was affected by the change in the flow due to the other stacked MPs, reducing $(Dcm)_{int}$. Therefore, it was suggested that the conditions in which three or more stacks ordered in the same direction, when the stacking is densely packed in the reactor, will decrease the effect of the structure and reduce the reactivity. Based on the above results, the flow direction was changed from the upper to the lower layer of the stacking, when the MPCs were packed densely in the reactor, such as condition “Five”. Moreover, it was confirmed that the reaction environment differed depending on the position of the MPC in the stacking.

Table 5.4-7 $(Dcm)_{int}$ in (d) TOP, (e) MIDDLE, (f) BOTTOM

Stacking Condition	(d) TOP	(e) MIDDLE	(f) BOTTOM
$(Dcm)_{int}$	0.49	0.35	0.26

That is, the reactivity under the catalytic reaction rate-limiting step is expected to be improved by stacking methods that consider the following two points.

・To increase the effect of the structure by not stacking MPCs too densely in the reactor

・To increase the effect of the structure by utilizing the directionality of the flow change

5.4.3 Effect of the number of MPC stacking on the reactivity for the WGS reaction

Similar to the SRM reaction, the effect of the number of MPC stacking on the reactivity for the WGS reaction was carried out under constant *W/F* comparison conditions. The stacking methods in each condition were consistent with the conditions applied for the SRM reaction, and the stacking image are already displayed in Fig. 5.4-1. The results of the conversions in the catalytic activity tests in terms of the number of MPCs stacking are presented in **Table 5.4-8** and **Fig. 5.4-12** and the Arrhenius plots as the reaction rate analysis are presented in **Table 5.4-9** and **Fig. 5.4-13**. It was provided that the reactivity was improved in condition "Three", while it was reduced in condition "Five". It was confirmed that there was no change in the rate-limiting step in the temperature range under these stacking conditions; it was confirmed that a rate-limiting step was a catalytic reaction.

These results were similar to the results of the SRM reaction. The reactivity improvement due to the increase in the number of MPC stacking, from 1 to 3, shown in condition "Three" and the reduced reactivity shown in condition "Five" could be due to the same reason as the SRM reaction focusing on a catalytic reaction rate-limiting step. Therefore, it was not investigated that the effect on streamlines, Dcm, and the reactant concentration distribution by simulations for the WGS reaction when changing the number of MPC stacking. Moreover, the effect of changing the position of MPC on the reactivity for the WGS reaction was not investigated by experiments. The results of the TOF ratio for the WGS reaction are displayed in **Table 5.4-10** and **Fig. 5.4-14**. For the WGS and SRM reactions under a catalytic reaction rate-limiting step, it was clarified the effect of improving reactivity tended to get larger at lower temperatures when changing the number of MPC stacking. The reasons for that already described in subsection 3.4.5. It was suggested that the reactivity under the catalytic reaction rate-limiting step can be improved by designing the structure of the catalyst even at low reaction temperatures.

Table 5.4-8 Conversions of (a) One, (b) Three, and (c) Five for the WGS reaction

T [K]	CO conversion [%]		
	One (MPC)	Three	Five
453	26.0	28.6	19.2
473	46.1	50.7	35.2
493	63.6	66.8	50.1
513	75.9	79.7	65.1
533	82.3	86.4	73.0

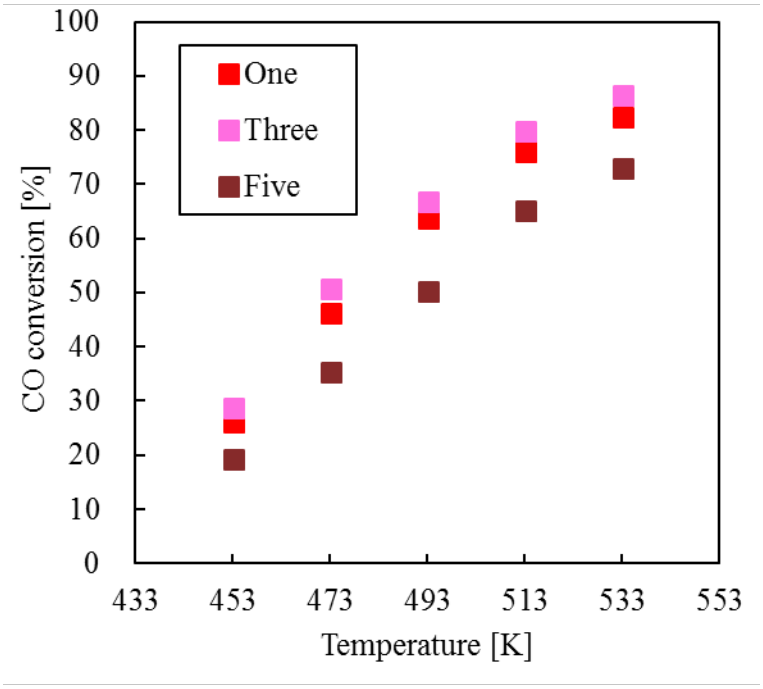

Fig. 5.4-12 Carbon monoxide conversions of (a) One, (b) Three, and (c) Five for the WGS reaction

Table 5.4-9 Reaction rate constant of (a) One, (b) Three, and (c) Five for the WGS reaction

T [K]	ln k_{WGS} [-]		
	One (MPC)	Three	Five
453	-8.9	-8.8	-9.3
473	-8.2	-8.1	-8.6
493	-7.7	-7.6	-8.1
513	-7.4	-7.2	-7.7
533	-7.2	-7.0	-7.4

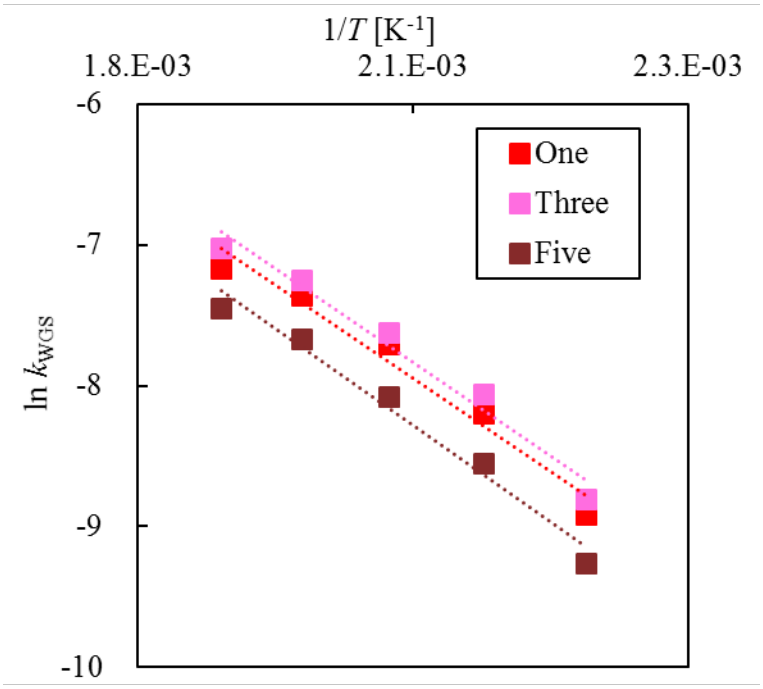

Fig. 5.4-13 Arrhenius plots of (a) One, (b) Three, and (c) Five for the WGS reaction

Table 5.4-10 TOF ratio for each stacking condition for the WGS reaction

Temperature	One (MPC)	Three	Five
LT	1.97	2.17	1.45
MT	1.68	1.76	1.32
HT	1.42	1.49	1.26

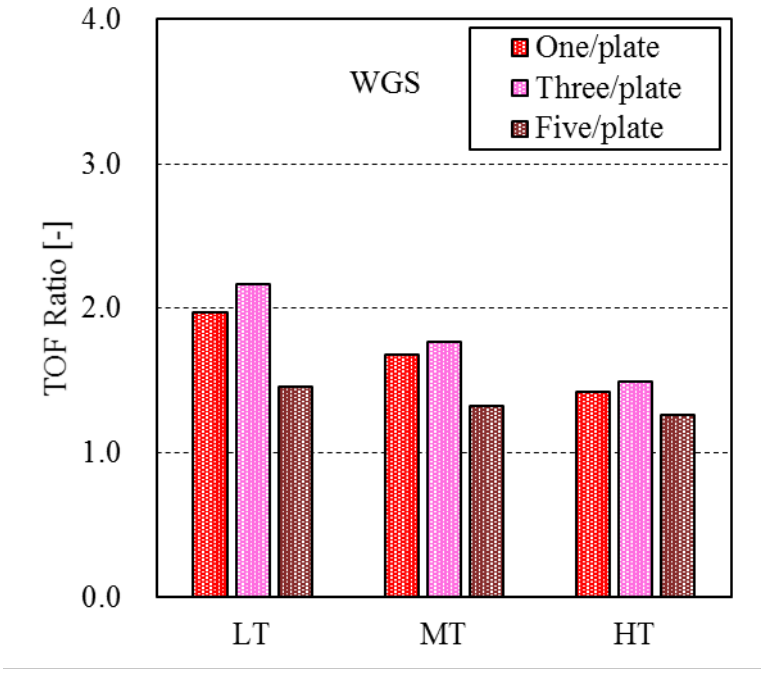

Fig. 5.4-14 TOF ratio for each stacking condition for the WGS reaction

5.4.4 Effect of the number of MPC stacking on the reactivity for the CHC reaction

Similar to the SRM and WGS reactions, the effect of the number of MPC stacking on the reactivity was carried out under constant *W/F* comparison conditions. The stacking methods in each condition were consistent with the conditions applied for the SRM and WGS reaction, and the stacking image are already displayed in Fig. 5.4-1. The results of the conversions in the catalytic activity tests in terms of the number of MPCs stacking are presented in **Table 5.4-11** and **Fig. 5.4-15** and the Arrhenius plots as the reaction rate analysis are presented in **Table 5.4-12** and **Fig. 5.4-16**.

It was provided that the reactivity was improved with the increase in the number of MPC stacking, and it was confirmed that there was no change in the rate-limiting step in the temperature range under these stacking conditions; it was confirmed that a rate-limiting step was an external mass transfer. It was indicated that a different tendency from the SRM and WGS reactions. However, the reactivity improvement was because the amount of catalyst in the reactor increased as the number of MPC stacking increase due to the constant *W/F* comparison condition. In other words, the reaction rate increased for the CHC reaction as the higher feed gas rate under an external mass transfer rate-limiting step.

Therefore, the catalytic activity tests were carried out under constant space velocity (SV) with a different number of MPC stacking. It was estimated that the reactivity would be similar under the catalytic activity test condition with a constant reactant feed rate regardless of the number of MPC stacking because the CHC reaction was an external mass transfer rate-limiting step. The results of hydrogen conversions are presented in **Table 5.4-13** and **Fig. 5.4-17**, and the Arrhenius plots as the reaction rate analysis are presented in **Table 5.4-14** and **Fig. 5.4-18**. The SV for the series of catalytic activity tests was set to the same as that in condition "One" (SV = 2400 h^{-1}), and the SV was calculated using the following equation (**Eq. 5.4-2**). As shown in these figures, the conversion increased with the increase in the number of MPC stacking in the reactor even under the constant feed gas rate conditions. The reason for it was the increased residence time of the reactant gas in the reactor. The reaction rate constant was also increased as the number of MPC stacking increased. It was confirmed that

the reactivity of the CHC reaction was improved by increasing the number of MPC stacking from 1 to 3. Moreover, in condition “Five” when the MPCs were densely stacked in the reactor, the reaction rate constant was higher than that obtained using condition “Three”. The reactivity of condition “Five” was not reduced because the Pe_M around the MPC stacking was not decreased for these reaction conditions in this study. Therefore, the external mass transfer was enhanced with an increase in the number of MPC stacking, and the reaction rate constant increased for the CHC reaction.

The results of the TOF ratio for the CHC reaction are displayed in **Table 5.4-15** and **Fig. 5.4-19**. Its value increased as the number of MPC stacking increased, which indicated the effect of MPC stacking when multiple MPCs were used under an external mass transfer rate-limiting step because the catalytic activity tests were carried out under constant *W/F* comparative conditions. The temperature dependence of the TOF ratio, as the effect of reactivity improvement, was almost constant and smaller under an external mass transfer rate-limiting step because of the little change in Pe_M, which contributes to the overall reactivity since the temperature dependence of the convection and diffusion of reactants was smaller.

$$\mathrm{SV} = \frac{(\mathrm{H_2}\text{ volume flow rate})\ [\mathrm{m^3/h}]}{(\text{Volume of catalyst part})\ [\mathrm{m^3}]} \qquad (\mathbf{Eq.\,5.4-2})$$

Table 5.4-11 Conversions of (a) One, (b) Three, and (c) Five for the CHC reaction (*W*/*F* constant)

T [K]	Hydrogen conversion [%]		
	One (MPC)	Three	Five
373	58.4	64.0	71.3
393	66.4	70.9	79.0
413	74.8	78.5	85.1
433	77.1	81.9	87.0
453	81.1	84.8	90.9

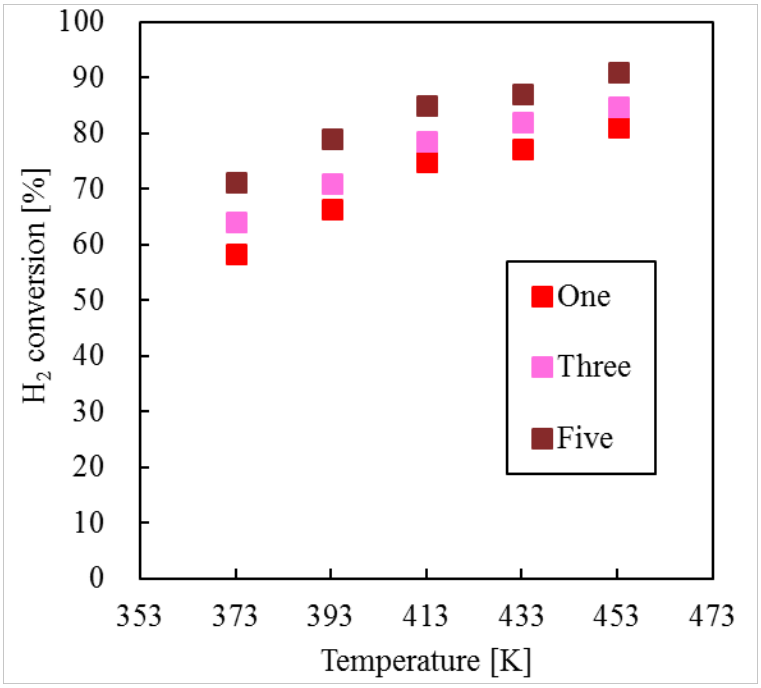

Fig. 5.4-15 Hydrogen conversions of (a) One, (b) Three, and (c) Five for the CHC reaction (*W*/*F* constant)

Table 5.4-12 Reaction rate constant of (a) One, (b) Three, and (c) Five for the CHC reaction (*W/F* constant)

T [K]	ln k_{CHC} [-]		
	One (MPC)	Three	Five
373	-3.9	-3.7	-3.5
393	-3.7	-3.5	-3.3
413	-3.4	-3.3	-3.1
433	-3.4	-3.2	-3.0
453	-3.2	-3.1	-2.9

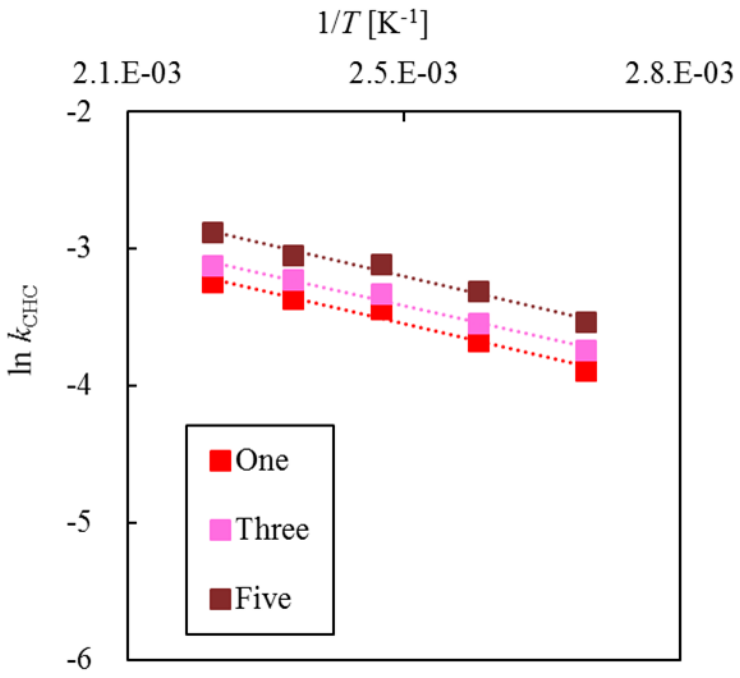

Fig. 5.4-16 Arrhenius plots of (a) One, (b) Three, and (c) Five for the CHC reaction (*W/F* constant)

Table 5.4-13 Conversions of (a) One, (b) Three, and (c) Five for the CHC reaction (SV constant)

T [K]	Hydrogen conversion [%]		
	One (MPC)	Three	Five
373	58.4	70.2	74.6
393	66.4	77.6	81.5
413	74.8	86.1	88.9
433	77.1	89.1	93.0
453	81.1	92.3	95.1

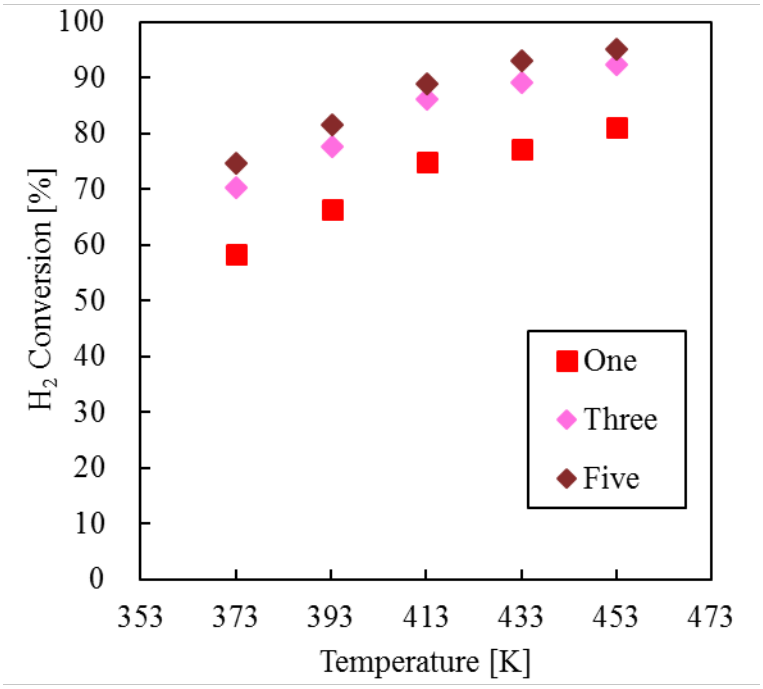

Fig. 5.4-17 Hydrogen conversions of (a) One, (b) Three, and (c) Five for the CHC reaction (SV constant)

Table 5.4-14 Reaction rate constant of (a) One, (b) Three, and (c) Five for the CHC reaction (SV constant)

T [K]	ln k_{CHC} [-]		
	One (MPC)	Three	Five
373	-3.9	-3.6	-3.4
393	-3.7	-3.4	-3.2
413	-3.4	-3.1	-3.0
433	-3.4	-3.0	-2.8
453	-3.2	-2.8	-2.7

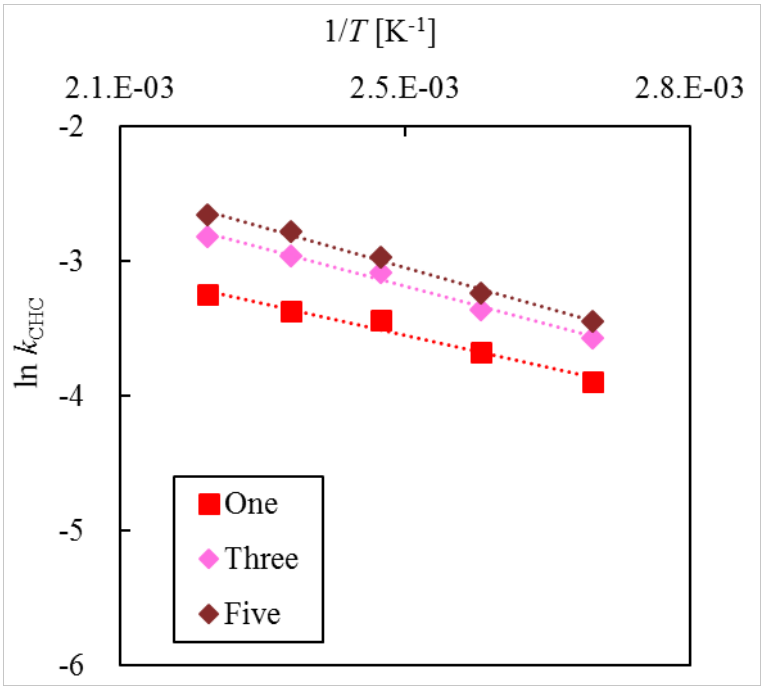

Fig. 5.4-18 Arrhenius plots of (a) One, (b) Three, and (c) Five for the CHC reaction (SV constant)

Table 5.4-15 TOF ratio for each stacking condition for the CHC reaction

Temperature	One (MPC)	Three	Five
LT	1.28	1.41	1.57
MT	1.27	1.33	1.44
HT	1.25	1.31	1.40

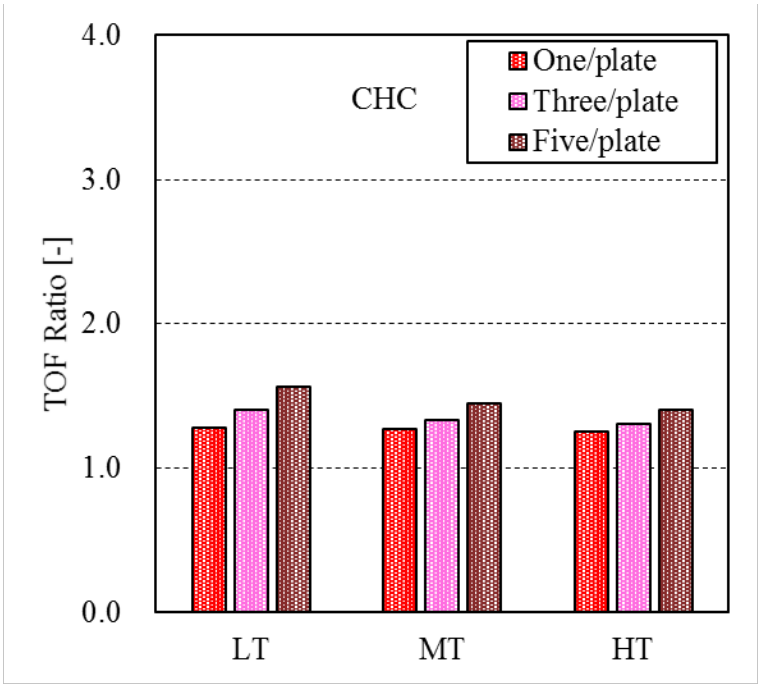

Fig. 5.4-19 TOF ratio for each stacking condition for the CHC reaction

For the CHC reaction, the overall reactivity evaluation index is Pe_M, not Dcm, because of an external mass transfer rate-limiting step, and it was calculated from Eq. 4.4-3 using numerical simulation in the direction of the MPC stacking. The Pe_M at 413 K for condition "Three" and "Five" are displayed in **Fig. 5.4-20 (b-4, c-4)**. For condition "One", the distribution of the Pe_M was already shown in Fig. 4.4-5 in chapter 4. The fluid flows from left to right in the figures, and the white area depicts the MPCs. It was indicated that the Pe_M was large in the whole MPC stacking for each stacking condition, and the distribution of Pe_M was small. Therefore, it was believed that the effect of the reactivity improvement due to the number of MPC stacking, got small as shown in Fig. 5.4-20.

Next, for the quantification of the Pe_M distribution, $(Pe_M)_{int}$ was evaluated using the calculation equation (**Eq. 5.4-3**) similar to the quantification of the Dcm distribution presented in Eq. 5.4-1. The results of the calculation of $(Pe_M)_{int}$ are displayed in **Table 5.4-16**. It was confirmed that the tendency of $(Pe)_{int}$ derived from the simulations was similar to the reactivity tendency derived from the experiments. In other words, it was provided the improvement of the overall reactivity by evaluating the Pe_M that varied due to the structure and its use for the whole stacking in the reactor under an external mass transfer rate-limiting step.

$$(\mathrm{Pe_M})_{\mathrm{int}} = \frac{(\text{Integrated value of } \mathrm{Pe_M} \text{ number in the designated domain})}{(\text{Volume of the designated domain for quantification})} \qquad (\mathbf{Eq.\,5.4-3})$$

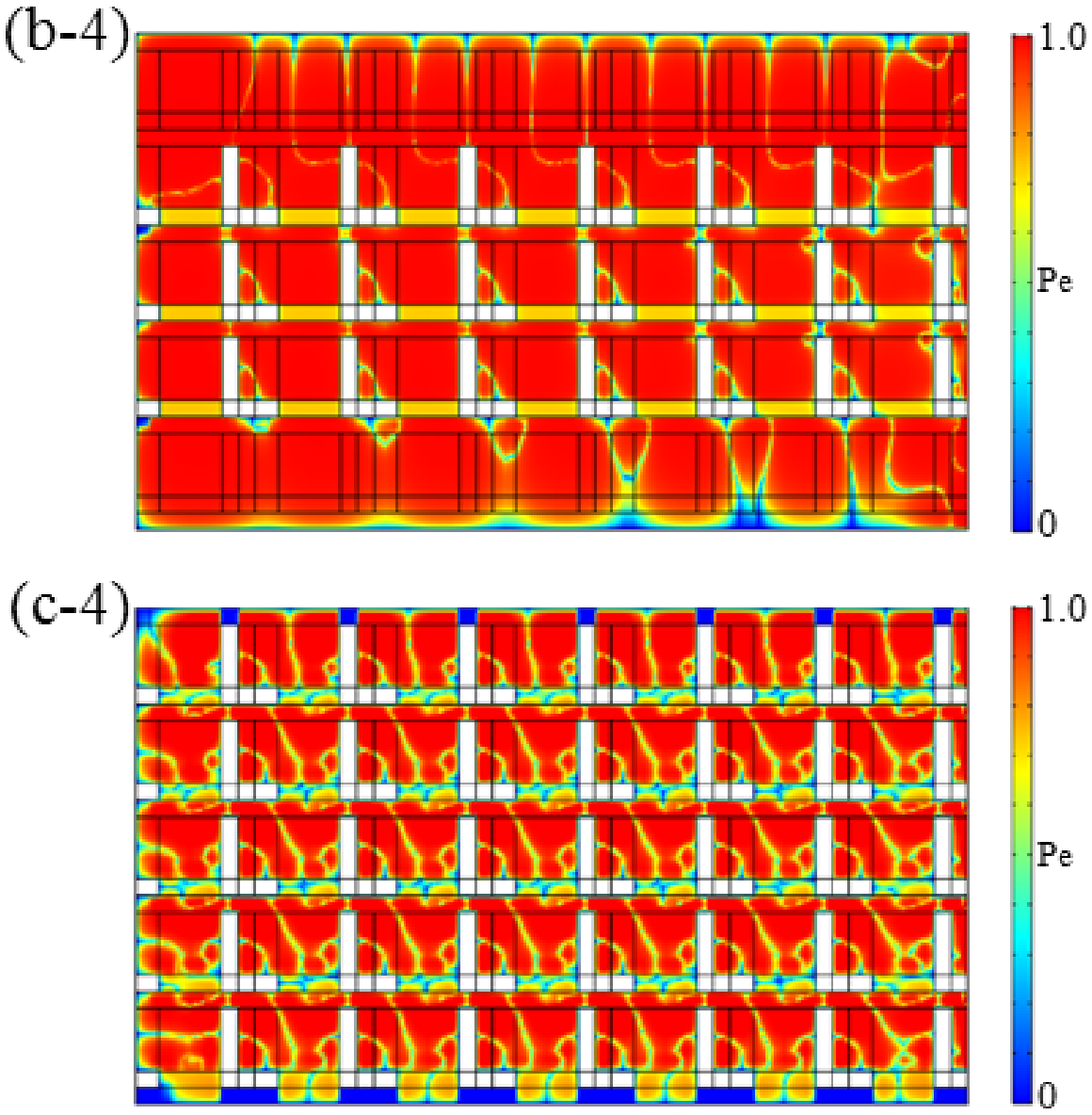

Fig. 5.4-20 Distribution of Dcm under condition “Three” and “Five” (413 K)

Table 5.4-16 $(Pe_M)_{int}$ in condition (a) One, (b) Three, (c) Five

Stacking Condition	(a) One	(b) Three	(c) Five
$(Pe_M)_{int}$	0.89	0.96	0.98

5.5 Conclusions of chapter 5

In this chapter, the effect of the number of MPC stacking on the reactivity was investigated by experiments and simulations for the SRM reaction, first. The effect of the structure was promoted by increasing the number of MPC from 1 to 3, and the reactivity was improved. The TOF ratio as the index for the effect of the reactivity improvement got larger at lower temperatures. On the other hand, the reactivity was significantly reduced when the MPCs packed densely in the reactor, and the effect of the reactivity improvement was small. The numerical simulation was performed in order to examine the reason for that, and streamline and Dcm, as the index for reactivity under a catalytic reaction rate-limiting step, were evaluated. The simulation results showed that, for condition “Five”, the effect of the structure was suppressed due to the densely stacked MPCs in the reactor, the flow change in the direction of MPC stacking was small, and the Dcm was small in whole the stacking. Moreover, a significant reactant concentration distribution was observed in the direction of MPC stacking.

The catalytic activity tests were conducted using the position of the catalyzed MP as a parameter because it was believed that the stacked MPCs in the reactor were not working uniformly due to the suppression of the effect of the structure. It was confirmed that the reactivity was different depending on the position of MPC. Especially condition “BOTTOM”, where the catalyst was positioned in the lowest part of the stacking, showed the reactivity reduction. It was suggested that the effect of the structure was smaller at lower part of stacking under conditions when the MPCs were densely packed in the reactor. It was confirmed that the catalyst was not working uniformly and the reason for the reduced reactivity for condition “Five” was identified. From these results, the reactivity under the catalytic reaction rate-limiting step is expected to be improved by stacking methods that consider the following two points.

- To increase the effect of the structure by not stacking MPCs too densely in the reactor
- To increase the effect of the structure by utilizing the directionality of the flow change

Catalytic activity tests with different number of MPC stacking were carried out for the WGS reaction under a catalytic reaction rate-limiting step, similar to the SRM reaction. The results showed a similar reactivity tendency as the SRM reaction; the reactivity was increased for condition “Three”, and decreased reactivity for condition “Five”. The reason was considered that the same as the SRM reaction because of the same rate-limiting step. Furthermore, for the CHC reaction, which was an external mass transfer rate-limiting step, catalytic activity tests were carried out with different number of MPC stacking. The reactivity improvement due to the number of MPC stacking could not be investigated under the constant *W/F* comparison condition under an external mass transfer rate-limiting step, so the comparison was performed under the constant SV condition. As the number of MPCs stacked for the CHC reaction increased, the reactivity improved and it was showed a different tendency than the SRM and WGS reactions under a catalytic reaction rate-limiting step. Furthermore, the TOF ratio as the effect of reactivity improvement was small and almost constant at each reaction temperature when the number of stacking was changed. These reasons were examined by evaluating Pe_M, the index for the reactivity under an external mass transfer rate-limiting step. The simulation results showed that the Pe_M was large and uniform in whole the MPC stacking. In other words, Pe_M was less affected due to the number of MPC stacking under the reaction conditions for the CHC reaction in this study, which reduced the effect of reactivity improvement.

Stacking condition	Results and factors for the reactivity for the SRM reaction
Number of MPC stacking	For condition “Five”, Reactivity decreased due to reactant concentration distribution in the stacking direction.
Position of MPC in the stacking	For condition “BOTTOM”, the effect of the structure was small and reactivity decreased.

Stacking methods to improve the reactivity under the catalytic reaction rate-limiting step.

- To increase the effect of the structure by not stacking MPCs too densely in the reactor
- To increase the effect of the structure by utilizing the directionality of the flow change

Fig. 5.4-21 Summary of chapter 5

Chapter 6

Proposal for Effective MPC Stacking Method

6.1 Abstract

In chapter 6, considering the results up to chapter 5, it was proposed the stacking methods of MPCs by using simulations to improve the reactivity, and experiments demonstrated the reactivity improvement due to the MPC stacking method. The effective MPC stacking method was proposed by considering the streamline and concentration distribution, and the evaluation index, Dcm. The stacking method with contrasting effects was also proposed, and the effects of these stacking methods on reactivity were examined from experiments. Furthermore, the evaluation index around the catalysts when the stacking method was changed was quantified by simulation, and the positive correlation was shown between the quantified values and the experimentally derived values about catalytic reactivity.

6.2 Purpose

Up to this chapter, the use of MPC was shown to improve the reactivity in the SRM, WGS, and CHC reactions, and the factors were revealed by experiments and simulations. Furthermore, the effect of the number of MPC stacking on the reactivity when the multiple MPCs stacked in the reactor was investigated, focusing on a rate-limiting step in each reaction. Although increasing the number of MPC stacking was effective in improving the reactivity, dense packing of MPCs into the reactor reduced the reactivity under a catalytic reaction rate-limiting step because it suppressed the effect of the structure. The purpose of this chapter was to propose an effective MPC stacking method and reaction environment for the reactivity improvement, considering the effects of the MPC structure and its usage on the reactivity that was revealed so far. First, the streamline and the distribution of Dcm were evaluated using the simulation, and then the effective stacking method and the contrasting method were proposed. Next, the catalytic activity tests were conducted to demonstrate the reactivity of the stacking methods in experiments. Furthermore, the effect of the effective stacking method on the reactivity

improvement and its tendency to the reaction temperature was evaluated by calculating the TOF ratio. The comparison and relationship between the index for overall reactivity calculated from the simulation proposed in each rate-limiting step and the index for reactivity calculated from experimental results were also presented.

6.3 Methodology

COMSOL Multiphysics software was used to propose the effective method of MPC stacking in the reactor to improve the reactivity under the condition of a catalytic reaction rate-limiting step. The effective MPC stacking methods for the reactivity was proposed by evaluating the streamline, Dcm, and reactant concentration. The overview of the prepared simulation models is shown in Fig. 2.6-1 and 2.6-2. The equations used for the calculations were described in Table 2.6-1. The results from those simulation models were verified as mesh-independent study, and it was confirmed that the calculation results did not change regardless of the number of meshes. Details of these numerical simulation methods were provided in Section 2.6.

The catalytic activity tests were performed in experiments using the proposed stacking method in simulation in order to validate if the predicted reactivity was obtained. The model catalyst reactions adopted the SRM and WGS reactions and CHC reactions for investigation of the proposed MPC stacking methods. MPCs were prepared as $Cu/ZnO/Al_2O_3$-MPC for the SRM and WGS reactions, and Pt/Al_2O_3-MPC for CHC reaction as described in Section 2.2. The catalytic activity test conditions for each reaction were shown in Section 2.5. Details of each experimental method were described in chapter 2.

6.4 Results and Discussion

6.4.1 Proposed effective stacking method for MPCs: Numerical simulation

A three-dimensional simulation for the SRM reaction was carried out to propose the effective MPC stacking methods because the SRM reaction had the largest effect of improving reactivity due to the structure of MPC. To improve the reactivity, the MPC stacking method that considered the following points was proposed to perform the experiments by referring to the $(Dcm)_{int}$, streamline, and reactant concentration distribution by simulation.

- To increase the effect of the structure by not stacking MPCs too densely in the reactor
- To increase the effect of the structure by utilizing the directionality of the flow change

The number of MPCs was fixed as four, to change the flow direction and increase in the effect of the structure. Furthermore, a part of the MPC orientation was changed to control the flow direction. The images of the proposed stacking method in the reactor and comparison packing methods are displayed in **Fig. 6.4-1 (g, h, i)**. The proposed suitable condition for improvement in the reactivity is referred as “OUTWARD”. Under it, the MPCs were stacked so that the fluid flowing through the center changed into the channel wall side, because the flow inside the channel is generally faster at the center and slower as it reaches the channel wall. Moreover, the comparison condition is referred as “NORMAL” when the stacking was orderly and referred as “INWARD” when the MPCs were stacked in the opposite orientation to condition “OUTWARD”. Condition “OUTWARD” was expected to get uniform the reactivity in the MPC stacking and improve the overall reactivity. Condition “INWARD” was assumed to reduce the overall reactivity, because of the larger distribution of the reactivity in the entire MPC stacking. The condition “NORMAL” implies condition “Four”. The inferred direction change of the fluid flow is depicted by red arrows in Fig. 6.4-1.

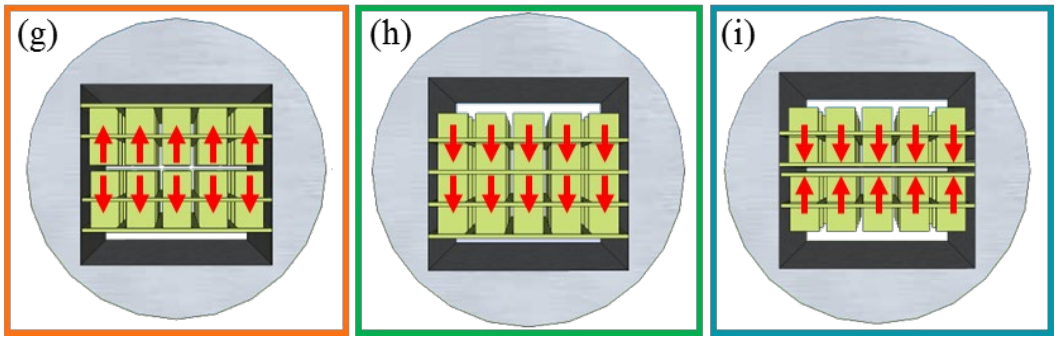

Fig. 6.4-1 Stacking methods of MPCs in the reactor (g) OUTWARD, (h) NORMAL, (i) INWARD

The streamline of each condition, the Dcm distribution, and the reactant concentration distribution are displayed in **Fig. 6.4-2 (g-1, h-1, i-1)**, **Fig. 6.4-3 (g-2, h-2, i-2)**, and **Fig. 6.4-4 (g-3, h-3, i-3)**. The changes in the distribution of reactant concentration with time are displayed in **Fig. 6.4-5**. The fluid flowed in accordance with the design concept. It was confirmed that the Dcm remarkably changed with the orientation of the MPC stacking, and it became larger under condition "OUTWARD" (g-2), whereas it became smaller under condition "INWARD" (i-2). These results demonstrated that it is possible to design the effect of the structure in considering the flow direction change by the orientation of the MPC stacking. $(Dcm)_{int}$ under each condition is listed in **Table 6.4-1**. The value was larger under condition "OUTWARD" and small under condition "INWARD". It was observed that the concentration distribution in the direction of the MPC stacking was small under condition "OUTWARD" (g-3), indicating a concentration distribution in the main flow direction, like in a plug flow reactor. It was expected that the stacked MPCs would work more uniformly, improving the reactivity. On the other hand, the reactant concentration distribution in whole MPC stacking was large under condition "INWARD" (i-3). It was assumed that the MPCs did not work uniformly and the reactivity was reduced.

Table 6.4-1 $(Dcm)_{int}$ in stacking condition (g) OUTWARD, (h) NORMAL, and (i) INWARD

Stacking Condition	(g) OUTWARD	(h) NORMAL	(i) INWARD
$(Dcm)_{int}$	0.79	0.68	0.41

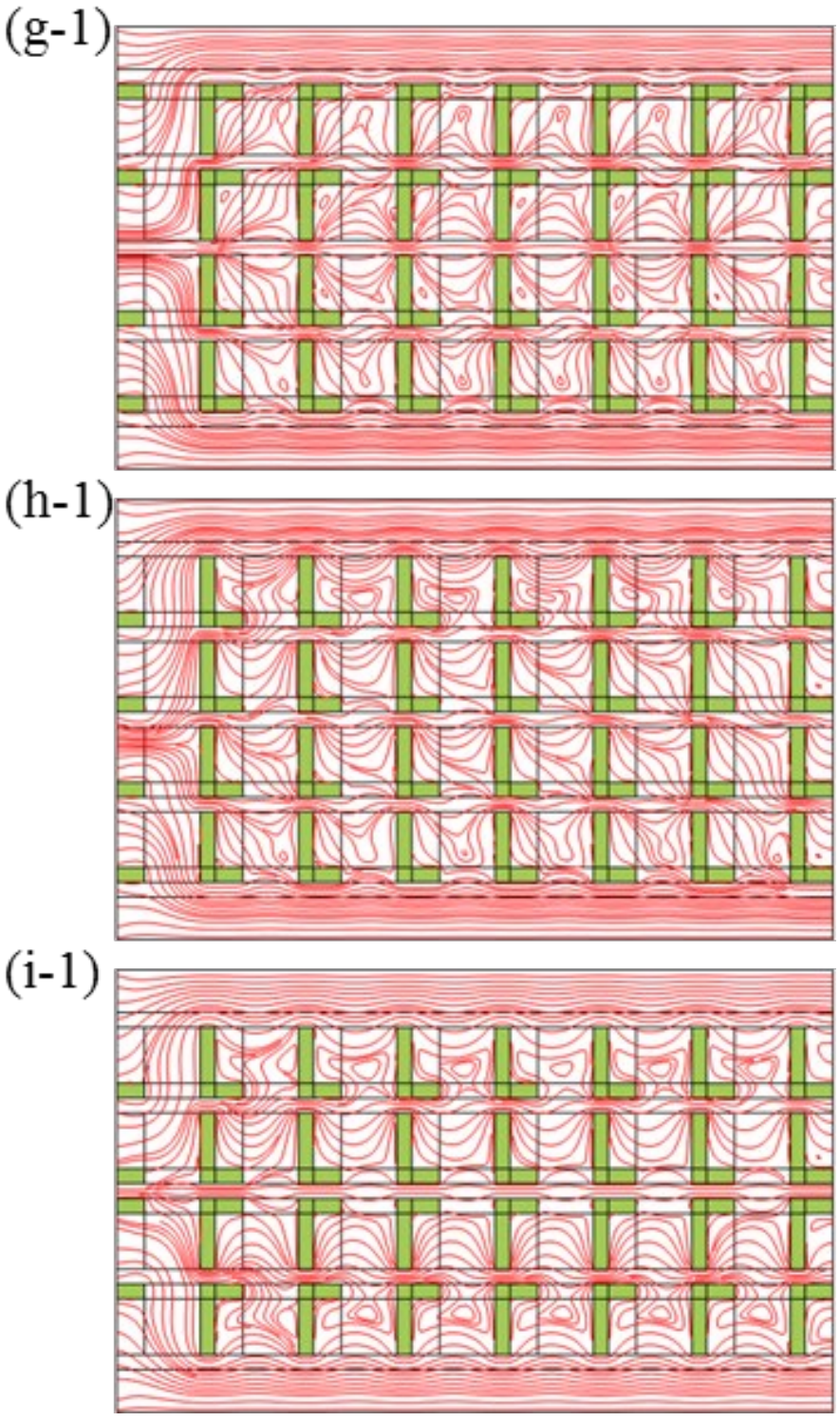

Fig. 6.4-2 Streamline in condition (g-1) OUTWARD, (h-1) NORMAL, and (i-1) INWARD

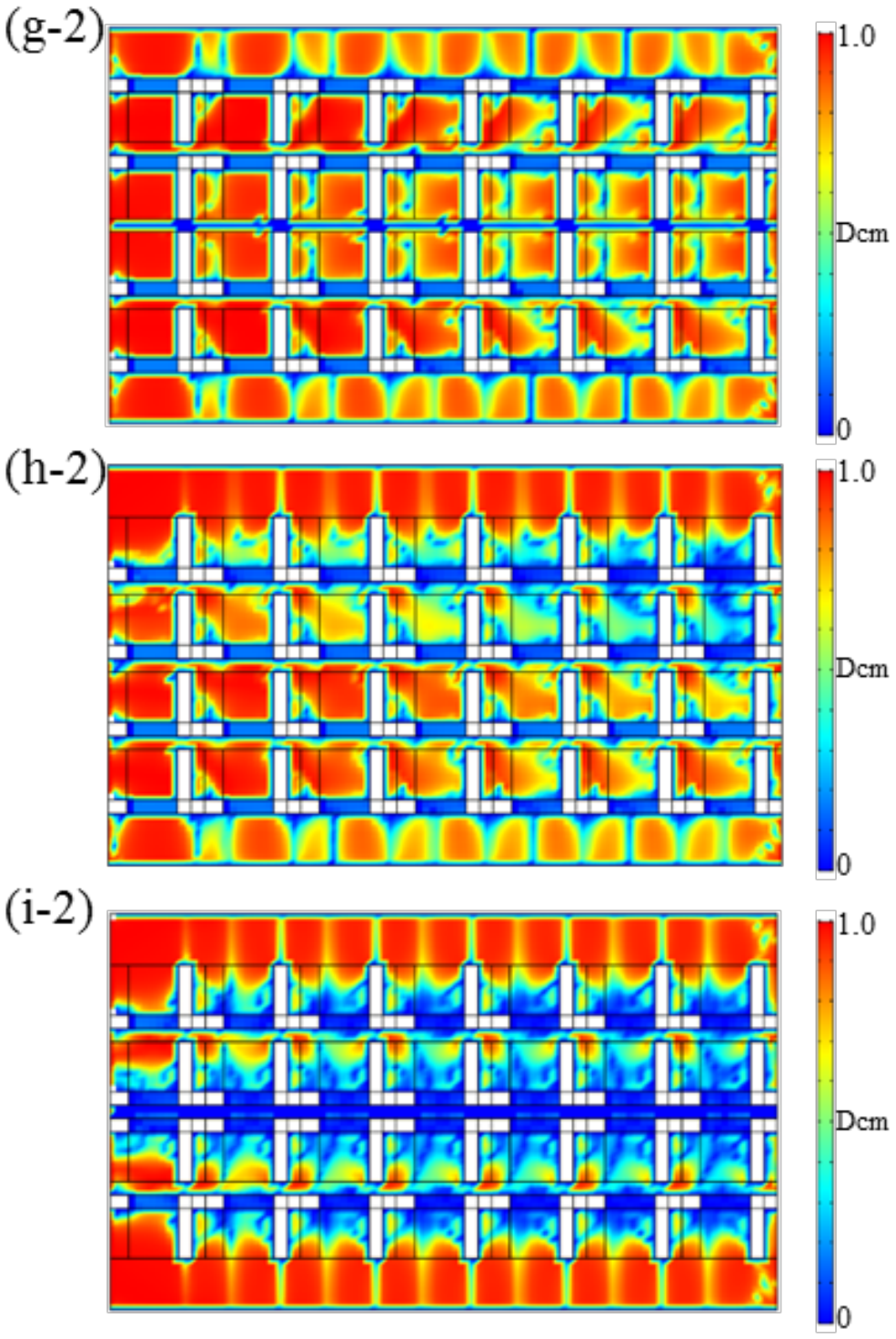

Fig. 6.4-3 Distribution of Dcm in condition (g-2) OUTWARD, (h-2) NORMAL, and (i-2) INWARD

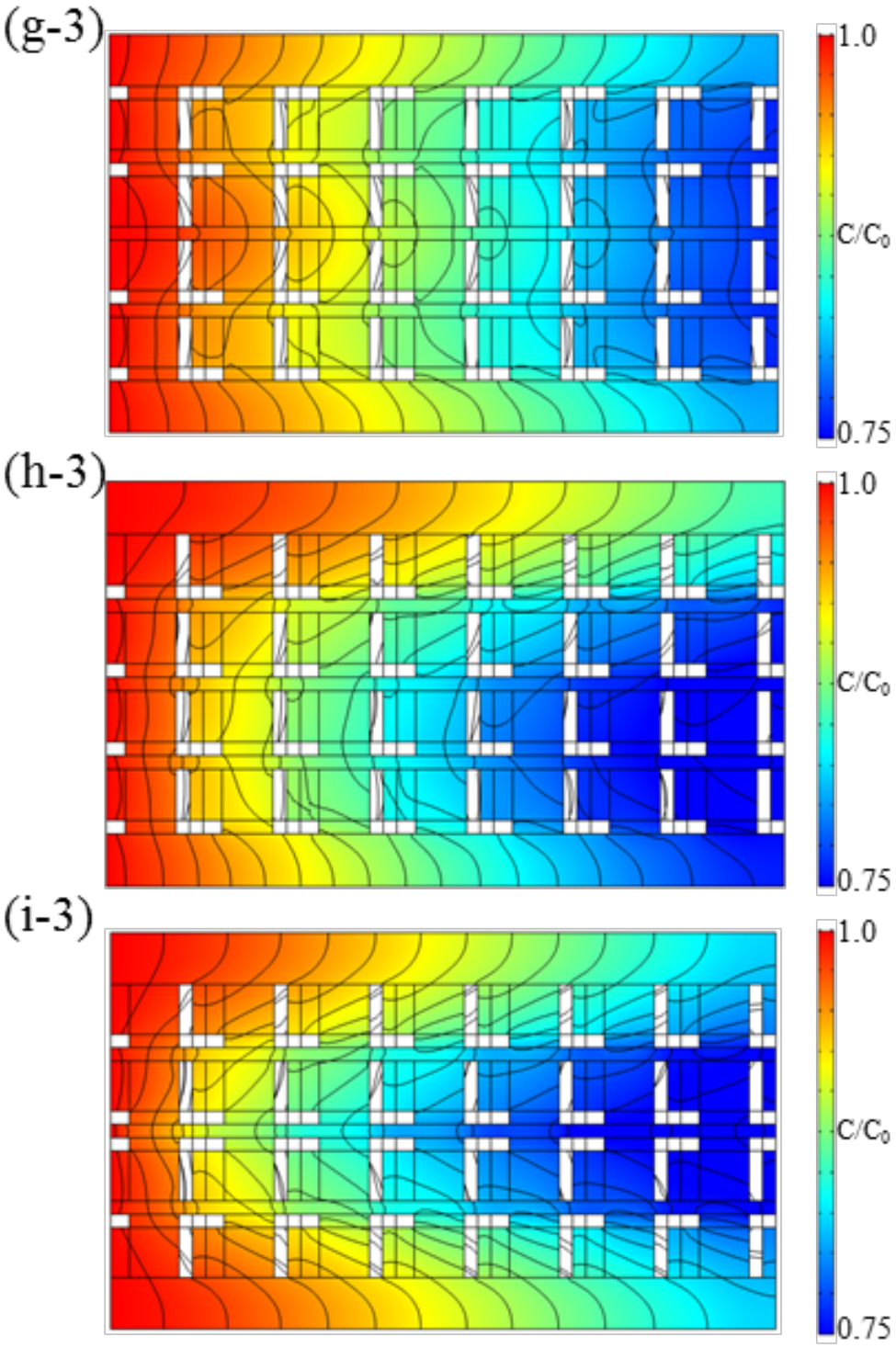

Fig. 6.4-4 Distribution of reactant concentration in condition (g-3) OUTWARD, (h-3) NORMAL, and (i-3) INWARD

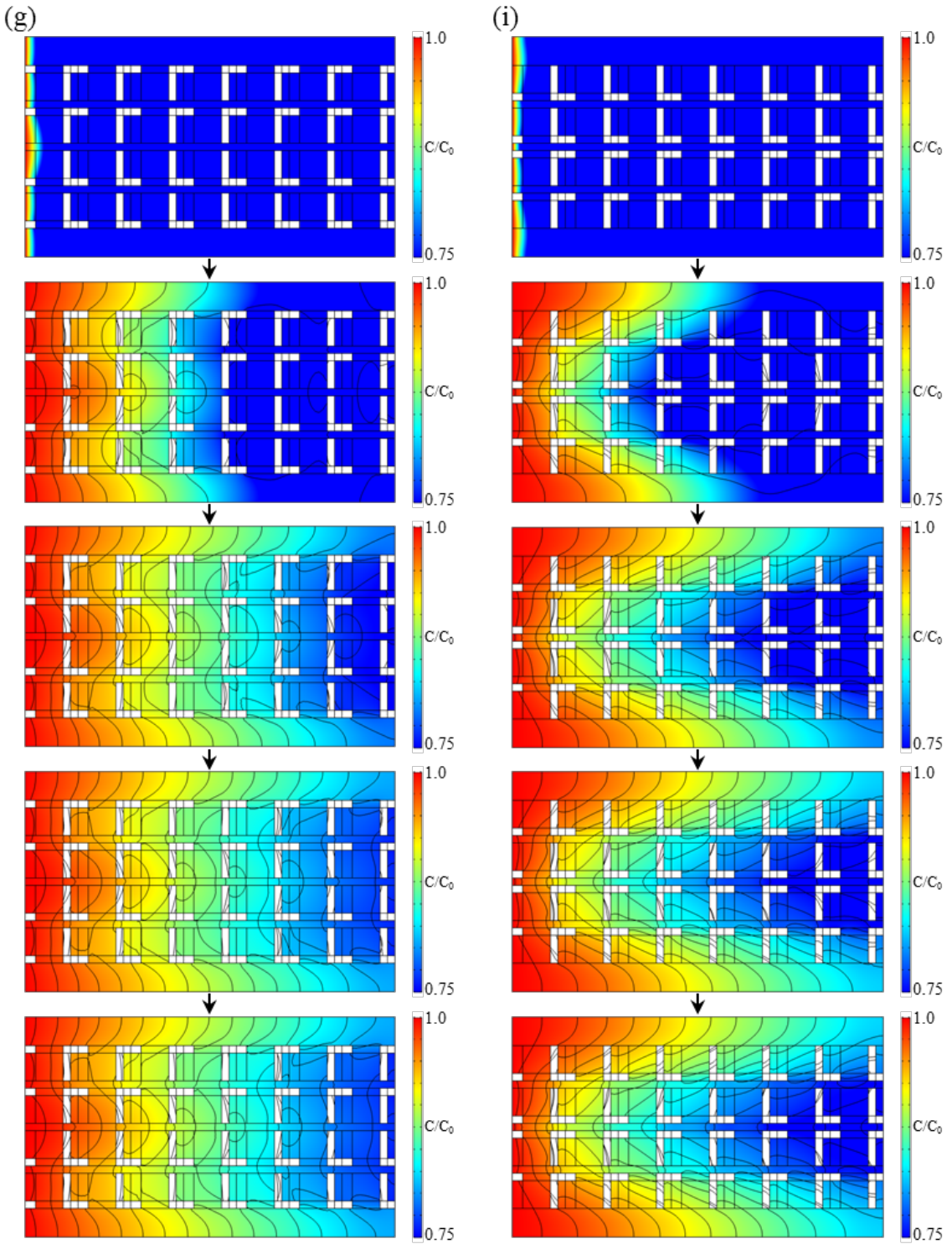

Fig. 6.4-5 Change in the distribution of reactant concentration with time in condition (g) OUTWARD and (i) INWARD

A number of strategies to improve the reactivity by making uniform the reactant concentration in the reactor have been implemented in membrane reactors [6-01, 6-02], microchannel reactors [6-03], and foamed structured catalysts [6-04]. We achieved making uniform the reactivity and improving $(Dcm)_{int}$ in the reactor by changing the stacking method of the unique structured catalyst into the reactor and suggested the improvement of the reactivity.

Furthermore, it was expected that the effect of the structure was changed by the influence of the MPC stacking distance, "d," thereby changing $(Dcm)_{int}$. The results of the calculated $(Dcm)_{int}$ are listed in **Table 6.4-2** under the condition "OUTWARD" changing the MPC stacking distance, "d" ("d" changed to 0.1, 2.0, 3.0 versus the conventional distance, "d" = 1.0). It was demonstrated that $(Dcm)_{int}$ became large at "d" = 1.0, and the conventional MPC stacking distance was appropriate. The streamlines and Dcm distributions for the MPC stacking distance condition ("d" = 0.1, "d" = 2.0 and "d" = 3.0) are displayed in **Fig. 6.4-6** and **Fig. 6.4-7**.

As depicted in these figures, when the stacking distance was short ("d" = 0.1), the fluid flowing through the holes was unable to flow out to the channel between the MPCs. This suggested that the synergistic effect of the structure is reduced. In addition, when the stacking distance was long ("d" = 3.0), the fluid through the holes flowed out to the flow channel between the MPCs, as each MPC was isolated. Moreover, as the synergistic effect of the structure became smaller, $(Dcm)_{int}$ decreased.

Table 6.4-2 $(Dcm)_{int}$ (MPC stacking distance "d" = 0.1, 2.0, and 3.0)

Stacking Distance "d"	0.1	1.0	2.0	3.0
$(Dcm)_{int}$	0.73	0.79	0.72	0.59

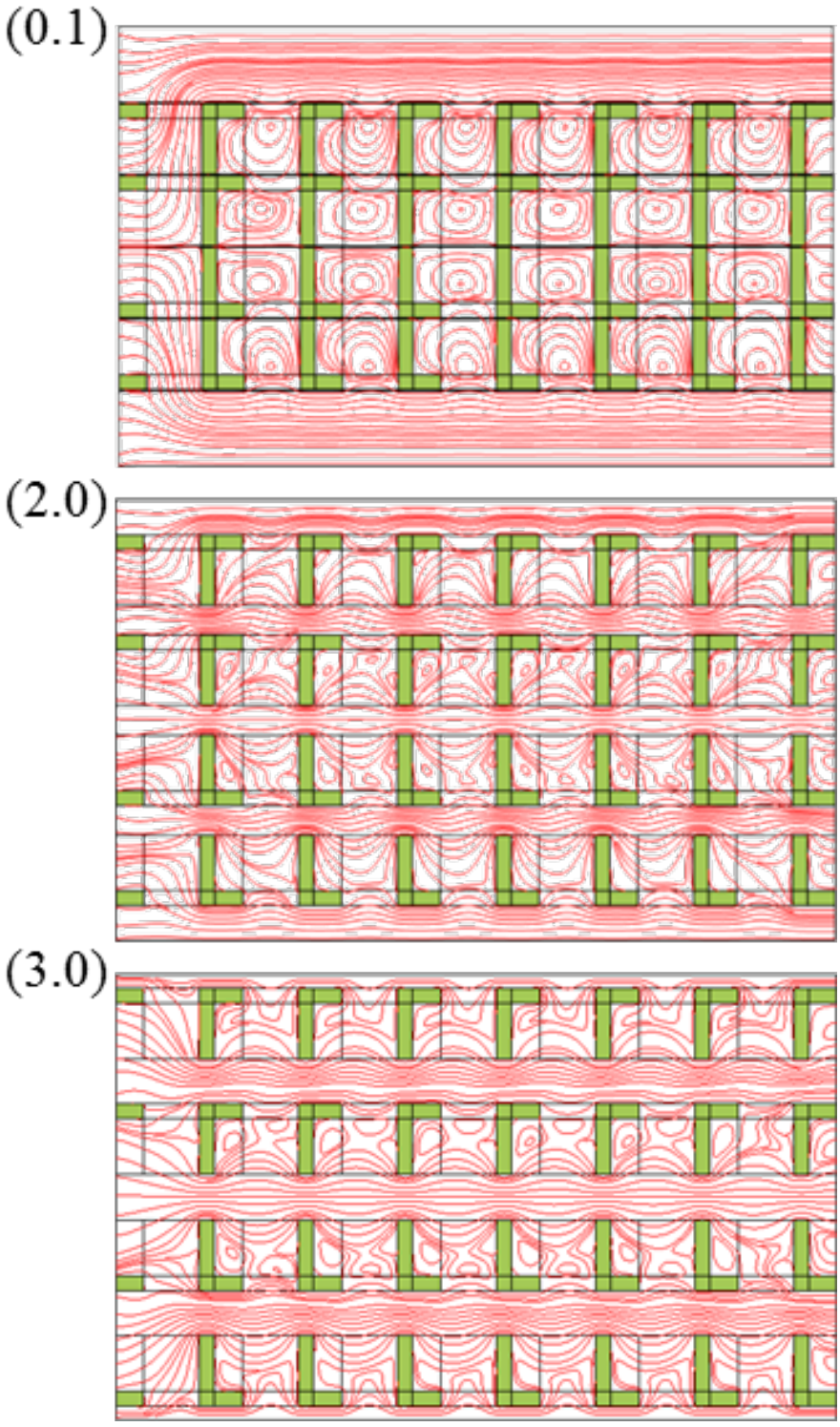

Fig. 6.4-6 Streamlines for the MPC stacking distance condition (“d” = 0.1, “d” = 2.0, and “d” = 3.0)

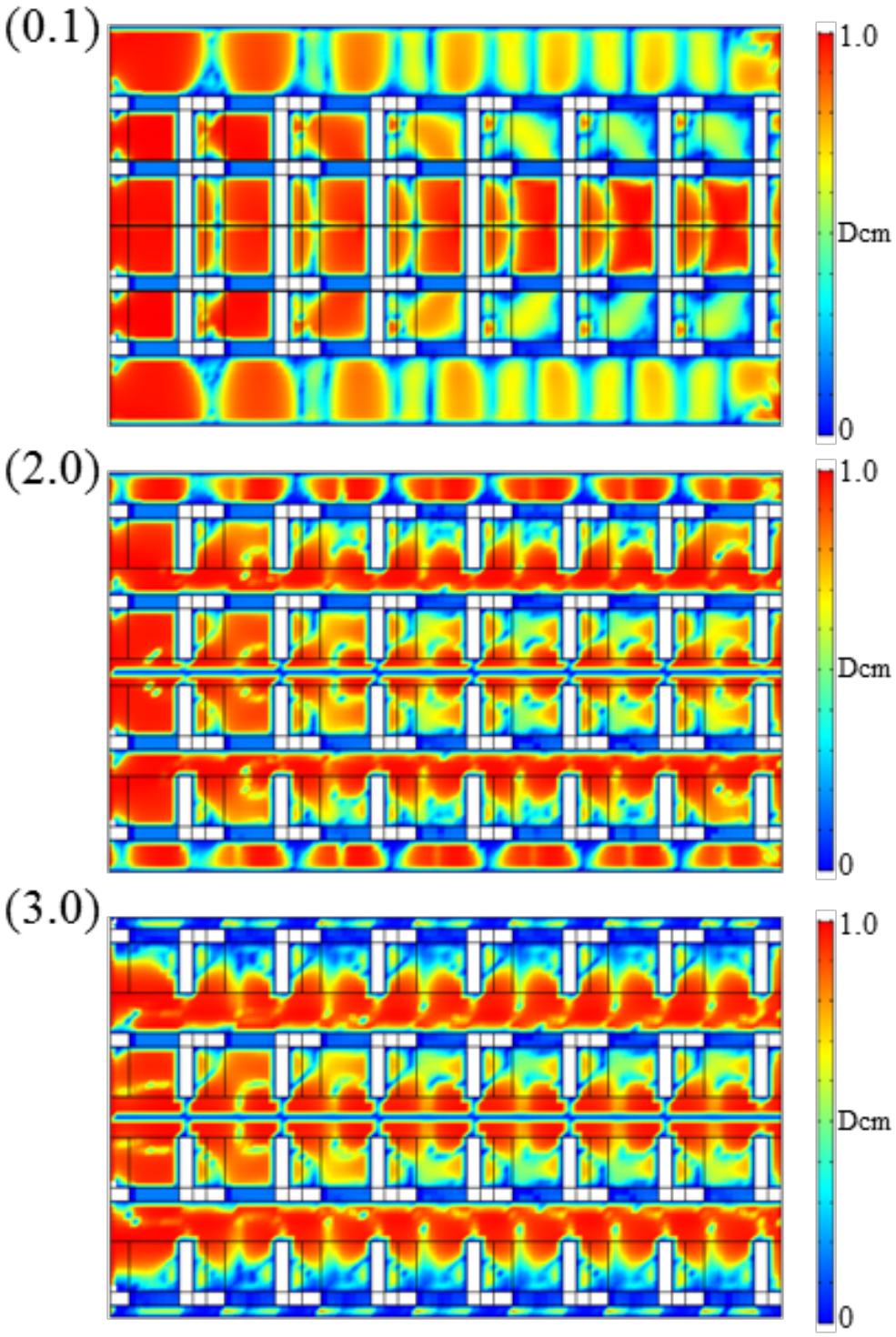

Fig. 6.4-7 Dcm distributions for the MPC stacking distance condition (“d” = 0.1, “d” = 2.0, and “d” = 3.0)

6.4.2 Demonstration of the reactivity improvement for the effective stacking method proposed

The catalytic activity tests for the SRM reaction, where the catalytic reaction was a rate-limiting step, were carried out in order to demonstrate the reactivity improvement of the proposed stacking method. The methanol conversions and Arrhenius plots of the activity tests under each condition are displayed in **Fig. 6.4-8** and **Fig. 6.4-9**, and the conversion under condition "Three" is also shown in the figure as a comparison. It was demonstrated that the methanol conversion is high under condition "OUTWARD" and low under condition "INWARD", and the rate–limiting step, which was the catalytic reaction, did not change in the temperature range of all conditions. Furthermore, the conversion under condition "NORMAL" was higher than that under condition "Three," and the reactivity was improved by the promotion of the effect of the structure by the MPC stacking.

These results presented the same tendency as $(Dcm)_{int}$ calculated by the simulation (Table 6.4-1), and the predicted reactivity was obtained. Specifically, high reactivity was achieved in the experiments by designing the MPC stacking method utilizing the simulation by making the entire stacked MPC work uniformly and promoting the effect of the structure. In addition, it was cleared of the effect of the stacking method on the reactivity since the reactivity was reduced under condition "INWARD" in the contrast design concept. The proposal for the effective MPC stacking method to improve the reactivity was achieved through experiments and simulations by evaluating $(Dcm)_{int}$ in a catalytic reaction rate-limiting step.

Table 6.4-3 Conversions of (g) OUTWARD, (h) NORMAL, and (i) INWARD for the SRM reaction

T [K]	Methanol Conversion [%]		
	OUTWARD	NORMAL	INWARD
473	9.9	8.4	6.5
493	24.3	20.8	15.6
513	46.9	43.3	32.3
533	77.7	72.8	63.1
553	95.5	93.1	88.2
573	100.0	100.0	98.7

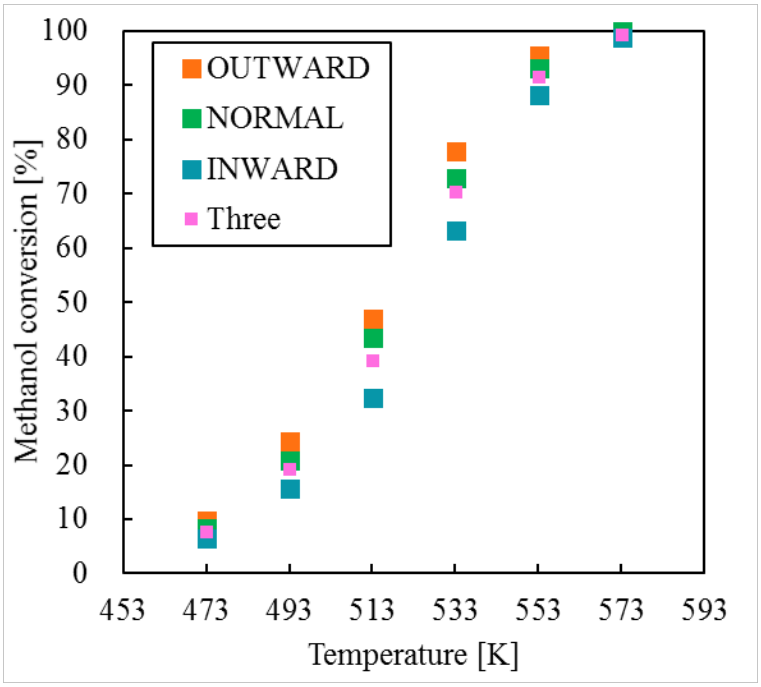

Fig. 6.4-8 Methanol Conversions in stacking condition (g) OUTWARD, (h) NORMAL, and (i) INWARD

Table 6.4-4 Reaction rate constant of (g) OUTWARD, (h) NORMAL, and (i) INWARD for the SRM reaction

T [K]	ln k_{SRM} [-]		
	OUTWARD	NORMAL	INWARD
473	-10.4	-10.5	-10.8
493	-9.4	-9.6	-9.9
513	-8.6	-8.7	-9.1
533	-7.7	-7.8	-8.1
553	-7.0	-7.1	-7.4
573	-	-	-6.6

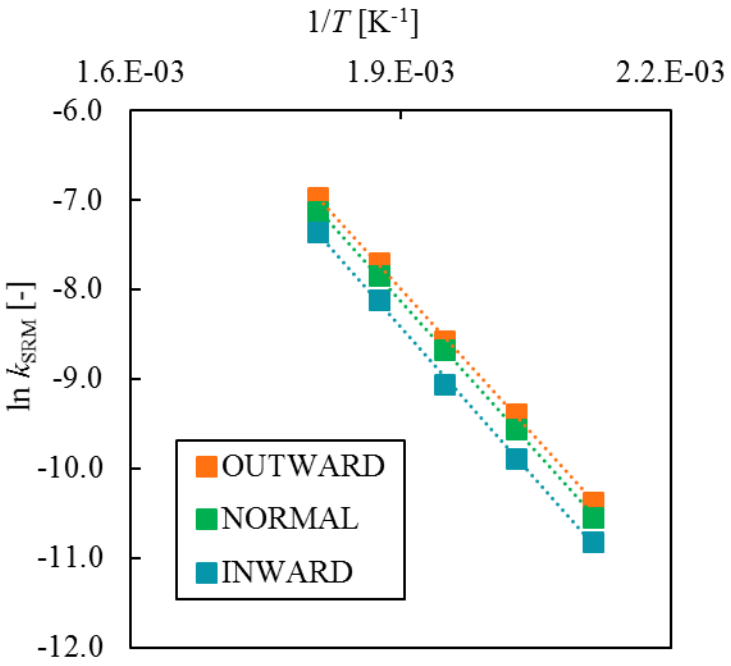

Fig. 6.4-9 Arrhenius plots in condition (g) OUTWARD, (h) NORMAL, and (i) INWARD for the SRM reaction

The TOF ratio was used to evaluate the effect of the reactivity improvement and the stacking method to improve the reactivity for the SRM reaction was evaluated for the results of the catalytic activity tests in this chapter. TOF was calculated using Eq. 3.4-6. These results are shown in **Table 6.4-5** and **Fig 6.4-10**. The TOF ratio showed the largest value with the effective stacking method proposed. Their values were larger at lower temperatures. It was considered that the reasons for that tendency were similar to those given in Subsection 3.4.5. The TOF ratio at HT for the SRM reaction was smaller than that at the other reaction temperature and did not change with the change in the stacking method because even the plate showed high reactivity.

It was suggested that the effective stacking method OUTWARD in the SRM reaction results in conversion efficiency of 3.8 times higher than that of the unprocessed plate-type catalyst under the low-temperature reaction environment because TOF is generally defined as the moles of reactant converted per unit time per mole of active catalytic sites. In other words, PI for a catalytic process was achieved by using structured catalysts such as MPC to improve the reactivity under low-temperature reaction environments. It was evaluated by Dcm, the unique index for a catalytic reaction rate-limiting step.

Table 6.4-5 TOF ratio for each stacking condition for the SRM reaction

Temperature	INWARD	NORMAL	OUTWARD
LT	2.4	3.2	3.8
MT	2.5	2.9	3.1
HT	1.4	1.4	1.4

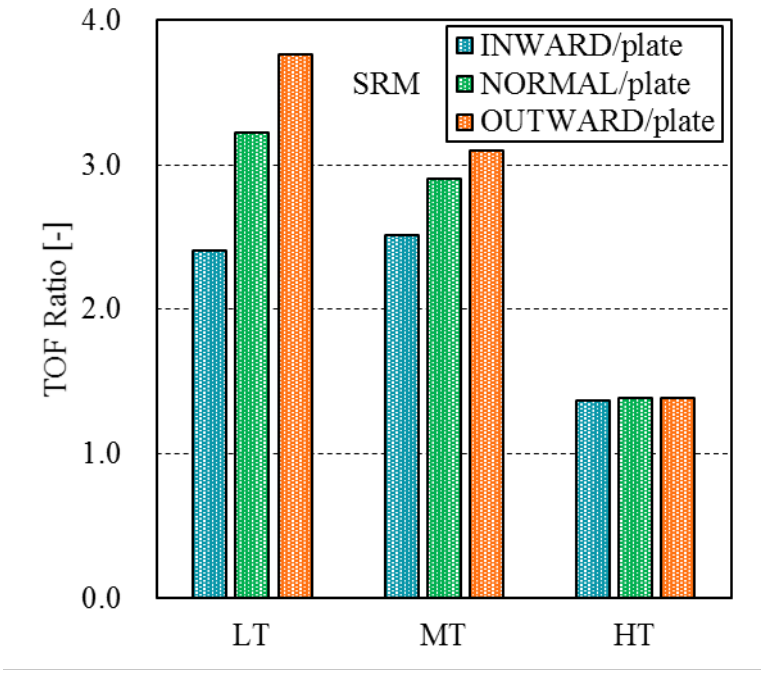

Fig. 6.4-10 TOF ratio for each stacking condition for the SRM reaction

Finally, for the SRM reaction, the relationship between the reaction rate constant k_{SRM} derived from the experimental results at 533 K and $(Dcm)_{int}$ calculated using the simulation under all the conditions of the MPC stacking method attempted in this study is displayed in **Table 6.4-6** and **Fig. 6.4-11**. Fig. 6.4-11 showed a good positive correlation, i.e., it reveals that by the MPC stacking method, $(Dcm)_{int}$ increased, which improved the reactivity. The slope of the linear plots increased at higher reaction temperatures because the reaction rate constant generally increases exponentially as the reaction temperature. The intercept of the linear plots was considered to represent the reaction rate constant for the catalytic reaction using the structured catalyst such as plate where there is no convection in the direction assessed for Dcm and mass transfer is dominated only by diffusion. In other words, it was suggested that the reaction rate obtained in the experiments using structured catalysts at a reaction temperature can be predicted by evaluating the $(Dcm)_{int}$ in the simulation.

Table 6.4-6 Comparison between $(Dcm)_{int}$ derived from simulation and the reaction rate constant k_{SRM} derived from experiments at 533 K as MT

	One (MPC)	Three	Five	TOP	TOP180
$(Dcm)_{int}$	0.49	0.60	0.21	0.49	0.49
k_{SRM} (533 K)	1.4×10^{-4}	1.7×10^{-4}	0.6×10^{-4}	1.6×10^{-4}	1.5×10^{-4}

	MIDDLE	BOTTOM	OUTWARD	NORMAL	INWARD
$(Dcm)_{int}$	0.35	0.26	0.79	0.68	0.41
k_{SRM} (533 K)	1.1×10^{-4}	0.8×10^{-4}	2.0×10^{-4}	1.7×10^{-4}	1.2×10^{-4}

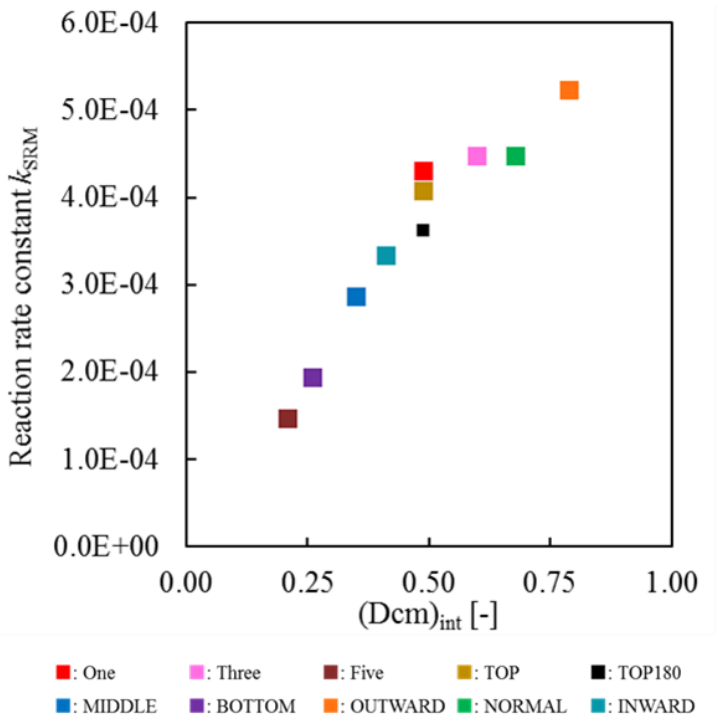

Fig. 6.4-11 Relation between $(Dcm)_{int}$ by simulation and reaction constant k_{SRM} by experiments (533 K as MT)

Next, for the WGS reaction, activity tests were carried out using the proposed stacking methods to investigate whether the results of reactivity were similar to those obtained for the SRM reaction. The CO conversions and Arrhenius plots of the activity tests under each stacking condition are displayed in **Fig. 6.4-12** and **Fig. 6.4-13**, and the conversion under condition "Three" is also shown in the figure as a comparison. It was demonstrated that the methanol conversion is high under condition "OUTWARD" and low under condition "INWARD", and the rate–limiting step, which was the catalytic reaction, did not change in the temperature range of all conditions. Furthermore, the conversion under condition "NORMAL" was higher than that under condition "Three", and the reactivity was improved by the promotion of the effect of the structure by the MPC stacking. These results were similar to those for the SRM reaction, with the expected reactivity.

The values of $(Dcm)_{int}$ for the WGS reaction calculated on the simulation were almost the same as those for the SRM reaction. Therefore, the experimentally obtained reactivity tendency for each stacking method was similar to the calculated $(Dcm)_{int}$ tendency in simulation. Focusing on the rate-limiting step, the reason for the improved reactivity of the effective stacking method for the WGS reaction was considered to be the same reason as for the SRM reaction, because the SRM and WGS reactions were the same rate-limiting step of a catalytic reaction. Therefore, it was further demonstrated that the effective stacking method was proposed to improved reactivity under a catalytic reaction rate-limiting step by evaluating the $(Dcm)_{int}$ in simulation.

TOF for the WGS reaction was also calculated as the effect of reactivity improvement by the same method for the SRM reaction, using Eq. 3.4-6. These results are shown in **Table 6.4-8** and **Fig 6.4-14**. The TOF ratio showed the largest value with the effective stacking method proposed. And, their values were larger at lower temperatures. It was considered that the reasons for that tendency were similar to those given in Subsection 3.4.5. However, the values for each reaction temperature for the WGS reaction were smaller than those for the SRM reaction. It was considered that the detailed comparison by thermodynamic studies or by quantum mechanics studies, as described in Subsection 3.4.5, is necessary for the factors contributing to this difference.

Table 6.4-6 Conversions of (g) OUTWARD, (h) NORMAL, and (i) INWARD for the WGS reaction

T [K]	CO Conversion [%]		
	OUTWARD	NORMAL	INWARD
453	30.7	28.5	21.8
473	54.9	52.3	38.9
493	70.9	67.8	56.7
513	83.8	81.1	70.4
533	89.9	87.2	75.2

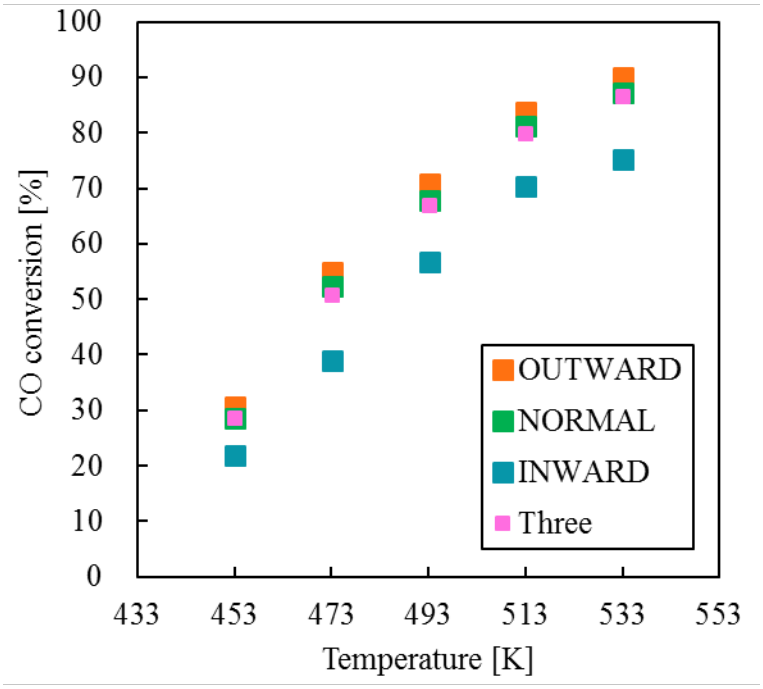

Fig. 6.4-12 CO Conversions in stacking condition (g) OUTWARD, (h) NORMAL, and (i) INWARD

Table 6.4-7 Reaction rate constant of (g) OUTWARD, (h) NORMAL, and (i) INWARD for the WGS reaction

T [K]	ln k_{WGS} [-]		
	OUTWARD	NORMAL	INWARD
453	-8.7	-8.8	-9.1
473	-7.9	-8.0	-8.4
493	-7.5	-7.6	-7.9
513	-7.1	-7.2	-7.5
533	-6.9	-7.0	-7.4

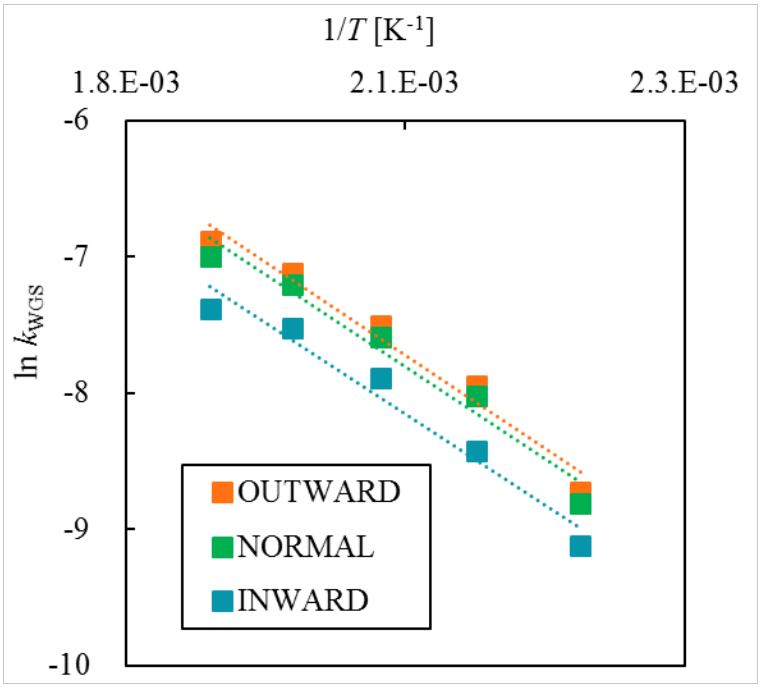

Fig. 6.4-13 Arrhenius plots in condition (g) OUTWARD, (h) NORMAL, and (i) INWARD for the WGS reaction

Table 6.4-8 TOF ratio for each stacking condition for the WGS Reaction

Temperature	INWARD	NORMAL	OUTWARD
LT	1.7	2.2	2.3
MT	1.5	1.8	1.9
HT	1.3	1.5	1.6

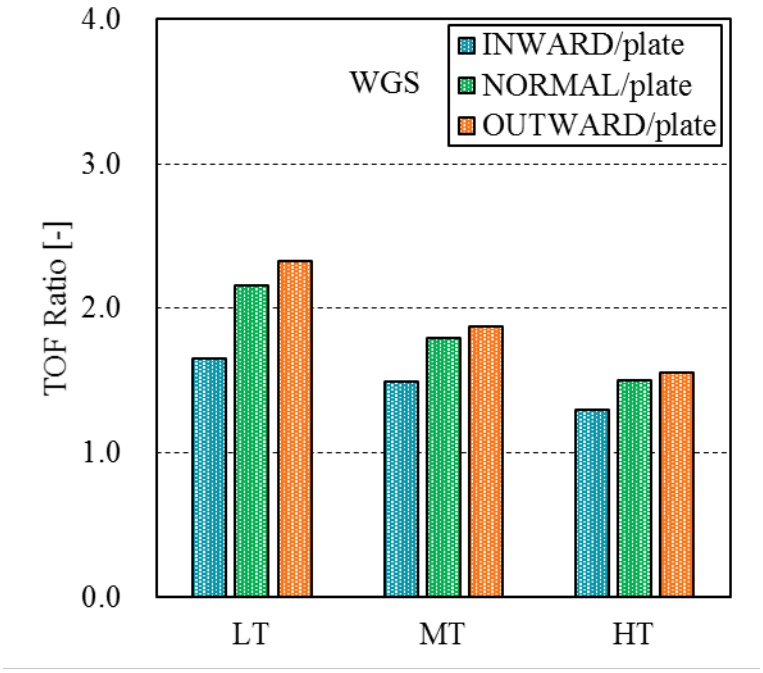

Fig. 6.4-14 TOF ratio for each stacking condition for the WGS Reaction

Finally, for the WGS reaction, the relationship between the reaction rate constant k_{WGS} derived from the experimental results at 493 K and $(Dcm)_{int}$ calculated using the simulation under all the conditions of the MPC stacking method attempted in this study is displayed in **Table 6.4-9** and **Fig. 6.4-15**. Fig. 6.4-15 showed a good positive correlation, i.e., it reveals that by the MPC stacking method, $(Dcm)_{int}$ increased, which improved the reactivity. These results were also similar to those of the investigation as the same method for the SRM reaction.

Table 6.4-9 Comparison between $(Dcm)_{int}$ derived from simulation and reaction rate constant k_{WGS} derived from experiments at 493 K as MT

	One (MPC)	Three	Five
$(Dcm)_{int}$	0.47	0.62	0.20
k_{WGS} (493 K)	3.2×10^{-2}	3.6×10^{-2}	4.4×10^{-2}

	OUTWARD	NORMAL	INWARD
$(Dcm)_{int}$	0.81	0.68	0.42
k_{WGS} (493 K)	4.0×10^{-2}	3.7×10^{-2}	3.4×10^{-2}

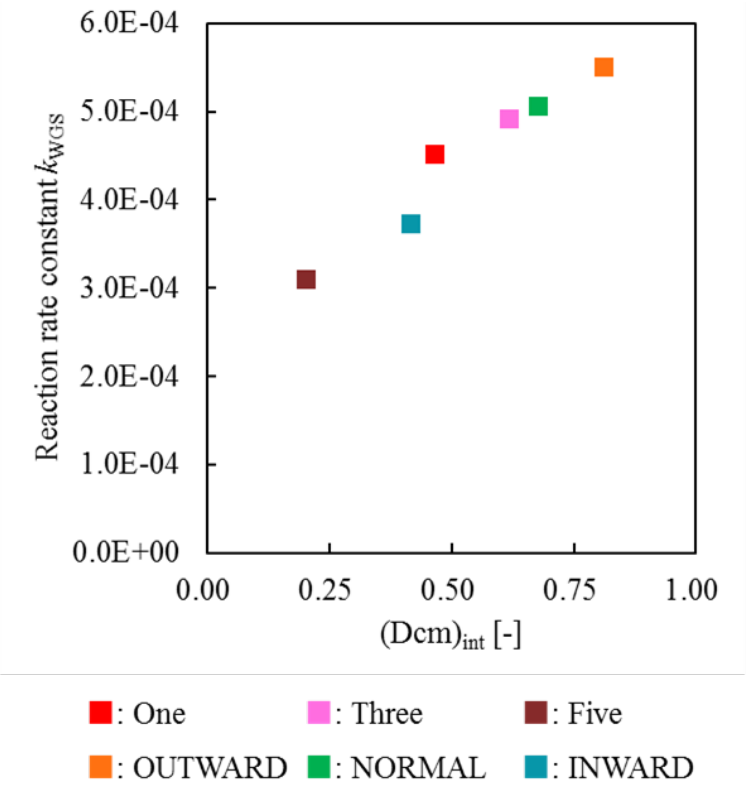

Fig. 6.4-15 Relation between $(Dcm)_{int}$ by simulation and reaction constant k_{WGS} by experiments (493 K as MT)

6.4.3 Application of the effective stacking method to the CHC reaction

For the CHC reaction, activity tests were carried out using the proposed stacking methods to investigate whether the results of reactivity were similar to those obtained for the SRM and WGS reactions. The hydrogen conversions and Arrhenius plots of the activity tests under each condition are displayed in **Fig. 6.4-16** and **Fig. 6.4-17**, and the conversion under condition "Three" is also shown in the figure as a comparison. By changing the orientation of MPC stacking, the reactivity was slightly higher under condition "OUTWARD" and slightly lower under condition "INWARD", and the rate-limiting step, which was an external mass transfer, did not change in the temperature range of all conditions. Furthermore, the conversion under condition "NORMAL" was slightly higher than that under condition "Three".

It was suggested that the promotion of the external mass transfer was slightly changed by the orientation of MPCs. The effect of changing the MPC stacking orientation on the reactivity was small because the external mass transfer was large and uniform throughout the MPC stacking under the experimental conditions of this study. Here, the simulation results for the distribution of Pe_M are shown in **Fig.6.4-18 (g-4, h-4, i-4)**. The Pe_M around the catalysts in the reactor was found to get large and uniform in the whole MPC stacking. For the CHC reaction, which was an external mass transfer rate-limiting step, the effect of changing in the MPC stacking method on the overall reactivity was small.

TOF for the CHC reaction was also calculated by same method for the SRM and WGS reaction, using Eq. 3.4-6. These results are shown in **Table 6.4-12** and **Fig 6.4-19**. The TOF, as the effect of reactivity improvement, ratios were smaller for all conditions, and the TOF ratios did not increase at the lower temperatures observed for the SRM and WGS reactions. And, it was considered that the reasons for that tendency were similar to those given in Subsection 3.4.5 and 5.4.4 for the CHC reaction by using MPCs and changing the number of MPC stacking. It was because Pe_M was large in the whole stacking of MPC and therefore Pe_M is less affected by temperature.

Table 6.4-10 Conversions of (a) One, (b) Three, and (c) Five for the CHC reaction

T [K]	Hydrogen conversion [%]		
	OUTWARD	NORMAL	INWARD
373	66.5	65.9	61.9
393	73.8	72.7	69.5
413	81.7	79.6	76.9
433	85.0	82.4	80.2
453	87.8	87.0	83.4

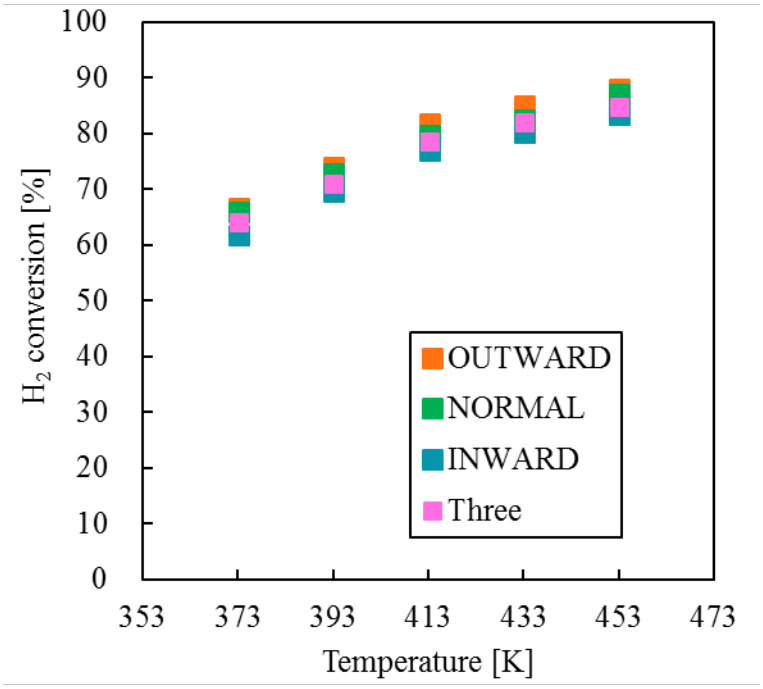

Fig. 6.4-16 Hydrogen Conversions in stacking condition (g) OUTWARD, (h) NORMAL, and (i) INWARD

Table 6.4-11 Reaction rate constant of (a) One, (b) Three, and (c) Five for the CHC reaction

T [K]	ln k_{CHC} [-]		
	OUTWARD	NORMAL	INWARD
373	-3.7	-3.7	-3.8
393	-3.5	-3.5	-3.6
413	-3.2	-3.3	-3.4
433	-3.1	-3.2	-3.3
453	-3.0	-3.0	-3.2

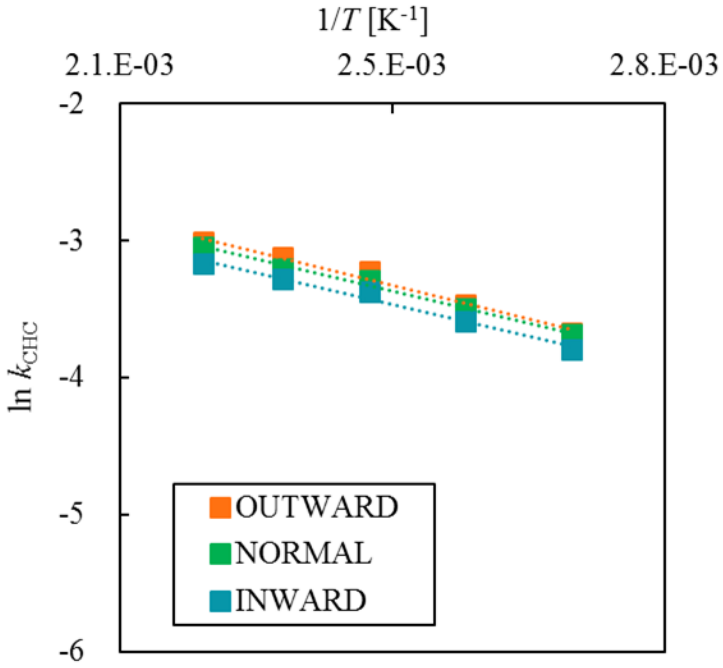

Fig. 6.4-17 Arrhenius plots in condition (g) OUTWARD, (h) NORMAL, and (i) INWARD for the CHC reaction

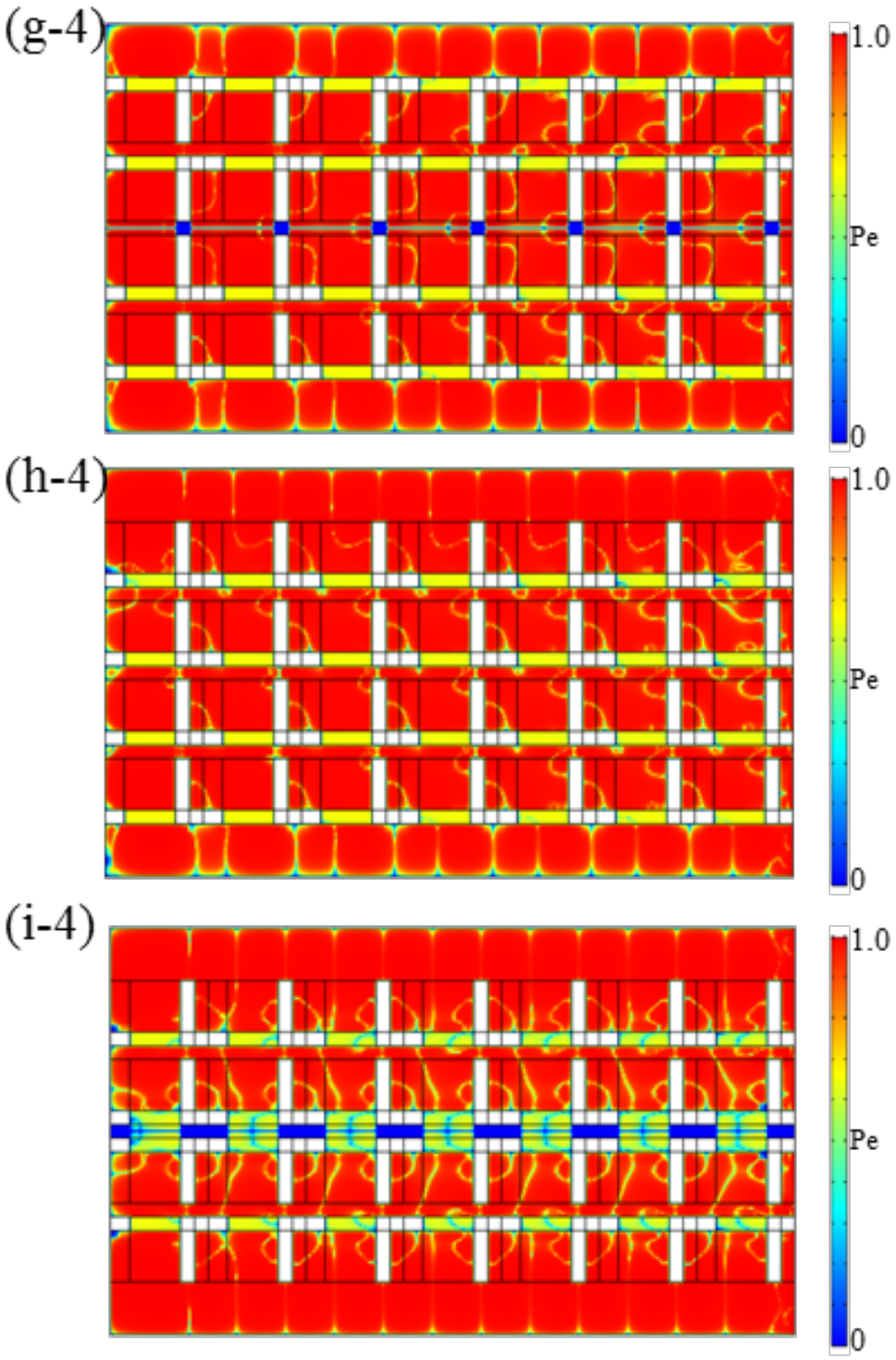

Fig. 6.4-18 Distribution of Pe_M in condition (g-4) OUTWARD, (h-4) NORMAL, and (i-4) INWARD

Table 6.4-12 TOF ratio for each stacking condition for the CHC reaction

Temperature	INWARD	NORMAL	OUTWARD
LT	1.36	1.45	1.46
MT	1.31	1.35	1.39
HT	1.29	1.34	1.36

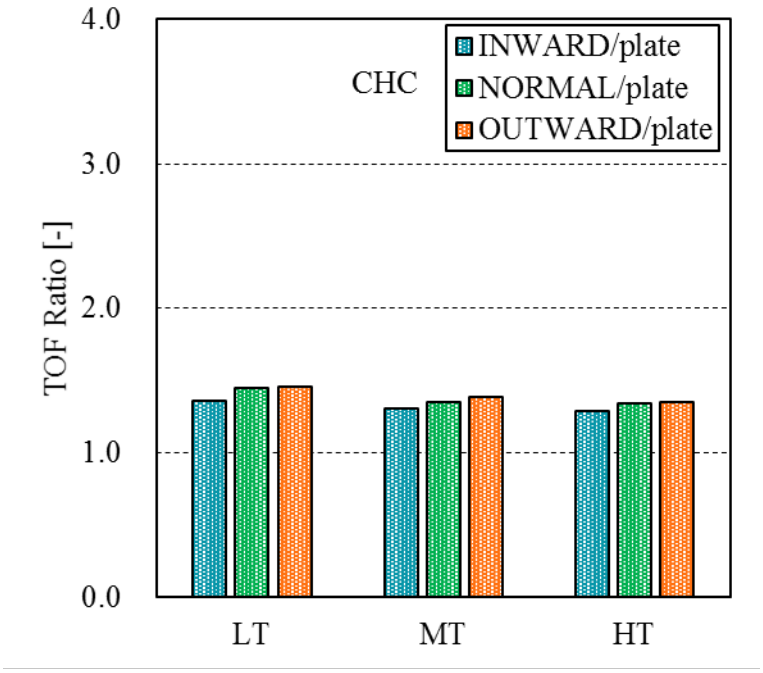

Fig. 6.4-19 TOF ratio for each stacking condition for the CHC reaction

The comparison and relationship were also discussed between the results of $(Pe_M)_{int}$ calculated from Eq. 5.4-3 and the results of the reaction rate constant, k_{CHC}, calculated from the experiments. These results are shown in **Table 6.4-13** and. **Fig. 6.4-20**. Although the reaction rate constant was higher for larger $(Pe_M)_{int}$, the effect of changing the MPC stacking method on the increase in reaction rate constant was smaller because of the very large $(Pe_M)_{int}$ for these experimental conditions in this study.

Table 6.4-13 Comparison between $(Pe_M)_{int}$ derived from simulation and reaction rate constant k_{CHC} derive from experiments at 413 K as MT

	One (MPC)	Three	Five
$(Pe_M)_{int}$	0.89	0.96	0.98
k_{CHC} (413 K)	3.2×10^{-2}	3.6×10^{-2}	4.4×10^{-2}

	OUTWARD	NORMAL	INWARD
$(Pe_M)_{int}$	0.97	0.97	0.93
k_{CHC} (413 K)	4.0×10^{-2}	3.7×10^{-2}	3.4×10^{-2}

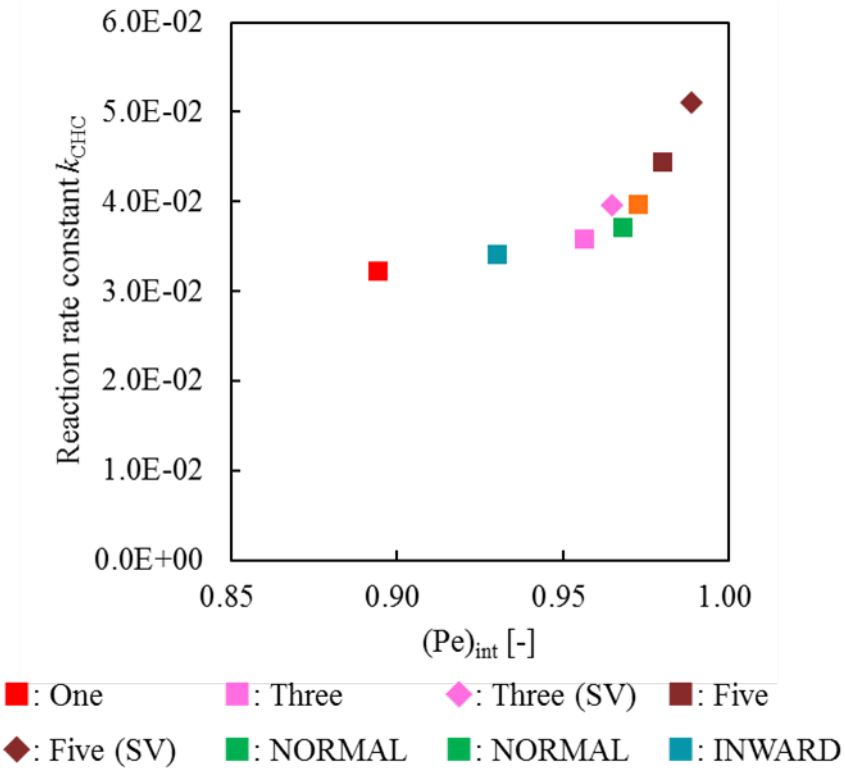

Fig. 6.4-20 Relation between $(Pe_M)_{int}$ by simulation and reaction constant k_{CHC} by experiments (413 K as MT)

6.5 Conclusions of chapter 6

In this chapter, the effective MPC stacking method was proposed for the SRM reaction under a catalytic reaction rate-limiting step, where the effect of structure on reactivity improvement was significant. Streamlines, Dcm, and reactant concentration distributions were evaluated using the numerical simulation, and the orientation and the distance of MPC stacking were investigated to improve the reactivity, and condition "OUTWARD" was proposed. Under condition "OUTWARD", the reactant concentration distribution in direction of MPC stacking was uniform, and the Dcm to evaluate the effect of the structure was large in whole the MPC stacking. Furthermore, the catalytic activity tests of its stacking method and the contrasting stacking method as a comparison condition were conducted, and the improved reactivity of the proposed stacking method was demonstrated by experiments. The results of the catalytic activity tests showed higher reactivity with the effective stacking method. The TOF ratio was evaluated as an effect of the reactivity improvement and the effect was larger at lower temperatures. It was achieved that the effective stacking method, condition "OUTWARD", for the SRM reaction results in the conversion efficiency of 3.8 times higher than that of the unprocessed plate-type catalyst by using the MPC and designing the stacking method under the experimental conditions in this study. The same stacking method was used for the WGS reaction, and similar results were obtained; the reactivity was improved. The same stacking method was applied for the CHC reaction under an external mass transfer rate-limiting step and its effect on reactivity was confirmed with catalytic activity tests. For the CHC reaction, the effect of the reactivity improvement was small. The tendency of the effect to reaction temperature was different from that of the SRM and WGS reactions.

In addition, the relationship between Dcm, which was the index for the proposed reactivity improvement calculated from simulations, and the reaction rate constants k calculated from the experimental results were evaluated, and it was suggested a positive correlation. In other words, it was demonstrated that the structural design of the structured catalyst and its stacking method by evaluating Dcm around the catalyst on the simulation for a catalytic reaction rate-limiting step provide the estimate for the experimental reaction rate.

6.6 References

[6-01] A. A. Lytkina, N. V. Orekhova, A. B. Yaroslavtsev; “Methanol Steam Reforming in Membrane Reactors,” Petroleum Chemistry 58 (2018) 911–922, https://doi.org/10.1134/S096554411811004X.

[6-02] X. Tan, K. Li; “Membrane microreactors for catalytic reactions,” Journal of Chemical Technology and Biotechnology 88 (2013) 1771–1779, https://doi.org/10.1002/jctb.4155.

[6-03] F. Yao, Y. Chen, G.P. Peterson; “Hydrogen production by methanol steam reforming in a disc microreactor with tree-shaped flow architectures,” International Journal of Heat and Mass Transfer 64 (2013) 418–425, https://doi.org/10.1016/j.ijheatmasstransfer.2013.04.057.

[6-04] Y. X. Liu, W. Zhou, Y. Lin, L. Chen, X. Y. Chu, T. Q. Zheng, S. L. Wan, J. D. Lin; “Novel copper foam with ordered hole arrays as catalyst support for methanol steam reforming microreactor,” Applied Energy 246 (2019) 24–37, https://doi.org/10.1016/j.apenergy.2019.03.199.

Chapter 7

Conclusions and Future Works

7.1 Conclusions

Chapter 1: Introduction

Chapter 1 provided a detailed description of the background, purpose, and organization of this dissertation. There is a need for PI approach in the field of chemical engineering in order to achieve a sustainable society. The structured catalyst is one of the various tools to realize PI, and attracting attention in recent years more and more because it has the characteristics to solve the problems of conventional catalytic reactor. In this study, the structured catalysts prepared and applied to the important reactions in the field of hydrogen energy. Furthermore, we focused on the improvement of catalytic reactivity due to the structure of the structured catalyst, while most of the previous studies on the use of structured catalysts have evaluated the improvement of the process performance as a catalytic process. One of the purposes of this dissertation was to clarify the detailed factors that contribute to improved reactivity using a structured catalyst through experiments and simulations. It was also the purpose to propose the index to quantitatively evaluate the improvement of reactivity due to the structure and to propose effective methods for using structured catalysts. The construction of this dissertation was shown in Fig. 1.1-1, and the outline was presented in Section 1.4.

Chapter 2: Methodology

In this chapter, the experimental and simulation methods related to this dissertation were provided. For the experiment, the method of preparing an anodized aluminum catalyst was adopted to catalyze a commercial structure made of aluminum. Cu/ZnO/Al_2O_3-MPCs with high catalytic activity and durability and low cost were prepared for the SRM and WGS reactions, and Pt/Al_2O_3-MPCs with low-temperature catalytic activity were prepared for the CHC reaction. The catalyst layer thickness, specific surface area, amount of catalyst loading, reduction properties, and active site characteristics were analyzed as the characterization of those catalysts.

Square channel reactors were prepared for the stacking of multiple MPCs and used in all catalytic activity tests. Catalytic activity tests were performed under constant *W/F* comparative conditions in each reaction, with care taken to identify the rate-limiting step.

For the simulation, the software used was COMSOL Multiphysics, which adopted 3D and 2D simulations, respectively. In all the simulation models, parallel calculations were performed for the fluid flow, heat transfer, and mass transfer to evaluate the physical phenomena around the catalyst. All simulation models were conducted and passed mesh independence verification.

Chapter 3: Comparison of Reactivity between MPC and Plate-type Structured Catalysts: Experimental studies

MPC was applied to the SRM, WGS, and CHC reactions, and the catalytic activity tests for comparing the reactivity to the unprocessed plate catalyst were carried out. MPC showed higher conversions than plate for all reactions, and reaction rate analysis according to the Arrhenius equation showed that there was no change in a rate-limiting step dependent on the reaction temperature and the activation energy was similar in both structures of MPC and plate for each reaction. Furthermore, the results of the reaction rate analysis revealed that the frequency factor was increased by the structure of MPC, suggesting that the contact frequency between reactants and catalysts was improved by the structure. The reactivity of the SRM and WGS reactions was improved under a catalytic reaction rate-limiting step, and this factor was investigated in detail because it was never reported. It is generally known that a frequency factor is expressed as a product of a number of collision molecules and a steric factor, and the improved a number of collision molecules or a steric factor due to the effect of the structure due to the structure of MPC was considered to provide the improvement of reactivity. On the other hand, for CHC reaction, the structure of MPC promoted the mass transfer around the catalyst and improved the reactivity for CHC reaction because the CHC reaction was an external mass transfer rate-limiting step.

The TOF, which is a general index of catalytic performance, was calculated and compared with that of the plate under each condition to quantitatively evaluate the effect of reactivity improvement due to the structure of

MPC. For the CHC reaction, which is an external mass transfer rate-limiting step, the effect was almost constant independent of the reaction temperature. On the other hand, the effects of the SRM and WGS reactions, which were a catalytic reaction rate-limiting step, were getting larger at lower temperatures. It was suggested that the contact frequency between the reactants and the catalysts was promoted at lower temperatures due to the effect of the structure. In this study, it was realized that the evaluation of the increase in the frequency factor as the effect of reactivity improvement by evaluating the TOF ratio.

Chapter 4: Investigation of Factors to Improve Reactivity due to the Structure of MPC and Proposal of Evaluation Index: Numerical Simulation

In this chapter, it was investigated the factors on reactivity improvement when the use of MPC comparing with unprocessed plate-type catalysts with COMSOL Multiphysics software as numerical simulations. The SRM reaction, which had the largest reactivity improvement effect due to the structure of MPC, and the CHC reaction, which had a smaller effect, were adopted in the simulation models. The initial and boundary conditions were set to match the experimental conditions, and the parameters related to the reaction rate were calculated from the experimental results. The results of the calculations for both reactions by their prepared simulation models showed similar conversion to those of the experimental results, thus confirming the validity of the simulation model. The change in streamline due to the structure of MPC using the simulation models was evaluated, and it was demonstrated that the MPC is a suitable tool for PI, as it showed that the MPC is capable of vector control of transport phenomena.

For the CHC reaction, which was an external mass transfer rate-limiting step, the Pe_M around MPC was calculated with simulation to evaluate the overall reactivity. The results showed that the use of MPC significantly increased the value of Pe_M around MPC. It was suggested that the factors of the reactivity improvement when the use of MPC for the CHC reaction.

Dcm, which evaluates the effect of the structure, was proposed as the index to evaluate the reactivity improvement due to the structure of MPC under a catalytic reaction rate-limiting step. The Dcm was defined as

the ratio of the mass transfer flux due to convection caused by the catalytic structure to the mass transfer flux due to diffusion, with a higher value indicating that the changes in the reactants fluid flow were larger. Dcm was evaluated in the direction of MPC fin height, considering the structure of MPC. Therefore, Dcm was found to be almost zero around the plate. On the other hand, Dcm around the MPCs was found to be larger in front of or behind the MPC fins. It was suggested that the factor of the reactivity improvement when the use of MPC for the SRM reaction. For the WGS reaction, it was the same reason for the reactivity improvement when MPC was used because a rate-limiting step was the same as the SRM reaction. In addition, numerical simulations were performed for the SRM reaction at different reaction temperatures in order to investigate the tendency of larger TOF ratios at lower temperatures as the effect of the reactivity improvement under a catalytic reaction rate-limiting step presented in Subsection 3.4.5 The evaluation of Dcm at each reaction temperature showed that the Dcm values around MPC were higher at lower temperatures, indicating good accordance between the calculated and experimental results. In other words, it was suggested that Dcm is a suitable index for evaluating the reactivity of structured catalysts such as MPC under a catalytic reaction rate-limiting step. It was a novel report for the field of process intensification of a catalytic reaction process using a structured catalyst.

Finally, the simulation model was prepared for the non-hole MPC and its streamlines and Dcm were evaluated. The streamlines and the value of Dcm around MPC indicated that the effect of the structure was small because there were no holes, and the reason for the decreased reactivity of the non-hole MPCs by experiments was verified. In other words, it was suggested that not only the fins but also the holes are important for improving the reactivity due to the structure of MPC.

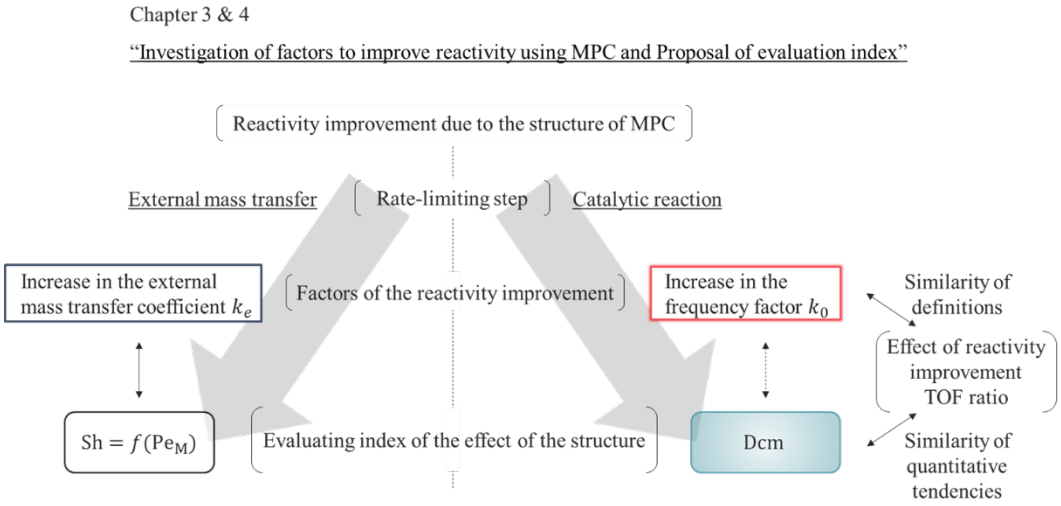

Fig. 7.1-1 Summary of chapter 3 & 4

Chapter 5: Investigation of the Effect of the Number of MPC Stacking on the Reactivity

In this chapter, the effect of the number of MPC stacking on the reactivity was investigated by experiments and simulations for the SRM reaction, first. The effect of the structure was promoted by increasing the number of MPC from 1 to 3, and the reactivity was improved. The TOF ratio as the index for the effect of the reactivity improvement got larger at lower temperatures. On the other hand, the reactivity was significantly reduced when the MPCs packed densely in the reactor, and the effect of the reactivity improvement was small. The numerical simulation was performed in order to examine the reason for that, and streamline and Dcm, as the index for reactivity under a catalytic reaction rate-limiting step, were evaluated. The simulation results showed that, for condition "Five", the effect of the structure was suppressed due to the densely stacked MPCs in the reactor, the flow change in the direction of MPC stacking was small, and the Dcm was small in whole the stacking. Moreover, a significant reactant concentration distribution was observed in the direction of MPC stacking.

The catalytic activity tests were conducted using the position of the catalyzed MP as a parameter because it was believed that the stacked MPCs in the reactor were not working uniformly due to the suppression of the

effect of the structure. It was confirmed that the reactivity was different depending on the position of MPC. Especially condition “BOTTOM”, where the catalyst was positioned in the lowest part of the stacking, showed the reactivity reduction. It was suggested that the effect of the structure was smaller at lower part of stacking under conditions when the MPCs were densely packed in the reactor. It was confirmed that the catalyst was not working uniformly and the reason for the reduced reactivity for condition “Five” was identified. From these results, the reactivity under the catalytic reaction rate-limiting step is expected to be improved by stacking methods that consider the following two points.

- To increase the effect of the structure by not stacking MPCs too densely in the reactor
- To increase the effect of the structure by utilizing the directionality of the flow change

Catalytic activity tests with different number of MPC stacking were carried out for the WGS reaction under a catalytic reaction rate-limiting step, similar to the SRM reaction. The results showed a similar reactivity tendency as the SRM reaction; the reactivity was increased for condition “Three”, and decreased reactivity for condition “Five”. The reason was considered that the same as the SRM reaction because of the same rate-limiting step. Furthermore, for the CHC reaction, which was an external mass transfer rate-limiting step, catalytic activity tests were carried out with different number of MPC stacking. The reactivity improvement due to the number of MPC stacking could not be investigated under the constant *W/F* comparison condition under an external mass transfer rate-limiting step, so the comparison was performed under the constant SV condition. As the number of MPCs stacked for the CHC reaction increased, the reactivity improved and it was showed a different tendency than the SRM and WGS reactions under a catalytic reaction rate-limiting step. Furthermore, the TOF ratio as the effect of reactivity improvement was small and almost constant at each reaction temperature when the number of stacking was changed. These reasons were examined by evaluating Pe_M, the index for the reactivity under an external mass transfer rate-limiting step. The simulation results showed that the Pe_M was large and uniform in whole the MPC stacking. In other words, Pe_M was less affected due to the number of MPC stacking under the reaction conditions for the CHC reaction in this study, which reduced the effect of reactivity improvement.

Chapter 6: Proposal for Effective MPC Stacking Method

In this chapter, the effective MPC stacking method was proposed for the SRM reaction under a catalytic reaction rate-limiting step, where the effect of structure on reactivity improvement was significant. Streamlines, Dcm, and reactant concentration distributions were evaluated using the numerical simulation, and the orientation and the distance of MPC stacking were investigated to improve the reactivity, and condition "OUTWARD" was proposed. Under condition "OUTWARD", the reactant concentration distribution in direction of MPC stacking was uniform, and the Dcm to evaluate the effect of the structure was large in whole the MPC stacking. Furthermore, the catalytic activity tests of its stacking method and the contrasting stacking method as a comparison condition were conducted, and the improved reactivity of the proposed stacking method was demonstrated by experiments. The results of the catalytic activity tests showed higher reactivity with the effective stacking method. The TOF ratio was evaluated as an effect of the reactivity improvement and the effect was larger at lower temperatures. It was achieved that the effective stacking method, condition "OUTWARD", for the SRM reaction results in the conversion efficiency of 3.8 times higher than that of the unprocessed plate-type catalyst by using the MPC and designing the stacking method under the experimental conditions in this study. The same stacking method was used for the WGS reaction, and similar results were obtained; the reactivity was improved. The same stacking method was applied for the CHC reaction under an external mass transfer rate-limiting step and its effect on reactivity was confirmed with catalytic activity tests. For the CHC reaction, the effect of the reactivity improvement was small. The tendency of the effect to reaction temperature was different from that of the SRM and WGS reactions.

In addition, the relationship between Dcm, which was the index for the proposed reactivity improvement calculated from simulations, and the reaction rate constants k calculated from the experimental results were evaluated, and it was suggested a positive correlation. In other words, it was demonstrated that the structural design of the structured catalyst and its stacking method by evaluating Dcm around the catalyst on the simulation for a catalytic reaction rate-limiting step provide the estimate for the experimental reaction rate.

Purpose of chapter 5 & 6

"Investigation of Effects of MPC Stacking and Proposal for effective Stacking Method"

Dcm was applied to evaluate the effect of the structure on the use of multiple MPCs.

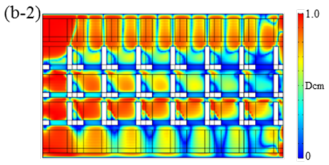

Strategies for stacking methods to improve the reactivity

- To increase the effect of the structure by not stacking MPCs too densely in the reactor
- To increase the effect of the structure by utilizing the directionality of the flow change

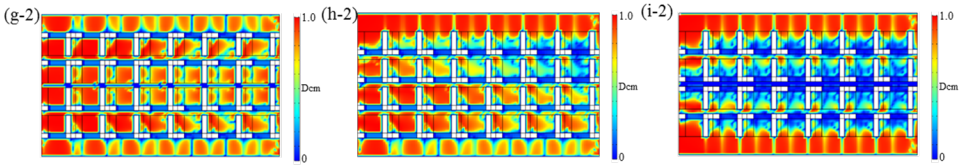

Reactivity reached 3.8 times higher at lower temperatures with the proposed stacking method

Fig. 7.1-2 Summary of chapter 5 & 6

7.2 Future works and Outlook

In this study, the reactivity improvement and the tendency of its effect under a rate-determining step of a catalytic reaction and under a rate-determining step of an external mass transfer were evaluated when the structured catalyst was used (**Table 7.2-1**). In addition, factors for those were investigated and the unique evaluation index, Dcm, was proposed (**Table 7.2-2**).

Table 7.2-1 Evaluating the effect of the reactivity improvement with a focus on a rate-limiting step

Reaction	Rate-limiting step in this study	Effect of reactivity improvement (TOF ratio)
SRM	Catalytic reaction	Largest
WGS	Catalytic reaction	Large
CHC	External mass transfer	Small

Table 7.2-2 Reactivity improvement factors and the evaluation indexes

Rate-limiting step in this study	Factor for reactivity improvement due to the structure of MPC	Evaluation index
Catalytic reaction	Increase in the frequency factor k_0	Dcm
External mass transfer	Increase in the external mass transfer coefficient k_e	Pe_M

As shown in Tables 7.2-1 and 7.2-2, the factors and indexes for the reactivity improvement using structured catalysts were suggested. Here, two of the targets that were not investigated in this study are provided below. First, the temperature dependence of the effect of the reactivity improvement when the structured catalyst was used under an external mass transfer rate-limiting step was not investigated in detail. The CHC reaction in this study was conducted under high flow rate conditions to evaluate the reactivity. However, the CHC reaction, when Pt catalyst was used, was proceeded very fast and was therefore under an external mass transfer rate-

limiting step in the experimental conditions. The Pe_M around the catalysts in the reactor was very large, and the Pe_M was less affected by the change in the MPC stacking methods and the reaction temperature. The tendency shown in the SRM and WGS reactions to get larger the effect of the reactivity improvement at lower temperatures is expected to be also confirmed for the CHC reaction because of the reaction environment, where was the low diffusion rate. It showed the tendency to increase slightly at lower temperatures in these experimental conditions, but it was not sufficient.

Therefore, the experimental conditions under an external mass transfer rate-limiting step, not limited to the CHC reaction, should be set up as in this study such as changing the MPC stacking method, and the change in the Pe_M around the catalysts and the temperature dependence due to the effect of the structure when changing the structure or use of the structured catalyst should be evaluated. In other words, the evaluation of the effects of the use of structured catalysts under an external mass transfer rate-limiting step provides expand the application of structured catalysts and accelerates the study and spread of structured catalyst technology. We believe that it will realize PI for a sustainable society.

Second, as described in Subsection 3.4.5, factors contributing to the difference in the effect of the reactivity improvement between the SRM and the WGS reactions were not investigated. It was suggested that the frequency factor, represented in the molecular collision theory in the field oh reaction kinetics, were increased by the effect of the structure due to the structure of MPC and improved the reactivity for the reaction under a catalytic reaction rate-limiting step. While it is well known that the frequency factor is expressed thermodynamically in the Absolute reaction rate theory as the Transition state theory [7-01]. In other words, it is possible to calculate the frequency factor to increase thermodynamically. Furthermore, the field of quantum mechanics, which developed after the development of reaction kinetics as a field of study, also had a significant impact on the field of reaction kinetics. In recent years, first-principles calculations of the electronic states of reactants and catalysts by quantum mechanical calculations of chemical reactions are being actively studied with the rapid increase in computational performance [7-02]. In addition, a number of machine learning-based catalyst designs have been reported for the selection of catalyst metals [7-03, 7-04]. The argument of this study should be examined in more detail regarding the improvement of the frequency factor from those approaches.

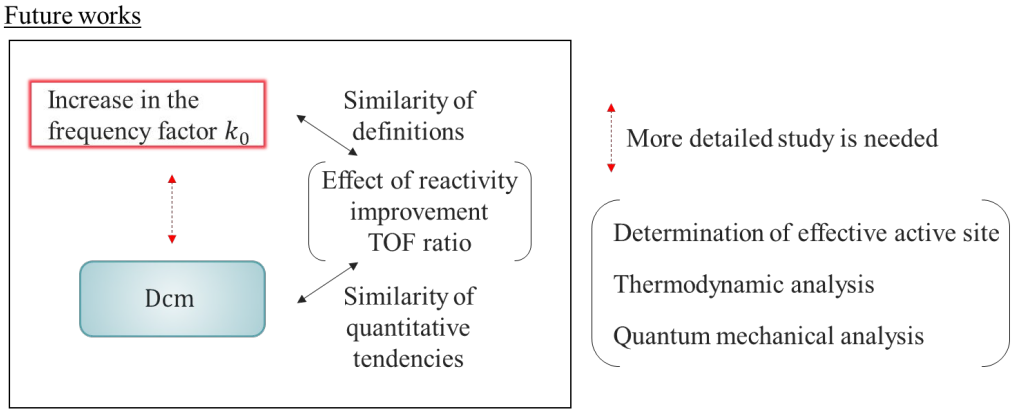

Fig. 7.2-1 Future works

The outlook of this study beyond the Future Works is the preparation and demonstration of structured catalysts with the appropriate structure for various reactions using a 3D printer. From the results of this study; the index for evaluating the effect of reactivity improvement due to the catalyst structure focusing on a rate-limiting step, we believe that structured catalysts are an applicable replacement for all conventional catalytic processes. The PI of the catalytic reaction process is realized by applying the structured catalysts, which have the proposed structure by simulation considering the reaction conditions and the characteristics of the target reactions. The structured catalyst will be prepared by using a 3D printer easily.

However, there are many challenges to the structured catalysts with a 3D printer. Depending on the hardware, software, printing paste properties, printing conditions, etc., the capacity and durability of the 3D printer structured catalyst will be influenced. Also, the composition of the printing paste has a significant effect on reactivity. However, the 3D printer structured catalyst technology is considered to be very attractive with the drastic improvement in computer performance and the rapid development of additive manufacturing technology in recent years, and it cannot help but hope that the study and use of structured catalyst technology will contribute to building a sustainable society.

7.3 List of published Journal related to this dissertation

1. **H. Sasaki**, M. Sakurai; “Proposal of index for reaction improvement using structured catalyst”, Journal of Chemical Engineering of Japan 53 (2020) 389–396, https://doi.org/10.1252/jcej.19we108.
2. **H. Sasaki**, M. Sakurai; “Proposal for effective stacking method of structured catalyst”, International Journal of Hydrogen Energy 46 (2021) 2036–2048, https://doi.org/10.1016/j.ijhydene.2020.10.067.
3. **H. Sasaki**, M. Sakurai; “Proposal of the reaction environment for effective use of structured catalyst”, Journal of Flow Chemistry (2021) “Accepted”, https://doi.org/10.1007/s41981-021-00150-9.

7.4 Presentation at conferences related to this dissertation

1. 佐々木浩允：「構造体触媒を用いたマイクロリアクタの開発」, 化学工学学生会 Poster Session’13, 2013.7
2. 佐々木浩允, 嶋田省吾, 桜井誠, 亀山秀雄 :「構造体触媒を用いたマイクロリアクタの開発」, 化学工学会 第 79 年会, 2014.3.18
3. 桜井誠、佐々木浩允：「構造体触媒マイクロリアクターによる反応性向上」, 化学工学会 第 48 秋季大会, 2016.9.7
4. Makoto Sakurai, Hiromi Hiramatsu, **Hiromu Sasaki**, Yuhei Sakai, Masashi Uehara, Hironari Sasagawa: “Process intensification using the micro reactor with a structured catalyst”, 5th International Workshop on Process Intensification (IWPI2016), 2016.9.29
5. 佐々木浩允、桜井誠 :「対流と拡散を考慮した構造体触媒反応器の設計」, 化学工学会 第 50 回秋季大会, 2018.9.18
6. **Hiromu Sasaki**, Makoto Sakurai: “Design of the Structured Catalyst Reactor Considering Convection and Diffusion”, 6th International Workshop on Process Intensification (IWPI2018), 2018.11.7
7. **Hiromu Sasaki**, Makoto Sakurai: “Study of packing method of the structured catalyst for reactivity improvement”, 18th Asian Pacific Confederation of Chemical Engineering Congress, 2019.9.24

7.5 References

[7-01] O. K. Rice, H. Gershinowitz; “Entropy and the Absolute Rate of Chemical Reactions I. The Steric Factor of Bimolecular Associations,” Journal of Chemical Physics 2 (12) (1934) 853–861, https://doi.org/10.1063/1.1749408.

[7-02] P. Geerlings and F. De Proft; “Conceptual DFT: the chemical relevance of higher response functions,” Physical Chemistry Chemical Physics 10 (2008) 3028–3042.

[7-03] T. Hattori, S. Kito; “Artificial intelligence approach to catalyst design,” Catalysis Today 10 (1991) 213–222, https://doi.org/10.1016/0920-5861(91)80066-I.

[7-04] T. Toyao, Z. Maeno, S. Takakusagi, T. Kamachi, I. Takigawa, K.-i. Shimizu; “Machine Learning for Catalysis Informatics: Recent Applications and Prospects,” ACS Catalysis 10 (2020) 2260−2297, https://doi.org/10.1021/acscatal.9b04186.

ACKNOWLEDGMENTS

I decided to quit the job and entered the Sakurai Lab. at Tokyo University of Agriculture and Technology in April 2018, where I used to work. Such a decision took a lot of courage, as this was a minority choice. I have people who have encouraged me to make this decision. In addition, there are people who supported me academically and emotionally after further education. I give a lot of acknowledgments to those not many people.

For Dr. Makoto Sakurai, I consulted with him on matters related to my life frequently and he listened to me intimately for hours at any time even before I entered the Sakurai Lab. After entering the Sakurai Lab., he accepted my ideas without denying them, and we have been working together to develop our research. From 2013, when I joined the Sakurai Lab., to today, I have spent the most time with him and shared many troubles, challenges, and joys with him. Dr. Sakurai is the person I respect the most. I look forward to your continued supervision.

I had many encounters with many people in the Sakurai Lab., where I worked for a long time. I appreciate the records and memories of the students who belonged to the Sakurai Lab., which have been passed down from generation to generation. I would like to especially thank those who have conducted similar research and shared their concerns about each other's research for giving me important approaches to my research. There are people who supported me even if it was not in the same Lab. The time we spent in dialogue about non-research matters gave me active energy for my research.

Dr. Masato Sakurai, who belongs to the Japan Aerospace Exploration Agency (JAXA), helped me a lot in making my decision. He provided us with a variety of information raging from research theme to post-degree career paths. I would like to appreciate your very kind response to my first rude email. On the other hand, I would like to apologize for not being able to develop the research themes that I attempted to share. I sincerely hope for the development of manned space science and technology, and I would like to be a person who further contributes to this field in the future.

I also acknowledge my colleagues, seniors, and superiors at the company I left. I received a lot of support from them who kept in touch with me after I left. They are the ones who connected my past with my future. And, I am very grateful to my old friends with whom I have shared some dialogue from time to time. The only true wisdom is in knowing you know nothing.

Finally, I especially thank my family for continuous support so far, and you.

Sincerely,

Hiromu Sasaki (2021.3.25)